

D R A F T

NCAR/TN -???+???

NCAR TECHNICAL NOTE

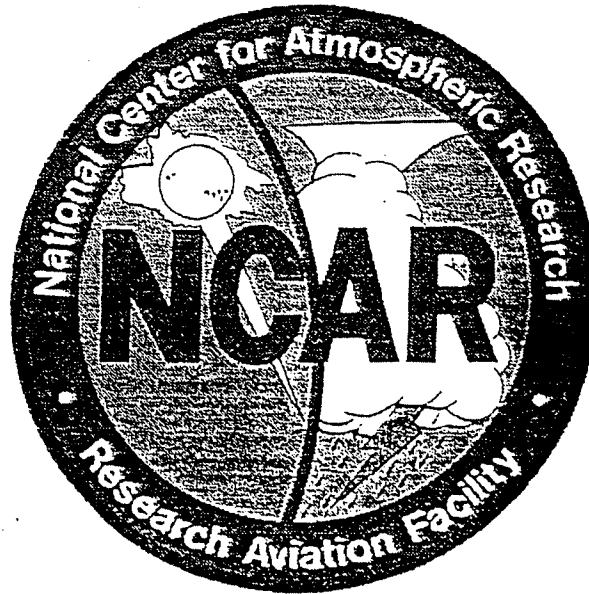
February 1997

RAF Sensor Summaries

June 1996

Julie A. Haggerty
Darrel Baumgardner

D R A F T



D R A F T

RESEARCH AVIATION FACILITY
ATMOSPHERIC TECHNOLOGY DIVISION
NATIONAL CENTER FOR ATMOSPHERIC RESEARCH
BOULDER, COLORADO

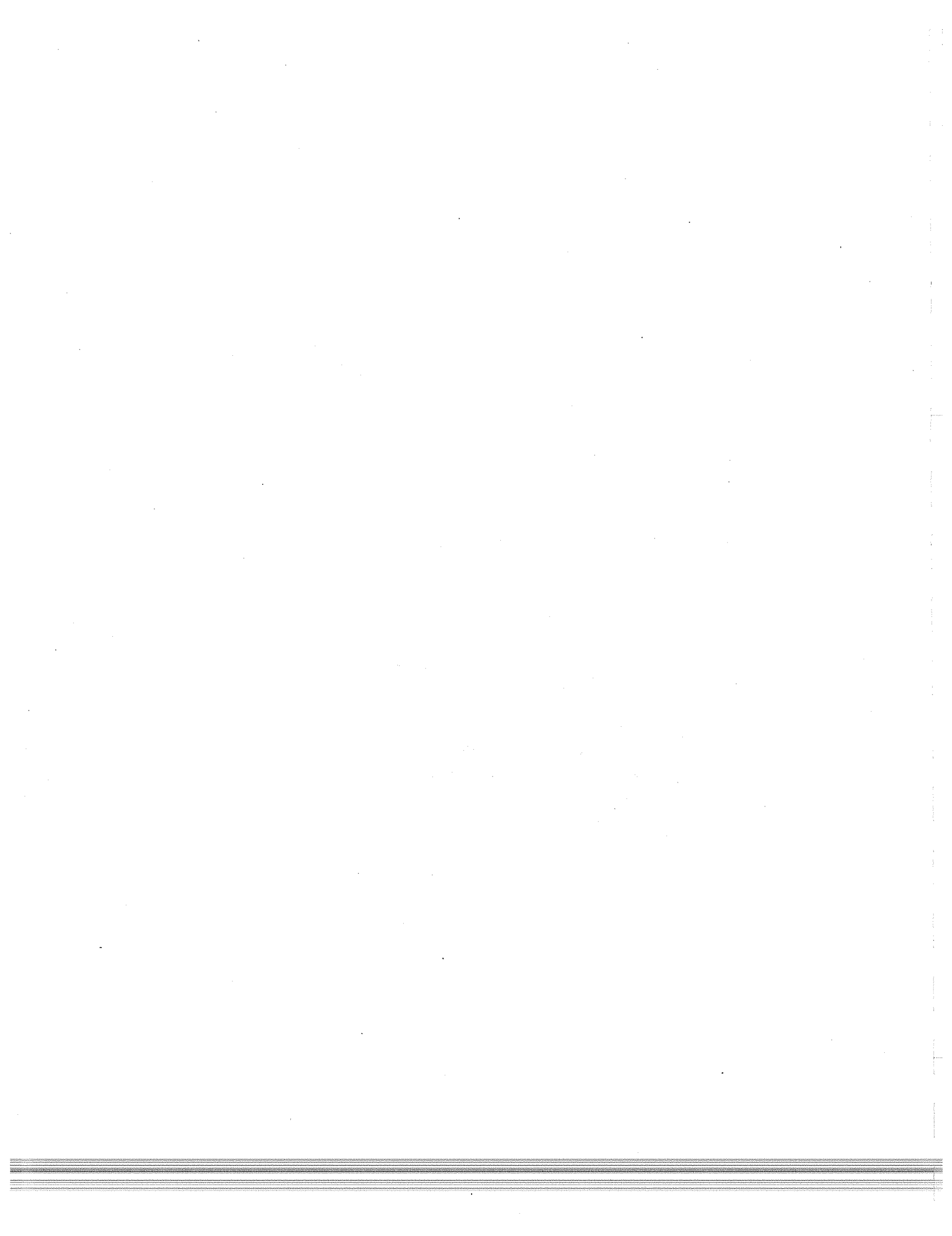


Table of Contents

SECTION 1—Meteorological Sensors	1
Standard Dewpointer	1
Lyman-Alpha Hygrometer	5
Cryogenic Frost-Point Hygrometer	9
Ultraviolet Hygrometer	14
OPHIR-III Radiometric Temperature	17
SECTION 2—Air Motion Sensors	21
Air Motion and Aircraft Position	21
Inertial System	21
Gust Probe	22
Global Positioning System (GPS)	23
Air Motion System	23
SECTION 3—Radiometric Sensors	28
Ultraviolet Radiometer	28
Pyranometer	33
Pyrgeometer	37
Precision Radiation Thermometer (PRT-5)	41
Heimann Radiation Pyrometer (KT19.85)	45
Spectral Vegetation Radiometer (SVR)	48
Multichannel Cloud Radiometer (MCR)	52
Airborne Imaging Microwave Radiometer (AIMR)	56
Scanning Aerosol Backscatter Lidar (SABL)	61
SECTION 4—Chemical Sensors	66
Nitrogen Oxide Analytical System	66
RAF "Fast" Ozone Analyzer	71
TECO 49 Ozone Analyzer	75
TECO 48 Carbon Monoxide Analyzer	78
SECTION 5—Aerosol Sensors	82
Passive Cavity Aerosol Spectrometer Probe	82
Forward Scattering Spectrometer Probe	86
CCN/IN Counter	88
Airborne Condensation Nucleus Counter	93
SECTION 6—Cloud Sensors	98
Counterflow Virtual Impactor	98
One Dimensional Optical Array Probe	103
Two Dimensional Optical Array Probes	107
Forward Scattering Spectrometer Probe	111
Rosemount Icing Detector	117
PMS/CSIRO Hot Wire Liquid Water Probe	121

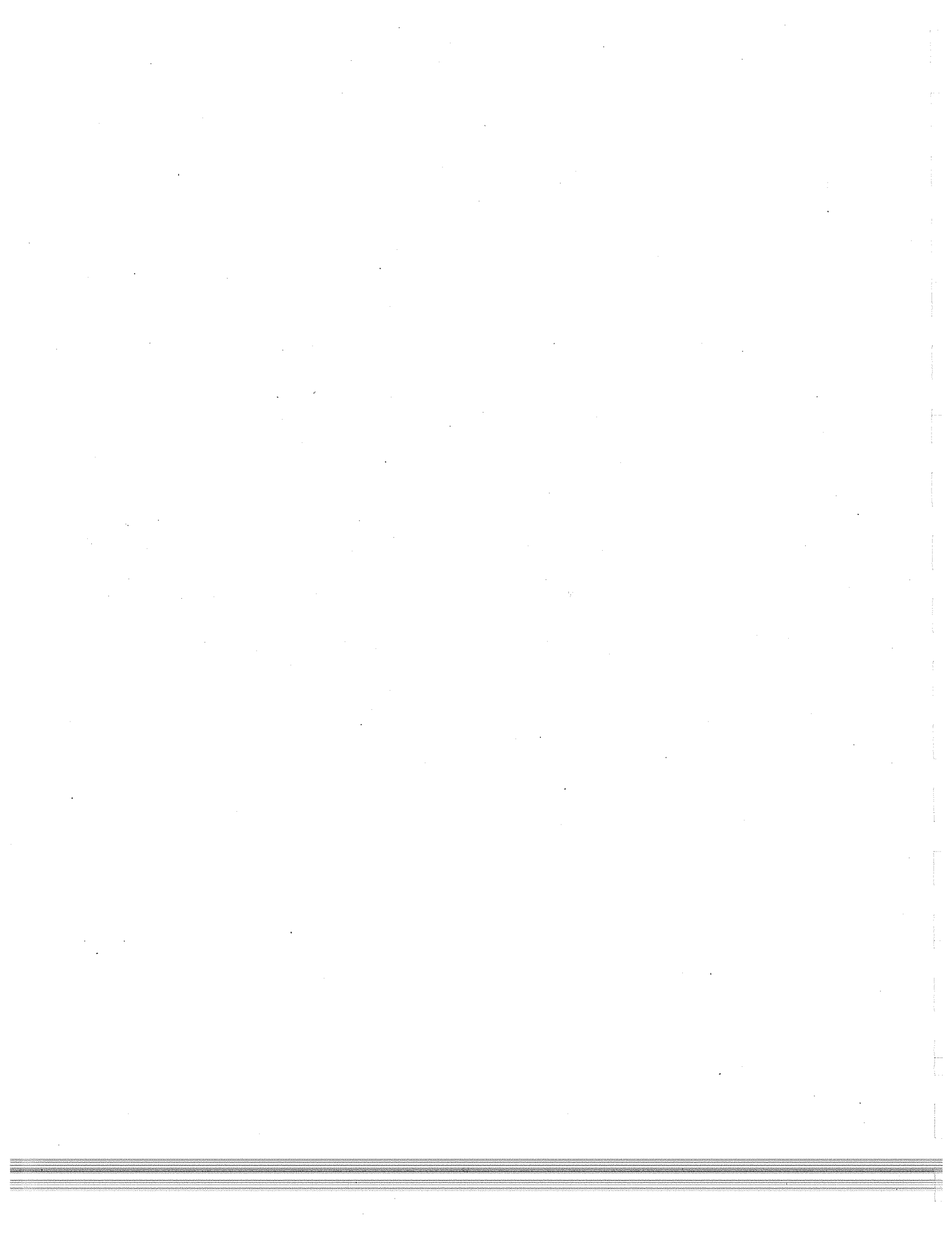
List of Figures and Table

Figure 1.1	Standard Dewpointer	3
Figure 1.2	An example of dewpoint measurements from the standard dewpointer	4
Figure 1.3	Lyman-Alpha Hygrometer	7
Figure 1.4	An example of mixing ratio data from the Lyman-Alpha hygrometer	8
Figure 1.5	Frost-Point Hygrometer	11
Figure 1.6	Graphical schematic of calculations to determine the ambient dew - or front-point temperatures	12
Figure 1.7	A vertical profile of dewpoint temperature measured over SE Wyoming on September 18, 1990	13
Figure 1.8	Mixing ratio as measured by the ultraviolet hygrometer	16
Figure 1.9	OPHIR-III Radiometric Temperature	19
Figure 1.10	A segment of OPHIR-III data from the TOGA-COARE Experiment	20
Figure 1.11	A segment of OPHIR-III data from the TOGA-COARE Experiment	20
Figure 2.1	Coordinate systems used in deriving equations for calculating the air velocity components. Aircraft attitude angles and wind incidence angles; attack (α), sideslip (β), ψ true heading, θ pitch, and ϕ roll	27
Figure 3.1	Ultraviolet Radiometer	30
Figure 3.2	Passband of Eppley TUVR Filter	31
Figure 3.3	Response of Eppley TUVR Selenium Barrier Layer Photocell	31
Figure 3.4	Example of data from the ultraviolet radiometer	32
Figure 3.5	RAF Pyranometer	35
Figure 3.6	Example of the instrument output from the pyranometer	36
Figure 3.7	RAF Pyrgeometer	39

Figure 3.8	Example of the instrument output from the pyranometer	40
Figure 3.9	Precision Radiation Thermometer (PRT-5)	43
Figure 3.10	Example of output from the PRT-5	44
Figure 3.11	Heimann Radiation Pyrometer (KT19.85)	46
Figure 3.12	Example of output from the Heimann Radiation Pyrometer	47
Figure 3.13	Spectral Vegetation Radiometer (SVR)	50
Figure 3.14	Example of the output from the Spectral Vegetation Radiometer	51
Figure 3.15	Multichannel Cloud Radiometer (MCR)	54
Figure 3.16	Cut-away drawing of the MCR	55
Figure 3.17	Example of one channel's output from the MCR	55
Figure 3.8	Airborne Imaging Microwave Radiometer (AIMR)	58
Figure 3.19	Block diagram showing relationships between the AIMR components	59
Figure 3.20	AIMR 90 Ghz image of Arctic ice from BASE. Bright areas represent leads in the ice	60
[Table 1]	SABL Specifications	63
Figure 3.21a	Scattering ratios at 532 nm	64
Figure 3.21b	Scattering ratios at 1064 nm	64
Figure 3.22	Ratio of scattering ratios	65
Figure 4.1	Nitrogen Oxide Analytical System	69
Figure 4.2	Plots of NO and NO _y concentrations	70
Figure 4.3	Plots of NO and NO _y concentrations	70
Figure 4.4	RAF "Fast" Ozone Analyzer	73
Figure 4.5	Example of output from the "Fast" Ozone Analyzer	74

Figure 4.6	TECO 49 Ozone Analyzer	77
Figure 4.7	TECO 48 Carbon Monoxide Analyzer - No Photograph Available	80
Figure 4.8	Diagram of the TECO 48 optics and electronics	81
Figure 4.9	Example of data from the TECO 48 Carbon Monoxide Analyzer	81
Figure 5.1	Passive Cavity Aerosol Spectrometer Probe (PCASP) optical path	84
Figure 5.2	Typical size distribution where the number, surface area, and volume concentration of particles in each size category is shown, normalized by the width of the size channel from the PCASP	84
Figure 5.3	Passive Cavity Aerosol Spectrometer Probe	85
Figure 5.4	The optical path of the Forward Scattering Spectrometer Probe (FSSP) Model 300	89
Figure 5.5	Variation of scattered light with particle diameter for the FSSP	90
Figure 5.6	Typical size distribution along with the number, surface area, and volume concentration of particles in each size category	90
Figure 5.7	Forward Scattering Spectrometer Probe	91
Figure 5.8	Schematic diagram of the CCN/IN counter	92
Figure 5.9	Airborne Condensation Nucleus Counter	96
Figure 5.10	Operation of the CCN Counter on NCAR aircraft	97
Figure 5.11	CN variation with height in summer near Denver, Colorado	97
Figure 6.1	Counterflow Virtual Impactor (CVI)	100
Figure 6.2	Schematic diagram of the CVI	101
Figure 6.3	Example of output from the CVI	102
Figure 6.4	Schematic diagram of the 260X OAP Cloud Probe	105
Figure 6.5	A size distribution of droplets as measured by the 260X OAP Cloud Probe ..	105

Figure 6.6	One Dimensional Optical Array Probe	106
Figure 6.7	Schematic diagram of the 2D Optical Array Probes	109
Figure 6.8	Images from the 2D probe in several different types of ice particles ranging from rain drops to pristine ice crystals to more complex heavily rimed ice particles	109
Figure 6.9	Two Dimensional Optical Array Probes (2D-C)	110
Figure 6.10	Schematic diagram of the Forward Scattering Spectrometer Probe (FSSP-100 Cloud Probe)	114
Figure 6.11	Variation of scattered light with particle diameter for the FSSP 100	115
Figure 6.12	Size distribution from the FSSP 100	115
Figure 6.13	Forward Scattering Spectrometer Probe	116
Figure 6.14	Schematic diagram of the Rosemount Icing Detector Model 871	119
Figure 6.15	Output from the Rosemount Icing Detector	119
Figure 6.16	Rosemount Icing Detector - No Photograph Available	120
Figure 6.17	Schematic diagram of the PMS/CSIRO Hot Wire Liquid Water Probe	123
Figure 6.18	PMS/CSIRO Hot Wire Liquid Water Probe	124



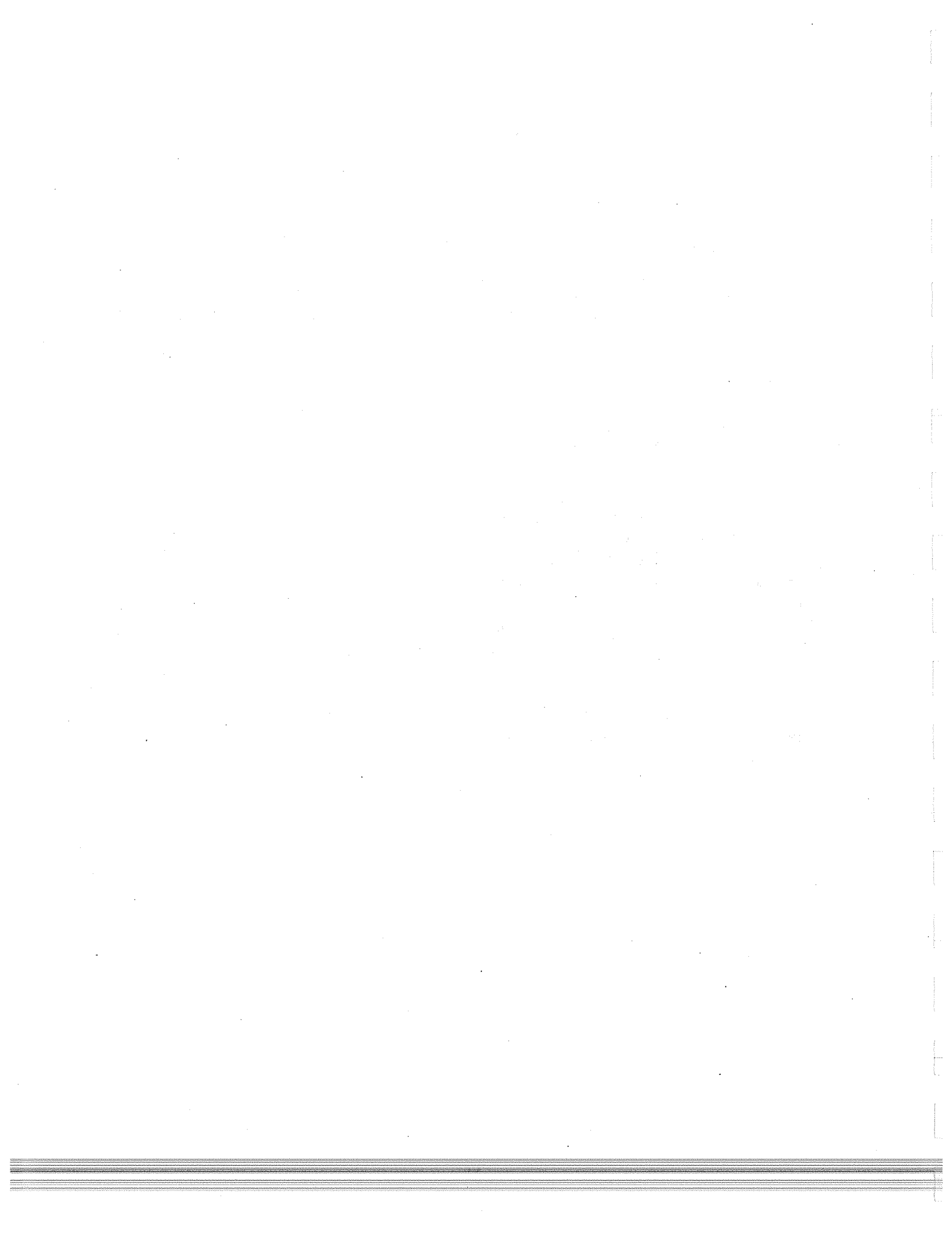
Preface

This document was compiled from material presented at a training workshop held in April 1995 for users of Research Aviation Facility aircraft and instrumentation. The workshop included presentations describing each sensor, discussions of flight planning, and a tutorial on RAF's real-time display software. The sensor presentations have been summarized and included in this technical report.

Contributions were provided by the RAF scientific staff as follows:

Darrel Baumgardner	(Aerosol and Cloud Sensors)
William A. Cooper	(Aerosol Sensors)
Richard Friesen	(Air Motion Sensors)
Julie Haggerty	(Radiometric Sensors)
Greg Kok	(Chemical Sensors)
Krista Laursen	(Radiometric Sensors)
Bruce Morley	(Radiometric Sensors)
Allen Schanot	(Meteorological Sensors)
Richard Schillawski	(Chemical Sensors)
Paul Spyers-Duran	(Meteorological Sensors)
Cynthia Twohy	(Aerosol and Cloud Sensors)

The services of Linda Banks, Barbara Knowles and Mary Ann O'Meara in preparing this document are gratefully acknowledged. Photographs were taken by Bob Bumpas.



SECTION 1—Meteorological Sensors

Standard Dewpointer (EG&G Model 137 Hygrometer & GE Model 1011b Hygrometer)

Introduction

The standard humidity measurement at RAF is performed using the chilled mirror technique for measuring dewpoint temperature. This system provides good accuracy and a response time adequate for mean humidity measurements with the ability to provide continuous readings over a wide range of environmental conditions. Figure 1.1 is a photograph of the instrument.

Operating Principles

The determination of dewpoint temperature by the chilled mirror technique has evolved into a system for routine operational aircraft use. The dewpointer hygrometer was chosen as the standard humidity measuring system at RAF because it represents one of the best and most reliable applications of this technology. With this type of system, the temperature of a reflecting surface is lowered until water vapor saturation is reached and a deposit of water (or ice) is formed. The saturated vapor pressure at the deposit temperature is equal to the partial pressure of the water vapor in the air passing over the deposit. This technique represents a fundamental measurement of the dewpoint temperature, which corresponds to the temperature at which condensation occurs. In temperature regimes falling below the standard freezing point (0C), the measured temperature actually represents the frost point. These values are converted back into equivalent dewpoint temperatures during data processing before any additional moisture calculations are performed.

The dewpointer employs Peltier thermoelectric junctions to control the temperature of its sensing mirror. The sensing mirror is in close thermal contact but electrically isolated from the Peltier thermoelectric junctions used for cooling and heating. The junctions are used to pump heat to and from the mirror and thus change the module (mirror and junction) temperature. As the mirror temperature reaches the dew (or frost) point, condensate forms on the mirror surface causing the reflective characteristics of the mirror to change. This change is detected by photo-resistors in the optical sensing bridge and converted to an electrical signal driving an amplifier whose output signal is fed back into the cooler and thus stabilizes the mirror temperature at a particular dew or frost layer thickness. The mirror temperature, which is measured with a platinum resistance thermometer, is taken to be the dewpoint temperature.

The manufacturer installs platinum thermometers in the mirror assemblies. The factory level calibration then consists of checking each system with a standard hygrometer calibration unit which is traceable to the gravimetric humidity standard of the National Bureau of Standards. RAF uses this calibration (C/ohm) to generate a system calibration based on simulated resistance changes in the sensing circuit. Calibrations are performed both before and after each project and are normally completed within a few days of the operations period. In addition, a second complete and collocated EG&G system is always included in every instrument package for a comparative analysis.

Sensor Output and Specifications

a) general information

Manufacturer: EG&G
RAF Resource Person(s): Allen Schanot, Bruce Morley

b) primary output

Parameter names: DPBC, DPTC
Plain language names: dewpoint temperature-thermoelectric bottom/top
Units: C
Accuracy: $\pm 0.5\text{C}$ (at dewpoint temperatures above 0C)
 $\pm 1.0\text{C}$ (at dewpoint temperatures below 0C)
Range: -50 to +50C
Response: varies from 2 sec in humid conditions to in excess of 20 sec at dewpoint depressions larger than 20C

Data Interpretation

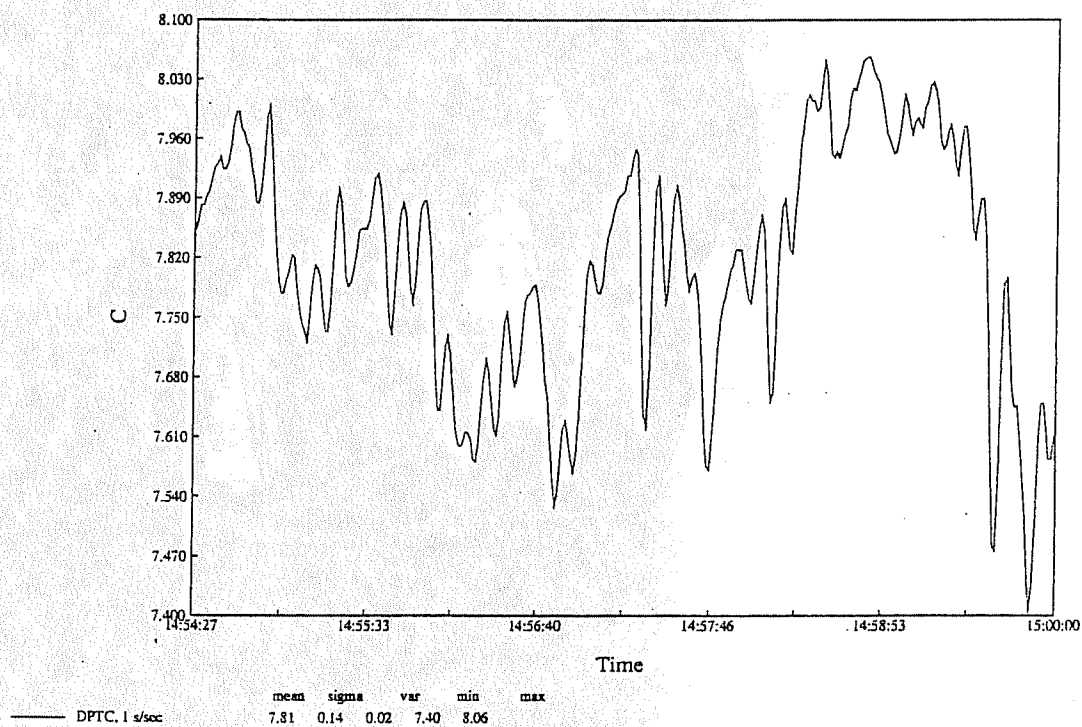
As a general rule, the dewpoint hygrometer has difficulty maintaining dewpoint depressions in excess of 20 to 25C (RH<10%). Figure 1.2 is an example of dewpoint measurements from this sensor.



Figure 1.1 — Standard Dewpointer

BOREAS - 818, Flight #20

9/3/1994 , 14:54:27-15:00:00



An example of dewpoint measurements from the standard dewpointer

Figure 1.2

Lyman-Alpha Hygrometer

Introduction

This instrument provides fast-response, high resolution measurements of humidity by monitoring emission in the lyman-alpha band of hydrogen atoms. A photograph is shown in Figure 1.3.

Operating Principles

The Lyman-alpha hygrometer was designed and built by NCAR to provide fast response, high resolution measurements of humidity. Lyman-alpha radiation is emitted by hydrogen atoms at a narrow line in the far ultraviolet portion of the spectrum (121.56 nanometers). It is produced by an electrical discharge in hydrogen. As the Lyman-alpha radiation passes across the sensing chamber, it is partially absorbed by atmospheric water vapor. An increase in absolute humidity results in increased absorption by the water vapor thus decreasing the detected signal. This signal change follows Beer's law such that:

$$I = I_0 \exp(-kxp/p_0)$$

where I = received signal; x = path length; I_0 = transmitted signal; k = absorption coefficient; p = concentration of water in the sensing volume; and p_0 = concentration of water vapor at standard temperature and pressure.

With I_0 , k , x , and p_0 being intrinsic properties of the system, the received signal provides a direct measure of water content within the sample volume.

In actual practice, liquid water, oxygen, and ozone will also absorb significant amounts of Lyman-alpha radiation and thus attenuate the received signal. Under the proper operating conditions, however, oxygen makes only a weak to moderate contribution to total absorption and its effects can be removed using measurements of temperature and pressure to calculate the fractional oxygen density. Ozone absorption does represent a true interferant but only becomes significant at extremely high altitudes (stratosphere) where the natural ozone concentrations routinely reach significant levels. Liquid water on the other hand, is often encountered at operational altitudes and its presence in the sampling chamber can result in a film of water forming on the window surfaces. Measurements made under these conditions are highly suspect and represent the basic limitation of this technique.

Due to the similarity from source to source, the calibration coefficients will only vary by about 6 percent on average. Sensor response is determined on a pre and post project basis using gases with known absorption characteristics at the Lyman-alpha wavelength. Response corrections are applied through the use of an equivalent sampling path length which covers collimation effects as well as source or detector changes. Any minor adjustments are made through the loose couple data processing procedure that references the Lyman-alpha response against the dewpointer units.

Sensor Output and Specifications

a) general information

Manufacturer: NCAR/RAF
 RAF Resource Person(s): Allen Schanot, Bruce Morley

b) primary output

Parameter names: MRLA, MRLA1, RHOLA, RHOLA1
 Plain language names: mixing ratio, Lyman-Alpha
 absolute humidity, Lyman-Alpha
 Units: g/kg, g/m³
 Accuracy: ±4% for relative humidity
 ±0.6C for dewpoint
 Range: 0.5 to 25 g/m³ absolute humidity
 Response: 2ms

Data Interpretation

In its current configuration the Lyman-alpha hygrometer is not an absolute, stand-alone system for airborne use (Friehe and Grossman, 1986; Spyers-Duran and Schanot, 1987). There is some drift inherent in the system which results in flight-to-flight and in-flight deviations of the mean humidity baseline derived from the Lyman-alpha measurements. In order to obtain a true absolute humidity, it is necessary to process the Lyman-alpha data in conjunction with the mean humidity data available from the more stable EG&G units. This processing technique loosely couples the two systems, removing baseline drift while not affecting the high-rate fluctuations. Although the coupling process continues to be effective through the full range of measurements, the drift in the instrument's response increases at the higher altitudes. The baseline drift adjustments soon approach the absolute value of the mean ambient humidity and therefore make the Lyman-alpha of limited use for low humidity, high altitude applications (Spyers-Duran, Schanot, 1987). Low level boundary layer applications provide much better data, with typical drift errors limited to approximately ±10%.

Figure 1.4 gives an example of mixing ratio data from this sensor.

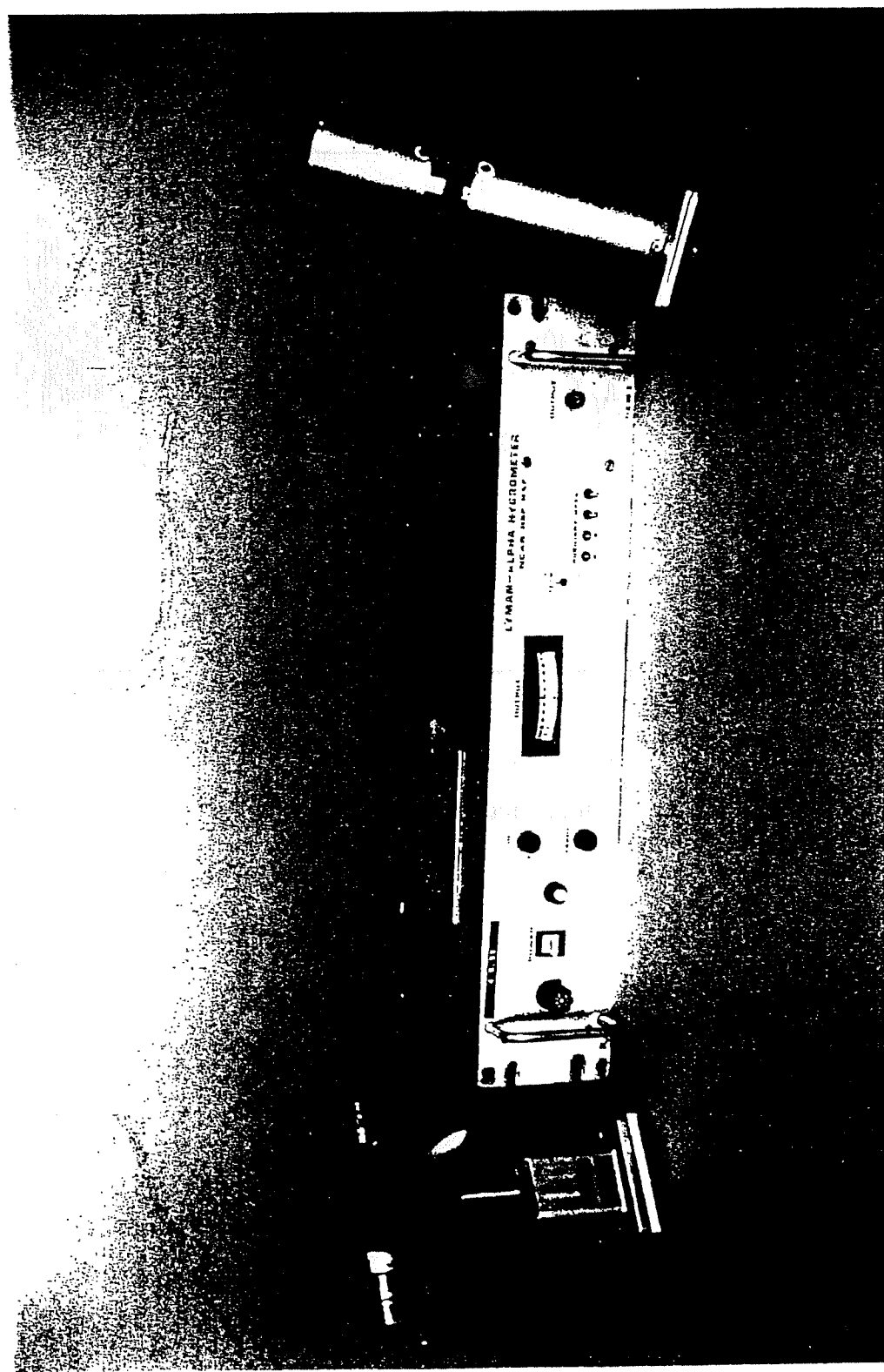
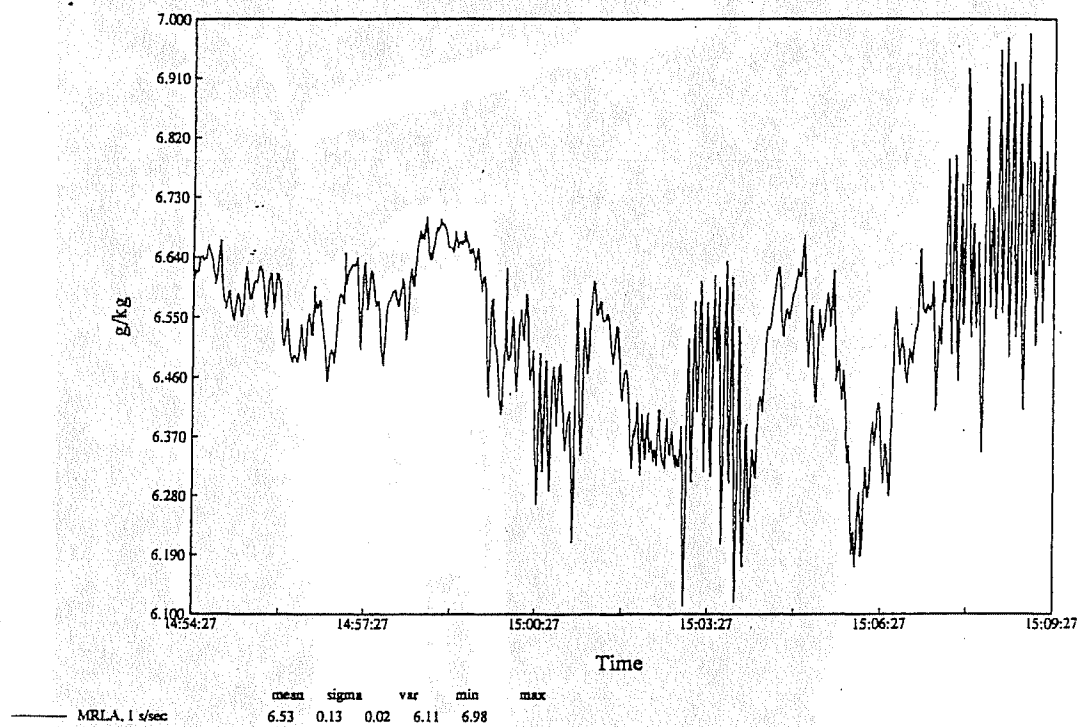


Figure 1.3 — Lyman-Alpha Hygrometer

BOREAS - 818, Flight #20

9/3/1994, 14:54:27-15:09:27



An example of mixing ratio data from the Lyman-Alpha hygrometer

Figure 1.4

Cryogenic Frost-Point Hygrometer

Introduction

This instrument addresses the need for measurements of low humidities in the middle to high troposphere and the lower stratosphere. It uses a mirror disk maintained at a temperature (dew or frost-point temperature) where a mass of condensate is stabilized. In the higher troposphere and lower stratosphere, the mirror condensate is always in the ice phase. Therefore, in the following discussions, the measured equilibrium temperature is referred to as the frost-point temperature. A photograph of the Frost-Point Hygrometer is shown in Figure 1.5

Operating Principles

The operation of this hygrometer is based on the fact that an equilibrium exists between the water vapor pressure in the air and over a water or ice surface at the dew or frost-point temperature. Mass transport will be away from the surface if the surface is above the equilibrium temperature, and mass transport will be to that surface if the surface temperature is lower than equilibrium. By monitoring the mass condensate, a feedback system can be used to control the surface at the equilibrium temperature.

This instrument is a chilled-mirror, condensation-type hygrometer that uses optical detectors for condensate sensing. The mirrors, optics, and electrical circuit make up a thermo-optical servo system, which maintains a condensate equilibrium at the frost-point temperature. The unique feature of the cryogenic hygrometer is the use of liquid nitrogen coolant as a heat-sink. The mirror temperature can then be changed rapidly, using electrical heating. It is this feature that allows the instrument to respond rapidly and maintain the required large dew-point depressions.

Sensor Output and Specifications

a) general information

Manufacturer: NCAR/RAF
RAF resource person(s): Allen Schanot

b) primary output

Parameter names:	CRHP, FPCR
Plain language names:	cryogenic sensing chamber pressure; cryogenic frostpoint temperature (uncorrected)
Frost-point range:	~-10 to -100C
Depression capability:	~106C
Thermistor calibration accuracy:	$\pm 0.13C$
Frost-point measurement uncertainty:	$\pm 0.43C$
Coolant load (LN_2):	2l
Operation time (for 2l LN_2 load):	3.5 h
Slew rate for heating:	$\sim 14C\ s^{-1}$
Slew rate for cooling:	$\sim 7C\ s^{-1}$
Response time:	2 s

Sample air trans. Time (from inlet to sensing): 0.1s (as flown on the NCAR Sabreliner)

Material (from inlet to sensing): stainless steel

Instrument Weight: 14 kg

Pump weight: 7.7 kg

c) derived parameters

RAF parameter names: FPCRC, DPCRC, CMRCR, RHOCR

Plain language names: Cryogenic frostpoint temperature; cryogenic dewpoint temperature; cryogenic mixing ratio, cryogenic absolute humidity

Data Interpretation

To calculate the frost-point temperature, a cubic spline approximation is used to convert the thermistor resistance to a frost-point temperature. By using functional relationships of the Goff-Gratch (1946) formulation, the ambient saturation vapor pressure can be characterized by either the ambient dew-point or frost-point temperature. During these calculations, the saturation vapor is corrected for the pressure measurements inside the cavity by using an iterative numerical technique (Newton's method). A graphical schematic shows this process in Figure 1.6.

It is important to understand the various factors which might limit the accuracy of the measurements. Any deviation of the mirror temperature from the frost-point temperature will affect the water vapor calculations. To establish accuracy, the first step is to characterize the parameters of this instrument in the laboratory under controlled conditions. The mirror thermistor calibration is accomplished by using a special calibrator block. The thermistor's change in resistance over the operating temperature range is non-linear; therefore, a non-precise fit to the temperature-resistance data will introduce measurement errors.

During field operations, the pressure in the instrument cavity is measured, to correct differences from ambient valued. A possible source of error that can affect the measurement accuracy is leakage of cabin air into the sensing cavity. Moisture evaporation from the outside surface of the aircraft can also affect the measurements. This instrument was designed to minimize these effects.

Figure 1.7 shows a vertical profile of dewpoint temperature measured with this sensor.

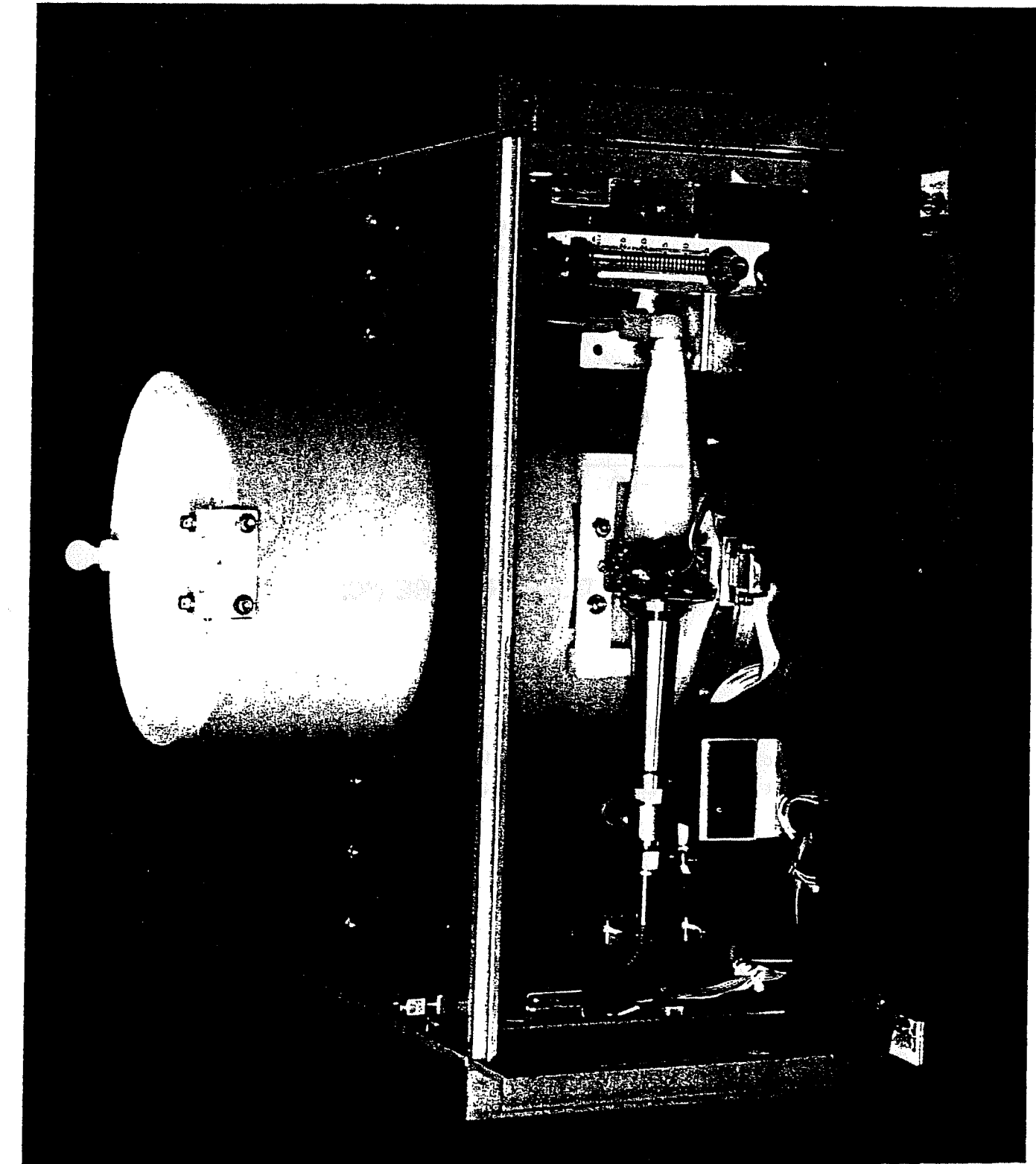


Figure 1.5—Cryogenic Frost-Point Hygrometer

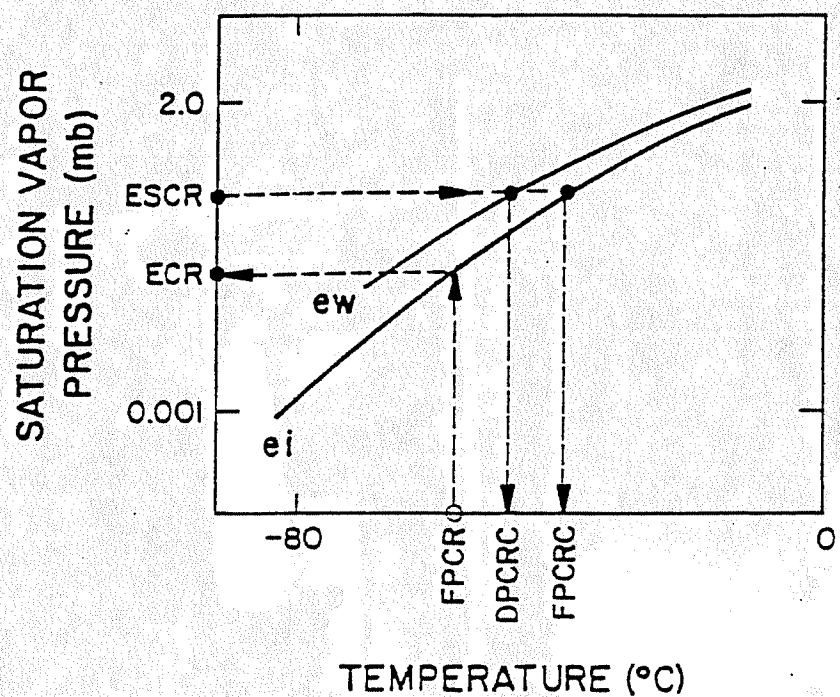


Figure 1.6—A graphical schematic depicts the flow of calculations to determine the ambient dew- or frost-point temperatures. The curve e_i is the saturation vapor pressure with respect to ice, and the curve for e_w is the saturation vapor pressure with respect to a plane water surface.

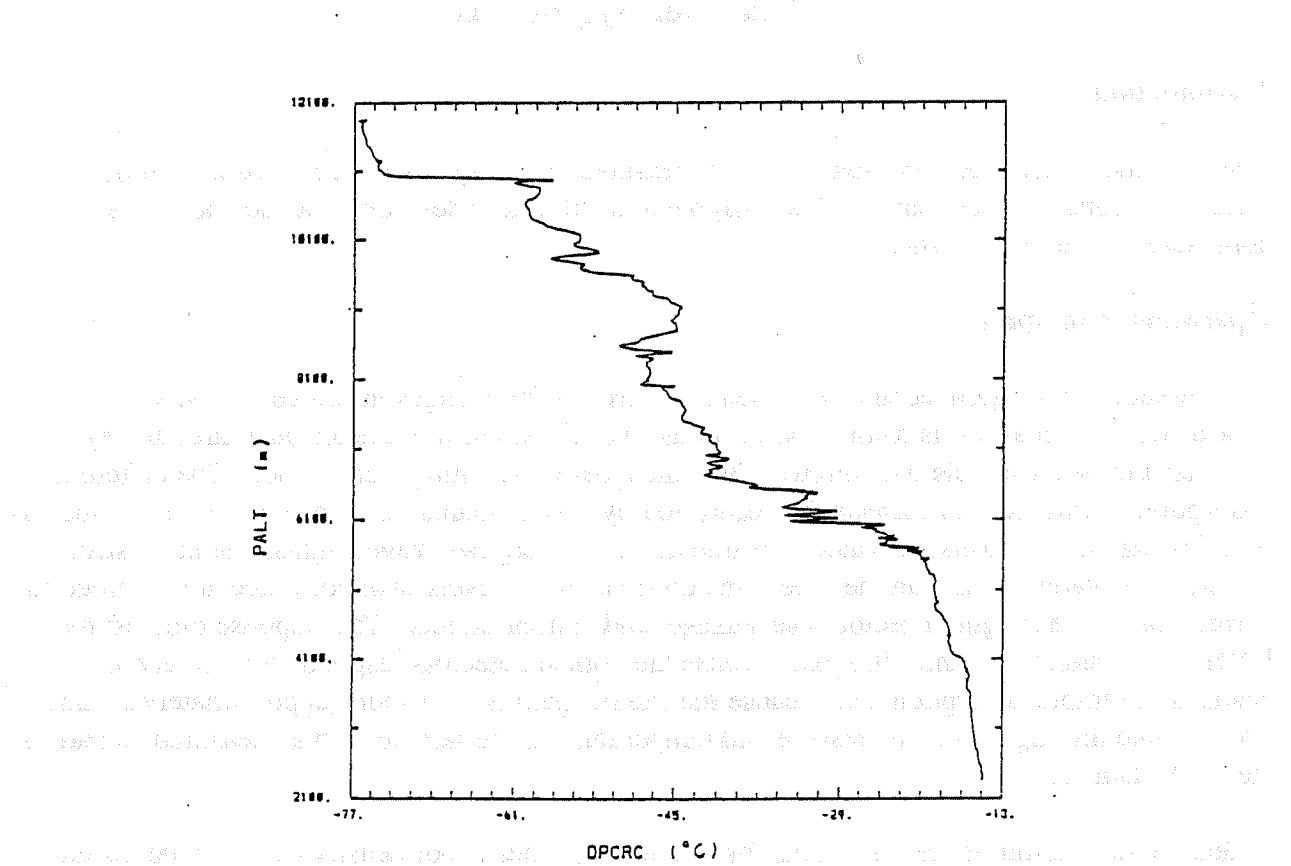


Figure 1.7—A vertical profile of dew point temperatures measured over SE Wyoming on September 18, 1990. The dewpoint (DPCRC-°C) is plotted against the pressure altitude (PALT-m).

Ultraviolet Hygrometer

Introduction

The airborne ultraviolet hygrometer (UVH) measures humidity based on the absorption of ultraviolet light by water vapor. This instrument is still under development and should be considered to be experimental.

Operating Principles

A differential absorption technique is used that corrects for changes in source intensity by measuring the signal levels from a source along two paths, one a reference path through dry nitrogen and one a sample path through the atmosphere containing water vapor. The differential absorption technique also corrects for absorption by contaminants other than water vapor, such as liquid water, salt deposits, or window degradation, by using two wavelengths, one more strongly absorbed by water vapor than the other. In addition, signal levels with no source are recorded to correct for ambient light, detector base leakage, and similar effects. The response time of the UVH is very short (less than 100 ms) because the optical detectors respond very rapidly to changes in sample absorption and because the sample path is very short (approximately 2 mm). To calculate mixing ratio, the pressure and temperature in the sample path is measured as part of the UVH data set.

A detailed derivation of the algorithms for calculating water vapor density from the measured signal levels is given in Weinheimer and Schwiesow (1992). In summary form, the water vapor mixing ratio is derived using four output signals and five calibration coefficients. Four of the five coefficients (C_1, C_3, C_4, C_5) depend on combinations of physical constants and can be derived theoretically. The fifth coefficient (C_2) depends on lamp outputs, detector sensitivity, and various other optical parameters. It is a dimensionless ratio determined experimentally.

The original plans for the instrument called for the determination of C_2 via a Licor dewpoint generator. However, the optical detectors used in the instrument proved to be less reliable than expected. Each detector exchange results in a new value for C_2 . For data processing purposes, the value of C_2 is determined through extensive data comparisons of UVH response with the designated reference dewpoint hygrometer. Unexpectedly, the instrument also demonstrates a small amount of in-flight baseline drift, ala the Lyman-alpha hygrometer. Like the lyman-alpha data processing, the UVH data need to be base lined against the reference hygrometer using the NCAR "Loose Couple" technique. The cause for this drift is under investigation.

Sensor Output and Specifications

a) general information

Manufacturer: NCAR/RAF
RAF Resource Person(s): Bruce Gandrud

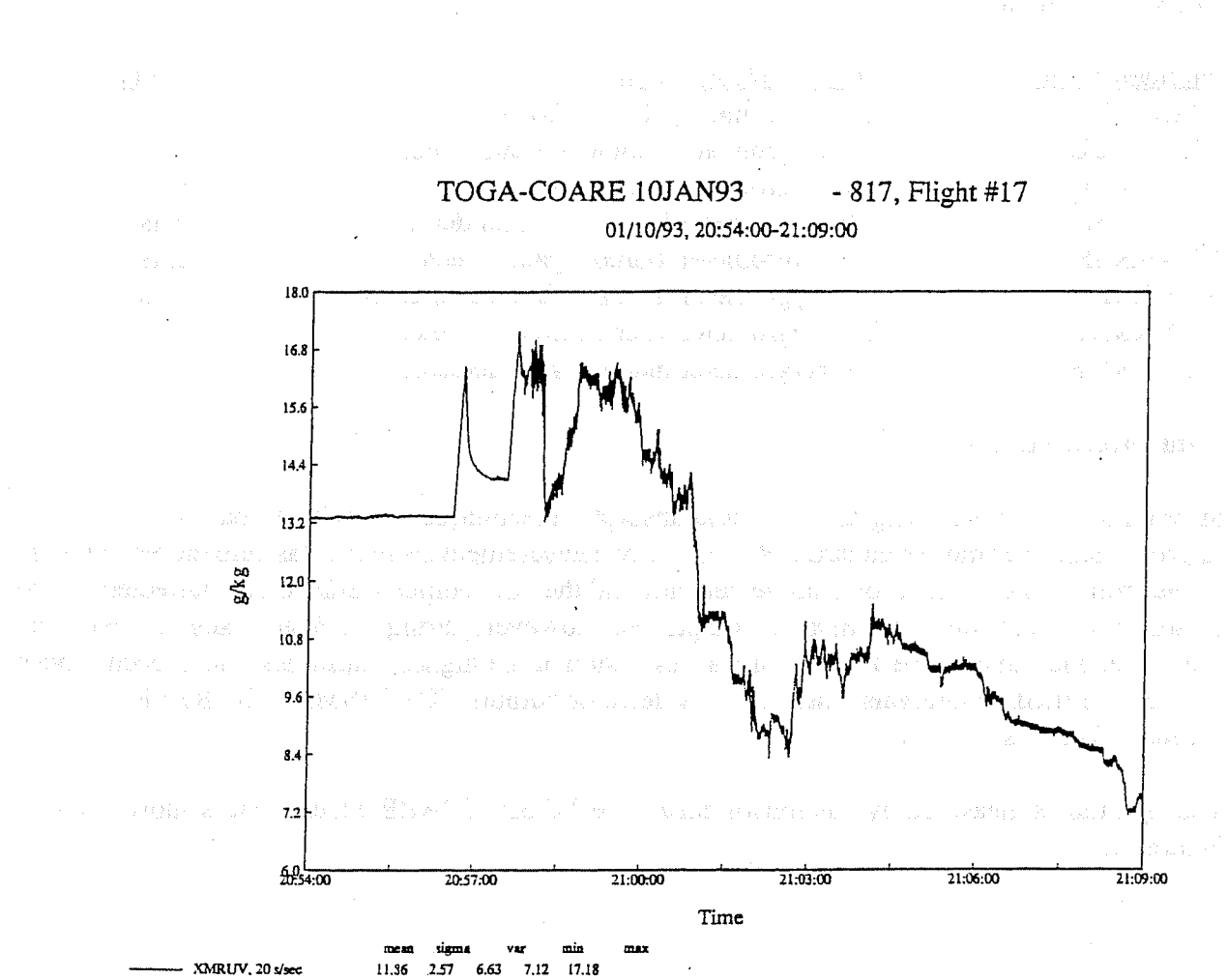
b) primary output

<u>Parameter Name</u>	<u>Plain Language Name</u>	<u>Units</u>
XMRUV	UV Hygrometer Mixing Ratio	g/kg
XUVTVOL	UV Hygrometer sample volume temp.	C
XUVPVOL	UV Hygrometer sample volume pres.	mb
XUVCHSP	UV Hygrometer lamp-off signal detector	cnts
XUVKRSP	UV Hygrometer klamp signal detector	cnts
XUVHREF	UV Hygrometer hlamp reference detector	cnts
XUVKRRF	UV Hygrometer klamp reference detector	cnts
XUVHSMP	UV Hygrometer hlamp signal detector	cnts

Data Interpretation

In general the two wavelength, differential absorption technique shows potential for improvement over more standard HRT humidity measurement systems. Instrument response is stable from flight to flight for a single detector and the data output seems to be unaffected by the presence of liquid water during the cloud passes. However, during the final stages of a detector's life cycle, one can observe a loss of signal resolution at the higher humidities. Such occurrences can be identified by intervals where the raw detector outputs (XUVHSMP, XUVKRSP) fall below 100 counts.

Mixing ratio as measured by this sensor during the TOGA-COARE experiment is shown in Figure 1.8.



Mixing ratio as measured by the ultraviolet hygrometer

Figure 1.8

OPHIR-III Radiometric Temperature

Introduction

The Ophir-III thermometer measures the temperature radiometrically by sensing the spectral radiance of CO₂ and determining the corresponding temperature of the emitting gas. The instrument is pictured in Figure 1.9.

Operating Procedures

The instrument operates at a wavelength of 4.255 μ m, where CO₂ is a strong emitter/absorber via vibrational/rotational transitions, and the sensed volume is a column extending about 10 m from the aircraft. The spectral radiance [power/(area*steradian*wavelength)] is a function of wavelength and the temperature of the CO₂ in this column of air. A thermo-electric cooler detector alternately "sees" infrared emissions from the atmosphere and a near ambient temperature reference blackbody as a highly reflective gold plated chopper wheel intersects the beam. Output from the detector is an electrical signal in the form of a sine-wave with peak-to-peak amplitude proportional to the difference in the radiative emissions of the atmosphere and the blackbody. Using a direct measurement of the blackbody temperature together with the detector amplitude and Planck's law of thermal radiation, a calculation of the ambient temperature is performed.

The calibration process for the Ophir-III is comprised of two parts. First of all, the calibration coefficients for the reference blackbody temperature sensor have to be established. Ophir uses an AD590 sensor for this purpose due to its excellent stability, long lifetime and broad dynamic range. The coefficients used in the processing are obtained directly from Ophir. The second part of the calibration process is more difficult. The instrument's response must be determined against a known target temperature, over the operational temperature range of the instrument. This portion of the calibration is completed through extensive data comparisons against the on-board reference temperature sensor (Rosemount Model- 102). Due to the potential errors in the reference temperature during cloud penetrations, only clear air data are used in the comparison process. Subtle flight-to-flight differences are common in these comparisons and lead to separate least square curve fits for each flight. More detailed information on the data processing will be made available on request.

Sensor Output and Specifications

a) general information

Manufacturer: Ophir
RAF Resource Person(s): Mike Spowart, Darrel Baumgardner

b) primary output

Parameter names:	XATO; XODS; OPHBBC
Plain language names:	1 Hz ambient temperature; high rate ambient temperature; blackbody reference temperature
Units:	C
Accuracy:	$\pm 1C$

Data Interpretation

In general, the Ophir instrument performs very well. In cloud temperature measurements will be of interest since the Ophir output is unaffected by the presence of liquid water in the sample volume. For clear air measurements, however, the standard reference temperature sensor is still the best source of data. The large range of ambient temperatures encountered during a typical research flight still cause some problems in the accuracy of the Ophir measurements over certain portions of a flight. For detailed analyses of short flight segments, Users may want to apply a separate baseline correction to the output values (XATO).

A segment of data from the TOGA-COARE experiment is shown in Figures 1.10 and 1.11. Plots of droplet concentrations (Figure 1.10) show that the aircraft was in a cloud between 0051 and 0057 UTC. Figure 1.11 shows corresponding temperature measurements from the RAF standard hot-wire device and from the OPHIR sensor. The temperature measurements show good agreement, except during the cloud penetrations. Wetting of the hot-wire system and subsequent evaporative cooling cause inaccurate temperature measurements, so the OPHIR measurements is more reliable in clouds.

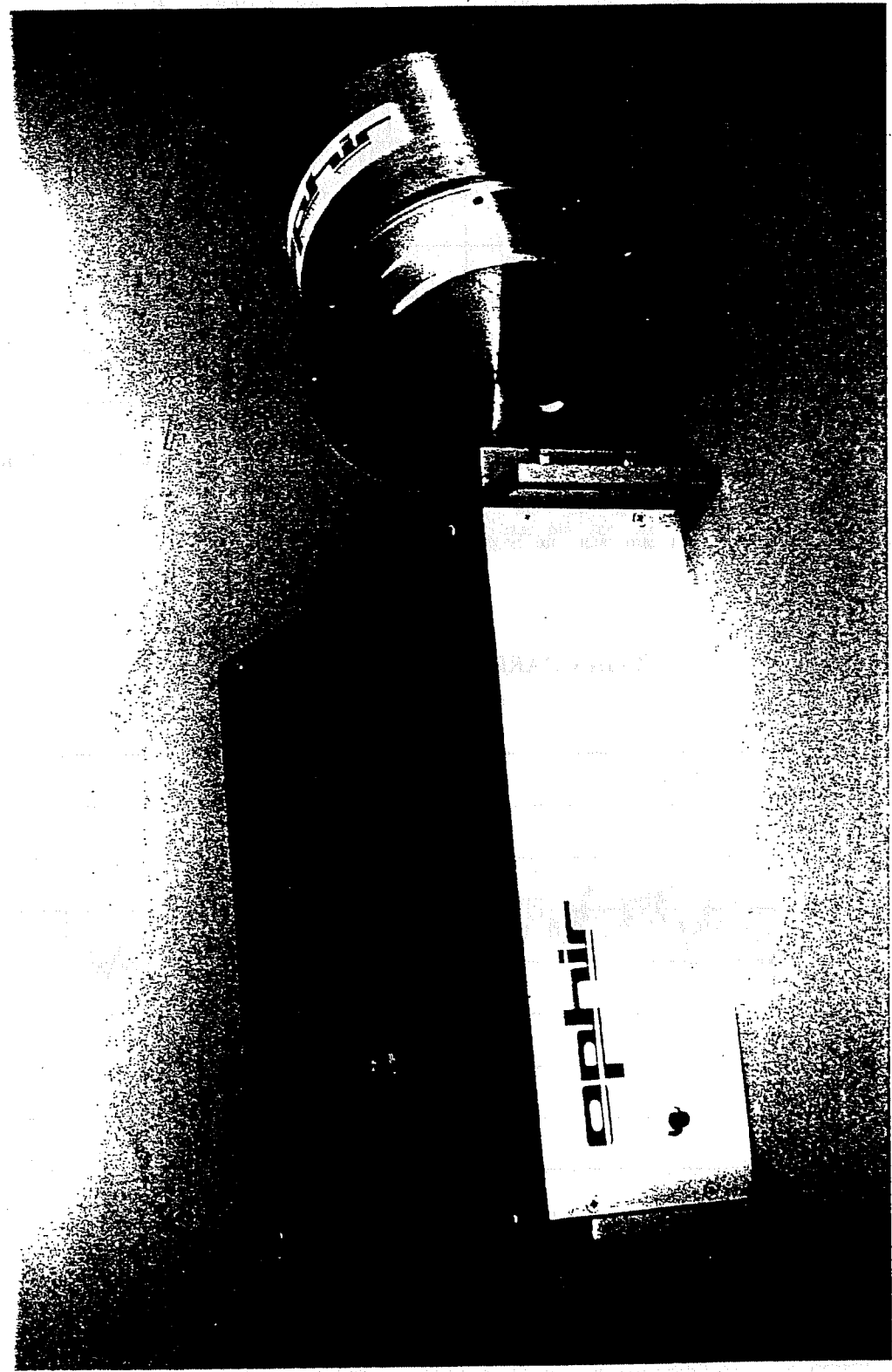


Figure 1.9—OPHIR-III Radiometric Temperature

02/18/93, 24:45:00-25:00:00

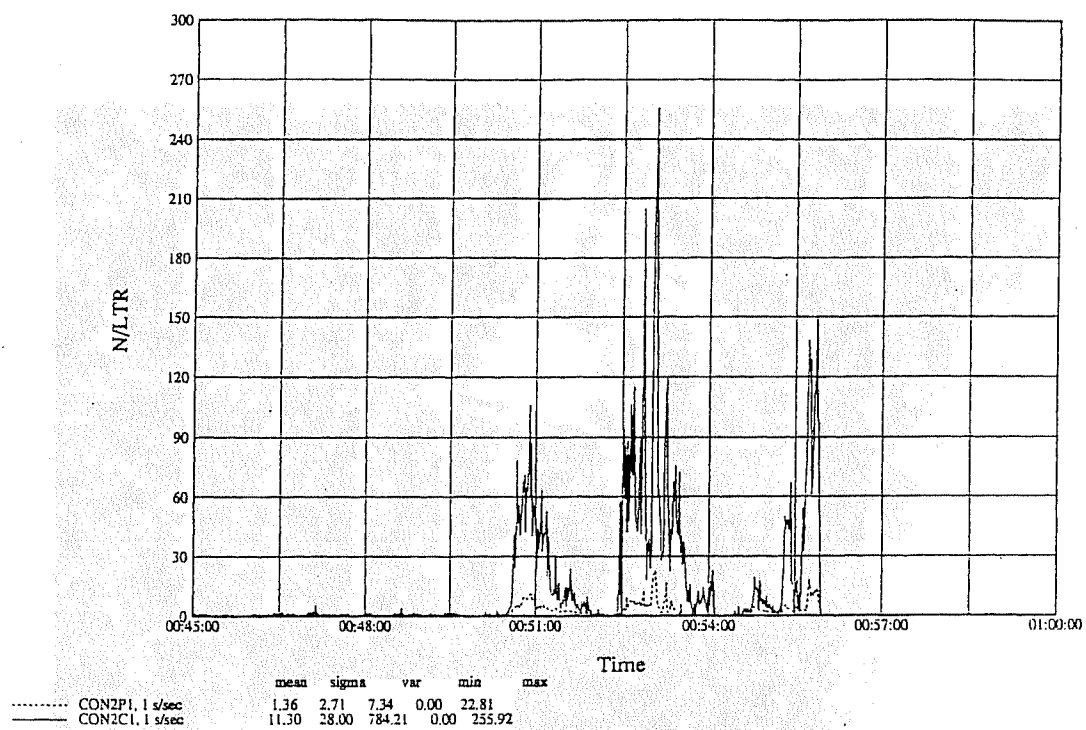


Figure 1.10

02/18/93, 24:45:00-25:00:00

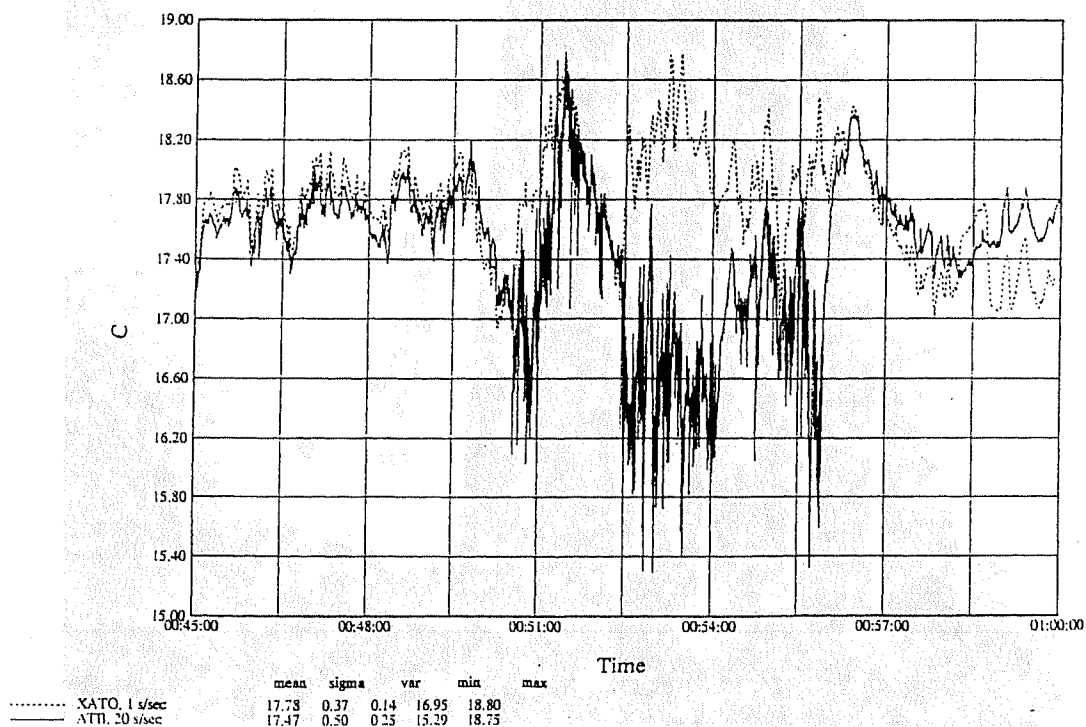


Figure 1.11

Segments of OPHIR-III data
from the TOGA-COARE Experiment

SECTION 2—Air Motion Sensors

Air Motion and Aircraft Position

Introduction

The air motion system is used to measure the mean wind velocity and direction and turbulence spectra and co-spectra. Vertical and horizontal fluxes of momentum and scalar quantities such as chemical constituents and state variables can be calculated from these measurements. The air motion system is comprised of several subsystems: a "radome" gust probe; an inertial reference unit (IRS); and a global positioning system (GPS). The gust probe uses differential pressure measurements from flush mounted ports in the aircraft nose radome to determine the incident angles (attack and sideslip) of the wind, i.e. the angle of the wind relative to the aircraft. This is the resultant of the aircraft's motion through the atmosphere and the atmospheric wind.

The IRS uses three orthogonally arranged gyros (laser solid state gyros in the NCAR aircraft) and accelerometers to measure the aircraft's position relative to the earth (latitude, longitude, altitude, and attitude) and velocity vector. Calculations combining measurements from the gust probe and the IRS give the three dimensional wind vector relative to the earth reference frame. The IRS is subject to unavoidable errors due to dynamic maneuvers of the aircraft and drift resulting from less than perfect initial alignment with the earth's reference frame and local gravity. These slowly varying errors can be largely removed by using the absolute accuracy of the GPS as a reference. The GPS is a highly accurate navigation system, externally updated once per second, using a constellation of orbiting satellites to determine the aircraft position and velocity.

Operating Principles

Inertial System

Mean horizontal wind calculations have always been an essential part of aircraft navigation. With the introduction of Inertial Navigation Systems highly accurate determination of the aircraft position, velocity and attitude have been possible. Faster and smaller digital computers have allowed inertial systems to sample the physical transducers (gyros and accelerometers) at higher input rates and produce calibrated outputs at higher rates (up to 50 HZ for RAF IRS's). Earlier inertial systems consisted of a stable platform that was aligned to local horizontal and kept in alignment as the aircraft moved over the earth with electromagnetic "torquers". The motion of the aircraft relative to the platform was measured by resolvers sensing the rotation of the gimbals and three orthogonal accelerometers measured the acceleration. These mechanical systems are being replaced by systems using solid state "ring laser" gyros. These systems are used as "strapdown" down systems, meaning that there is no gimbaled platform. The rotation of the aircraft is sensed by the laser gyros and the software program resolves the acceleration and angles. Laser strapdown systems are not inherently more accurate than the mechanical systems, however, they are more reliable and less complex due to fewer moving parts. They are subject to the same of the same errors as mechanical systems such as schuler oscillation and accelerometer drift and bias.

Ideally the inertial system cluster of gyros and accelerometers are collocated with the gust probe and perfectly aligned to the same axes. On the RAF aircraft the inertial systems are rigidly mounted to the aircraft structure near the center of gravity and the location of the system relative to the gust probe is precisely measured so position corrections can be applied. Non-rigid mechanical coupling of the gust probe and the inertial system (relative motion due to the bending and twisting of the airframe) and less than perfect alignment between the gust and inertial systems account for small dynamic and static errors. (For a more detailed discussion of Inertial Navigation Systems, see Kayton, 1969, Broxmeyer, 1964, and Lenschow, 1986.) The RAF currently uses Inertial Reference Systems (IRS) instead of Inertial Navigation Systems (INS), the hardware is the same the distinction being that the IRS does not provide the software interface that calculates navigation functions for the aircraft.)

Gust Probe

All of the RAF aircraft use a five hole differential pressure gust probe installed in the nose radome. Five small (~ 0.6 cm) holes are drilled in the tip of the radome arranged in a cruciform pattern. The five holes are arranged symmetrically with respect to the center hole which is located near the stagnation point of the airflow around the nose of the aircraft. The alignment of the holes is referenced to the vertical stabilizer and wings with a transit. A differential pressure probe is connected between the two outer holes in the lateral axis to measure the sideslip angle and another between the outer holes in the vertical plane to measure the attack angle. A third differential pressure transducer is connected between the center hole and the static pressure ports located further back on the aircraft fuselage to give a measurement of the dynamic pressure at the radome. The angles of attack (α) and sideslip (β) are the flow angles of the air with respect to the longitudinal axis of the aircraft in the vertical and lateral directions, respectively (see Figure 2.1). The attack and sideslip angles and the true airspeed, which is calculated from the dynamic pressure, air temperature and static pressure, define the wind (gust) velocity vector relative to the aircraft.

Traditionally, incident angles have been measured with various types of gust probe transducers mounted on booms that physically extend the point of measurement beyond the aircraft disturbed flow field (~ 1.5 fuselage diameters ahead of the aircraft). The radome gust probe technique measures the pressure distribution on the nose of the aircraft. This technique has the advantage of simplicity, elimination of boom vibration, and allows for a nose mounted radar that can "see" through the fiberglass radome but would be distorted by a metal boom structure. Distortion of the velocity field by the aircraft body alters the pressure field on the surface of the radome and by measuring this altered pressure field we can infer the undistorted velocity field away from the aircraft. Using potential flow theory for flow around a sphere it can be shown that the equation

$$\alpha = \frac{\Delta P}{kQ_c}$$

for determining the incident angles is

OR

$$\beta = \frac{\Delta P}{kQ_c}$$

al. 1983 for details of the derivation). In the above equation ΔP is the differential pressure measured across attack or sideslip angle holes in the radome, Q_c is the dynamic pressure measured at the radome center hole and k is a sensitivity factor determined from in-flight calibration maneuvers ($k \sim 0.079 \text{ deg}^{-1}$ for Mach number < 0.55). Theory shows that the radome gust system is capable of measuring mean winds and turbulent eddies to a scale approximating the diameter of the aircraft fuselage (~ 4 to 5 meters). Smaller scales would be distorted by "blocking" by the fuselage.

Both the Electra and the C-130 have heated radomes to prevent the build up of ice which will distort the distribution around the pressure ports or completely close off the ports. Water can enter the ports when flying in precipitation and there are drain lines located inside of the radome that keep ingested water from blocking the pressure lines.

Global Positioning System (GPS)

The GPS is a constellation of 21 satellites in six circular orbital planes at an altitude of 20,200 km. The satellites are arranged so that there will always be at least four satellites above 5 degrees elevation for an aircraft near the earth's surface. Four satellites are needed to determine an independent three dimensional position of the aircraft. Multichannel receivers are used on the RAF aircraft so that several satellites can be tracked simultaneously without interruption. A multichannel receiver allows for 1 second updates without loss of data in high dynamic situations. Highly accurate satellite ephemeris and clock data are received by the on-board system in the navigation message sent from the satellites and this is transformed into aircraft three dimensional position and ground speed. The GPS is managed by the Department of Defense and, for reasons of national security, it has deliberately degraded the system by adding errors to the clock and ephemeris data. The resulting accuracies are 100 meters in the horizontal and 140 meters in the vertical (3 standard deviations). (see Forssell, 1991).

The RAF uses the uses the GPS information to correct the IRS position and ground speed drift and bias errors. (See Leach, et al., 1991, for a discussion of a correction algorithm using Kalman filtering techniques.)

Air Motion System

The combination of the three subsystems described above comprises the air motion system. The primary output is the aircraft position and the u, v, and w wind components. Fluxes may be calculated from these components and other scalar quantities recorded on the RAF data system (ADS) because time offsets have been removed.

Error analysis of the entire system is extremely complex and it would serve no useful purpose to present it here. They are detailed by Brown et al (1993). The primary errors result from physical misalignment of system components, drift and bias offsets, airflow distortion around the sensors and time phasing offsets primarily between the gust probe and the IRS. Data analyses have shown that the various system components have different contributions to the spectral content of the wind dependent upon the frequency range considered. The same is true of the error sources. For the "mean" winds ($< .05 \text{ Hz}$) IRS measurements and the true airspeed (TAS) dominate and drift, offsets and calibration errors are largest. In the range $> .05 \text{ Hz}$ and $< 2 \text{ hz}$, contributions of the IRS, TAS and gust probe are approximately balanced with the IRS becoming less important near the higher frequency. Above 2 Hz the gust probe and TAS are dominate and the IRS has

little influence due to the aircraft inertia filtering out the high frequency aircraft motions. (For an in depth discussion of derivation of the air motion equations see Lenschow, 1986.)

Air Motion System Output and Specifications

Inertial Reference System

Honeywell Laseref SM IRS. Laser gyro, strapdown, inertial reference system.

Primary outputs: Ground speed, north/south (VNS), east/west (VEW); Attitude angles, pitch (PITCH), roll (ROLL), true heading/yaw (THDG); aircraft vertical velocity (VSPD); position, latitude (LAT), longitude (LON), inertial altitude (ALT).

Accuracies/resolution/units: Ground speed, .51/.06/m/sec; Attitude angles, pitch, roll, .05/.01/degrees, heading .2/.01/degrees; position, .41(m/sec/hr of flight)/.06/m/sec; vertical velocity, 0.15/.005/m/sec; inertial altitude, 1.52/0.30/m (inertial system only, requires pressure altitude and aircraft altitude input).

Calibration: Initial calibration is performed by manufacturer. Scale factors, calibration coefficients, are entered in the operational software. Alignment on aircraft is performed at JeffCo using a theodolite and leveling the aircraft.

RAF Resource Person(s): Don Lenschow, Dick Friesen

Gust Probe system

Radome: All RAF aircraft have the five hole differential system in a fiberglass radome. The aircraft radomes have limited spherical geometry and the holes are positioned at 33 degrees with respect to the longitudinal axis. (Maximum theoretical sensitivity is at 45 degrees. The resultant loss of sensitivity is ~ 8%).

Pressure transducers: Three differential pressure transducers are mounted in the nose for measuring the attack differential pressure (ADIFR), sideslip differential pressure (BDIFR), and radome dynamic pressure (QCR). An absolute pressure transducer is used to measure the static pressure (PSFD) from ports on the fuselage. QCR is the difference between the pressure at the center hole of the radome and PSFD. ADIFR is the difference between the top and bottom differential pressure, Rosemount 1221 F1vl, 2 psid absolute pressure, Rosemount 1501, psia

Calibration: In-house with a dead weight standard traceable to NIST standard.

RAF Resource Person(s): Dick Friesen, Don Lenschow, Dave MacFarland

Global Positioning System (GPS)

GPS receiver: Trimble Navigation TANS, 6-Channel GPS receiver.

Primary outputs: Three dimensional position; Latitude (GLAT), Longitude (GLON), altitude (GALT); aircraft ground speed; east/west (GVEW), north/south (GVNS), vertical velocity (GVZI).

Accuracy: Position, 100 meters with selective availability (SA) enabled, 25 meters without (horizontal), 140 meters with SA, vertical; velocity, 0.02 meters/second without SA and steady state (non-maneuvering). These are manufacturers specifications unverified by RAF.

Calibration: Self-calibration. Depends on satellite ephemeris and clock.

RAF Resource Person(s): Dick Friesen

Derived Outputs for Air Motion System

Derived outputs for the air motion system are primarily a three dimensional wind vector. The RAF computes these in the geographic reference frame and the aircraft reference coordinates.

Geographic: East/west component of windspeed, VEW; North/south, VNS; Wind direction, WD; Total (resultant) windspeed, WS

Aircraft components: Latitudinal component of windspeed, VY; Longitudinal, UX.

Vertical wind velocity, WI, is the same in both coordinates.
GPS corrected winds have a "C" appended to the

mnemonic: VEWC, VNSC, WDC, WSC, VYC, UXC, WIC.

Processing dependencies: parameters necessary to derive winds are: true airspeed, TAS; angles of attack and sideslip, ATTACK, SIDESLIP; aircraft ground speed, VNS, VEW; aircraft vertical velocity, VSPD; pressure altitude, PALT; aircraft attitude angles, ROLL, PITCH, THDG (true heading).

Accuracy: The RAF states a nominal accuracy of mean winds (<1Hz) of 1.0 meter/sec. The primary sources of error are drift in the IRS and true airspeed uncertainty. The RAF specifies the error as $1.0 \text{ meters/sec} + 0.5t$, where t is the time in hours from start of flight, to account for the IRS drift(see RAF Bulletin #23). This assumes the worst case manufacturer's specification. With GPS correction techniques the accuracies of 0.25 meters/sec (absolute) are achievable. For short-term, <10 minutes, relative accuracy of 0.1 meters/sec is achievable.

Data Interpretation

The RAF uses various in-flight calibration maneuvers to check the dynamic response of the system and to calibrate and verify the long wavelengths of the turbulence and mean winds (see RAF Bulletin #23). Aircraft intercomparisons are also useful to gain confidence in the systems performance. Power spectra, maximum entropy, covariance, wavelet analyses are techniques for verifying the validity of the data, especially in the shorter wavelengths.

The RAF does not routinely calculate fluxes in the standard processing.

RAF does not calculate fluxes in the standard processing. If you want to do flux calculations, you must do it yourself.

RAF does not calculate fluxes in the standard processing.

RAF does not calculate fluxes in the standard processing. If you want to do flux calculations, you must do it yourself.

RAF does not calculate fluxes in the standard processing.

RAF does not calculate fluxes in the standard processing.

RAF does not calculate fluxes in the standard processing. If you want to do flux calculations, you must do it yourself.

RAF does not calculate fluxes in the standard processing. If you want to do flux calculations, you must do it yourself.

RAF does not calculate fluxes in the standard processing. If you want to do flux calculations, you must do it yourself.

RAF does not calculate fluxes in the standard processing.

RAF does not calculate fluxes in the standard processing. If you want to do flux calculations, you must do it yourself.

RAF does not calculate fluxes in the standard processing. If you want to do flux calculations, you must do it yourself.

RAF does not calculate fluxes in the standard processing. If you want to do flux calculations, you must do it yourself.

RAF does not calculate fluxes in the standard processing. If you want to do flux calculations, you must do it yourself.

RAF does not calculate fluxes in the standard processing. If you want to do flux calculations, you must do it yourself.

RAF does not calculate fluxes in the standard processing. If you want to do flux calculations, you must do it yourself.

RAF does not calculate fluxes in the standard processing. If you want to do flux calculations, you must do it yourself.

RAF does not calculate fluxes in the standard processing. If you want to do flux calculations, you must do it yourself.

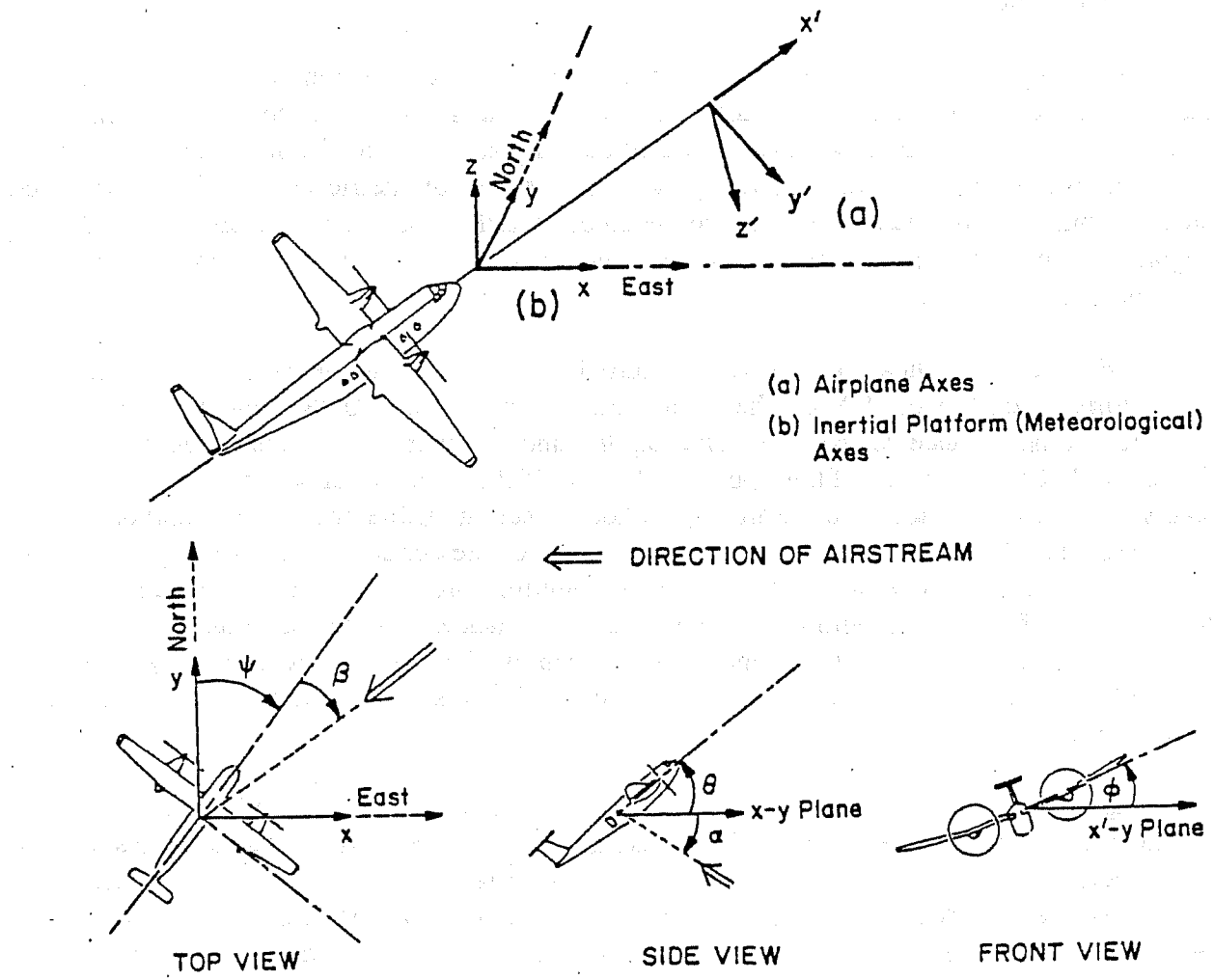


Figure 2.1 — Top: Coordinate systems used in deriving equations for calculating the air velocity components. Bottom: Aircraft attitude angles and wind incidence angles; α attack, β sideslip, ψ true heading, θ pitch, ϕ roll.

SECTION 3—Radiometric Sensors

Ultraviolet Radiometer

Introduction

The NCAR Research Aviation Facility (RAF) provides instruments for the airborne measurement of hemispheric ultraviolet radiation. These measurements are obtained through the use of modified instruments from Eppley Laboratories, Inc. This write-up provides an overview of the ultraviolet radiation instruments along with a discussion of their performance characteristics.

Operating Principles

All types of hemispheric radiometers supported by the RAF have been modified within the facility to make them suitable to the airborne measurement environment and to make them compatible with the RAF airborne data acquisition system. One modification is the addition of a high quality electronic amplifier circuit to the output of the radiometric sensor. The unamplified outputs from the coordinates are small, on the order of millivolts, and are therefore susceptible to degradation by local noises. The gain of the added amplifiers is set to 100 and provides a radiometer output in the range of 0 to 1 volt.

The RAF ultraviolet radiometer, shown in Figure 3.1, is a repackaged version of the Eppley Laboratories, Inc., Model TUVR. The modification of the Eppley TUVR made by RAF was the reduction of the distance between the diffusing disc and the filter. RAF reduced the height of the Eppley TUVR to match that of the Eppley PIR's and PSP's. This modification results in a sensor that is much easier to mount on the aircraft without affecting visible or infrared radiation measurements. The radiation sensors are mounted close together and a standard Eppley TUVR would shadow the other sensors without special mounting hardware being constructed. Modification of the sensor, without degrading its performance, was the best solution to the problem. No difference in angular sensitivity between the RAF sensor and an Eppley has been observed and the only difference from the unmodified Eppley is that the RAF sensor has a larger signal range.

Incoming radiation impinges on an opaque quartz disc where it is diffused and passed through to the filter and detector. The design of the diffusing disc gives the instrument a cosine response to hemispheric radiation. Several centimeters behind the diffusing disk is the passband filter. It is an interference filter with a passband of .295 to .385 μm , as shown in Figure 3.2. Immediately behind the filter is the detector, a selenium barrier-layer photocell. The frequency response of the detector is shown in Figure 3.3. (The information in Figures 3.2 and 3.3 was provided by Eppley Laboratories.) Experience with the TUVR at the RAF has indicated virtually no temperature sensitivity (actually, much less than the Eppley specification of 0.1% $^{\circ}\text{C}$).

Sensor Output and Specifications

a) general information

Manufacturer:

Eppley Laboratories

RAF Resource Person(s):

Krista Laursen, Bruce Morley, Julie Haggerty

Calibration Method:

Comparison with calibrated tungsten iodine lamp

b) primary output description

RAF parameter name:	UVB and UVT
Plain language name:	Ultraviolet radiation bottom and top
Temperature Dependence:	0.1%/C from -40 to +40°C
Linearity and Range:	± 2% from -0 to 700 Wm ⁻²
Response Time:	Milliseconds
Directional Sensitivity:	±2.5% from normalization, 0-70° Zenith angle
Orientation:	No effect on instrument performance
Mechanical Vibration:	Capable of withstanding up to 20 g's
Size:	146 mm diameter, 171 mm high
Weight:	1.8 kg

The yrtravuiket ubstrynebts are periodically returned to Eppley Laboratories for calibration. The TUVR exhibits excellent stability. The calibration technique for the instrument is based on work by Ångstrom and Drummond (1962). This technique involves exposing the radiometer to a NIST calibrated tungsten-iodine lamp. A combination of the spectral characteristics of the calibration lamp, the radiometer filter, and the radiometer detector is used to determine the sensitivity of the radiometer in the spectral band of .295 to .385 μm.

Figure 3.4 is an example of data from this sensor.

See RAF Bulletin No. 25 for information on all RAF radiation measurements.

The RAF resource people are Krista Laursen, Bruce Morley and Julie Haggerty.

Measurement Problems

See "Measurement Problems" discussion for the pyranometer.

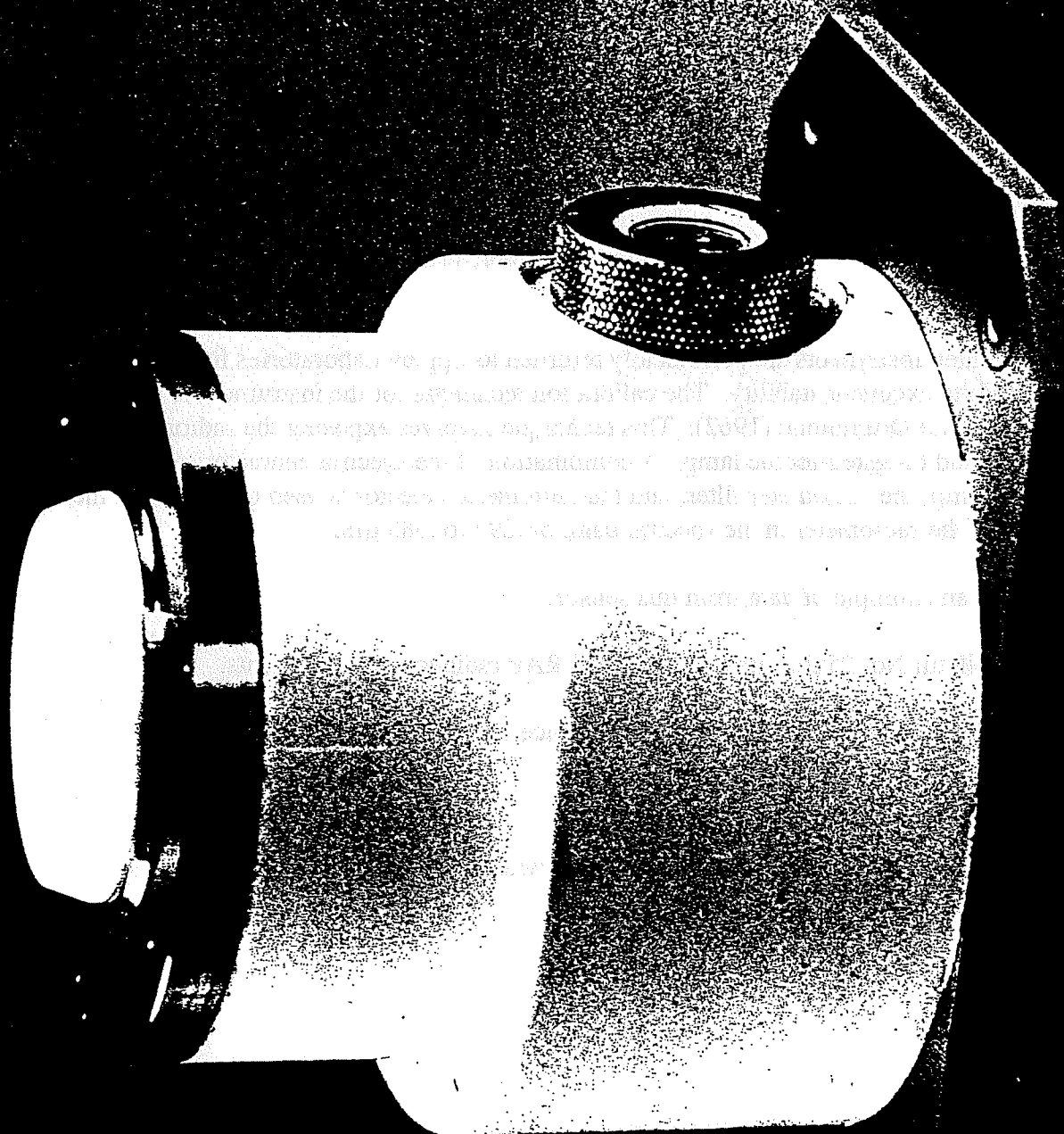


Figure 3.1 — Ultraviolet Radiometer

TYPICAL TRANSMITTANCE
OF EPPLY MODEL TUVR FILTER

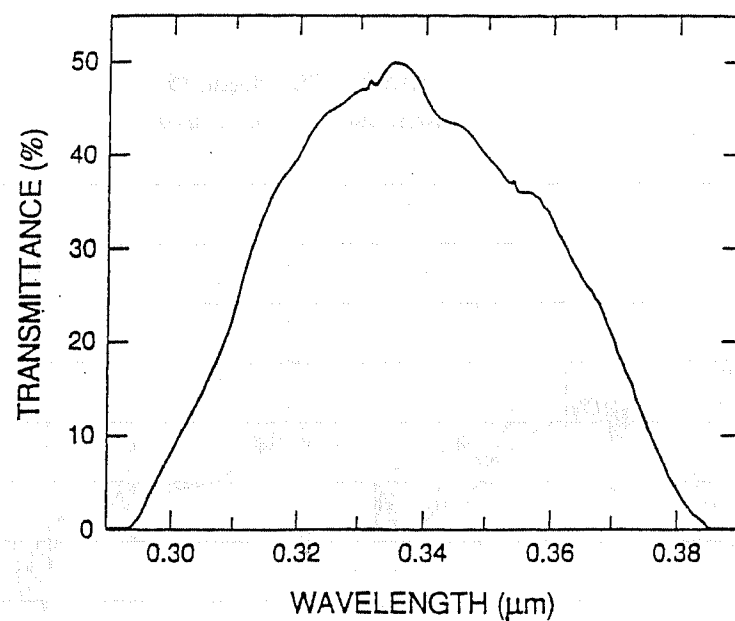


Figure 3.2 — Passband of Eppley TUVR Filter

RELATIVE SPECTRAL RESPONSE
SELENIUM BARRIER-LAYER PHOTOCELL

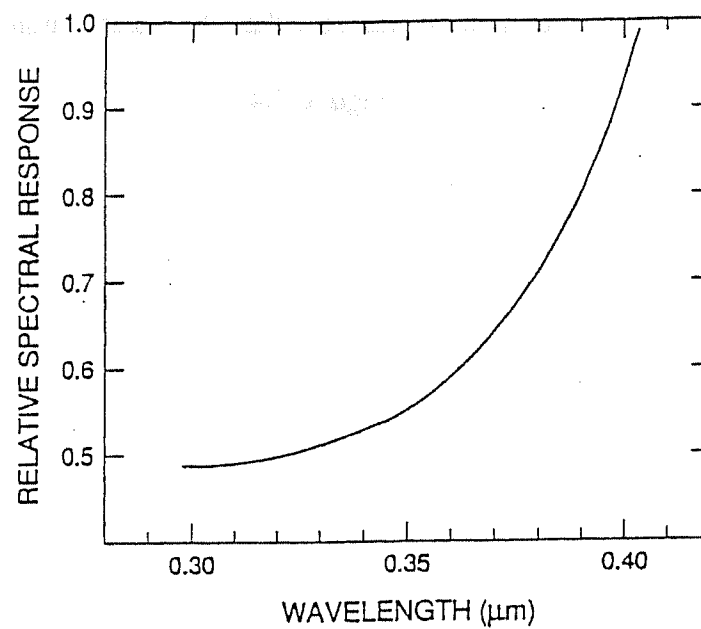
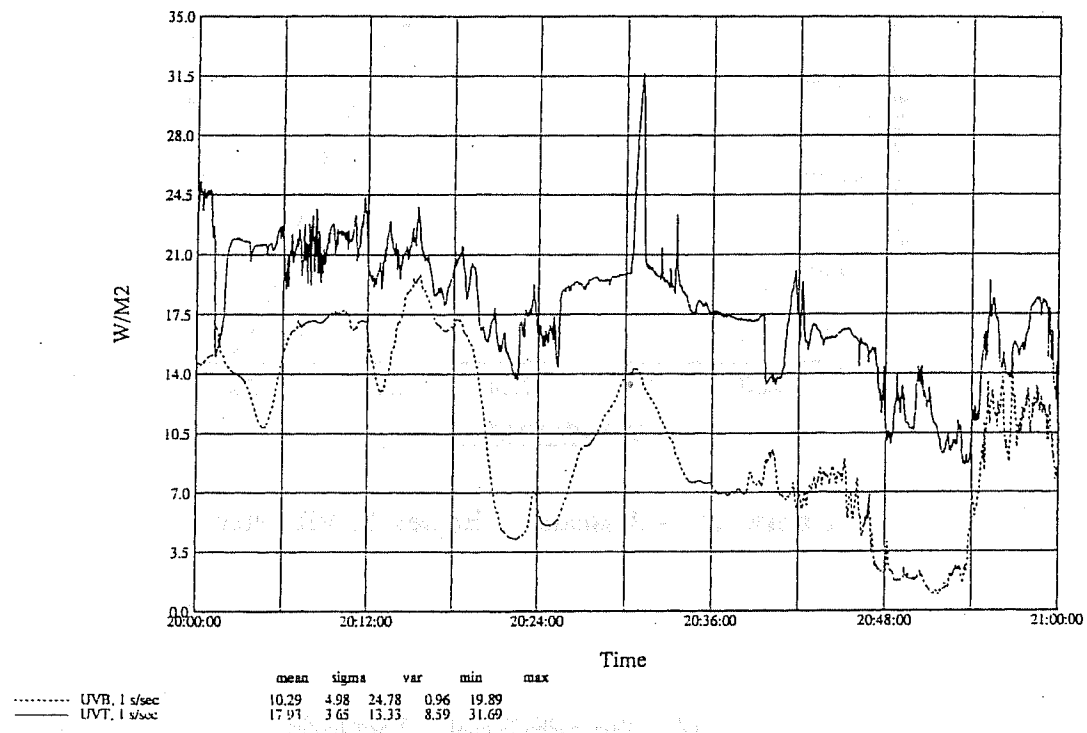


Figure 3.3 — Response of Eppley TUVR Selenium Barrier Layer Photocell

BASE - 120, Flight #5

09/26/1994 , 20:00:00-21:00:00



Example of data from the ultraviolet radiometer

Figure 3.4

Pyranometer

Introduction

Used for measuring hemispheric visible radiation, the pyranometers operated at RAF are modified versions of the Eppley PSP pyranometer. The RAF has repackaged the PSP sensor and filters into a modified housing that is more suitable for aircraft mounting and to provide space for an internal signal amplifier. Lighter weight materials were used in fabricating the modified housing, and the white collar on the Eppley PSP pyranometer, used for regulating the housing temperature, that covered the radiometer (except for the dome) was removed. In the RAF pyranometer, housing temperature is regulated by ventilation due to aircraft true airspeed and ambient temperature. The internal signal amplifier added by RAF to the pyranometer has a gain of 100 and boosts the normal PSP signal output, usually on the order of millivolts, to the range of 0 to 1 volt.

The RAF pyranometer is shown in Figure 3.5, and an example of the instrument output is given in Figure 3.6.

Operating Principles

Incoming radiation is sensed with a thermopile of copper-constantan junctions which are coated with Parson's black lacquer. This absorption is essentially independent of wavelength for the passband of the pyranometer.

The passband of the radiometer is determined by the filter characteristics of the domes. Usually, the pyranometer is fitted with two domes of WG295 Schott filter glass yielding a passband of 0.285 to 2.80 μm . Other filter combinations can be used to obtain different passbands. However, the user should be aware that the RAF does not stock all of these filters and that the pyranometers are calibrated using the WG295 filters.

Sensor Output and Specifications

a) general information

Manufacturer:	RAF-modified Eppley instrument
RAF Resource Person(s):	Krista Laursen, Bruce Morley, and Julie Haggerty
Calibration Method:	Comparison with reference pyranometer and to a hemisphere of tungsten-filament lamps (done at Eppley Laboratories)

b) primary output descriptions

RAF Parameter Names:	SWT and SWB (W/m^2)
Plain Language Name:	Short wave radiation, top and bottom
Range:	0-1 Volt
Directional Sensitivity:	$\pm 1\%$ deviation from 0 to 70° zenith angle; $\pm 3\%$ deviation from 70 to 80° zenith angle
Orientation:	No effect on instrument performance
Linearity:	$\pm 0.5\%$, 0 to 2800 W m^{-2}
Temperature Dependence:	$\pm 1\%$, -20 to +40° C (nominal)
Response Time:	1 sec (63% response to step function)
Mechanical Vibration:	Capable of withstanding up to 20 g's

Measurement Problems

Normal aircraft maneuvers can produce errors in the measured irradiances. Another problem stemming from airborne use of the pyranometer is that changes in aircraft heading, pitch and roll can vary the contributions of the direct and diffuse components of the irradiance. Methods for treating these and other difficulties have, however, been suggested by Bannehr and Glover (1991), and have been implemented in the processing of measurements from projects after 1995.

The aircraft's orientation and the angle of the sun relative to the aircraft's orientation are important factors in determining the irradiance measured by the pyranometer. If the aircraft is oriented such that the sun is directly behind the aircraft, the pyranometer will measure only the direct component of the solar radiation. If the aircraft is oriented such that the sun is directly in front of the aircraft, the pyranometer will measure only the diffuse component of the solar radiation. If the aircraft is oriented such that the sun is at an angle to the aircraft's orientation, the pyranometer will measure both the direct and diffuse components of the solar radiation.

The aircraft's orientation and the angle of the sun relative to the aircraft's orientation are important factors in determining the irradiance measured by the pyranometer.

The aircraft's orientation and the angle of the sun relative to the aircraft's orientation are important factors in determining the irradiance measured by the pyranometer.

The aircraft's orientation and the angle of the sun relative to the aircraft's orientation are important factors in determining the irradiance measured by the pyranometer.

The aircraft's orientation and the angle of the sun relative to the aircraft's orientation are important factors in determining the irradiance measured by the pyranometer.

The aircraft's orientation and the angle of the sun relative to the aircraft's orientation are important factors in determining the irradiance measured by the pyranometer.

The aircraft's orientation and the angle of the sun relative to the aircraft's orientation are important factors in determining the irradiance measured by the pyranometer.

The aircraft's orientation and the angle of the sun relative to the aircraft's orientation are important factors in determining the irradiance measured by the pyranometer.

The aircraft's orientation and the angle of the sun relative to the aircraft's orientation are important factors in determining the irradiance measured by the pyranometer.

The aircraft's orientation and the angle of the sun relative to the aircraft's orientation are important factors in determining the irradiance measured by the pyranometer.

The aircraft's orientation and the angle of the sun relative to the aircraft's orientation are important factors in determining the irradiance measured by the pyranometer.

The aircraft's orientation and the angle of the sun relative to the aircraft's orientation are important factors in determining the irradiance measured by the pyranometer.

The aircraft's orientation and the angle of the sun relative to the aircraft's orientation are important factors in determining the irradiance measured by the pyranometer.

The aircraft's orientation and the angle of the sun relative to the aircraft's orientation are important factors in determining the irradiance measured by the pyranometer.

The aircraft's orientation and the angle of the sun relative to the aircraft's orientation are important factors in determining the irradiance measured by the pyranometer.

The aircraft's orientation and the angle of the sun relative to the aircraft's orientation are important factors in determining the irradiance measured by the pyranometer.

The aircraft's orientation and the angle of the sun relative to the aircraft's orientation are important factors in determining the irradiance measured by the pyranometer.

The aircraft's orientation and the angle of the sun relative to the aircraft's orientation are important factors in determining the irradiance measured by the pyranometer.

The aircraft's orientation and the angle of the sun relative to the aircraft's orientation are important factors in determining the irradiance measured by the pyranometer.

The aircraft's orientation and the angle of the sun relative to the aircraft's orientation are important factors in determining the irradiance measured by the pyranometer.

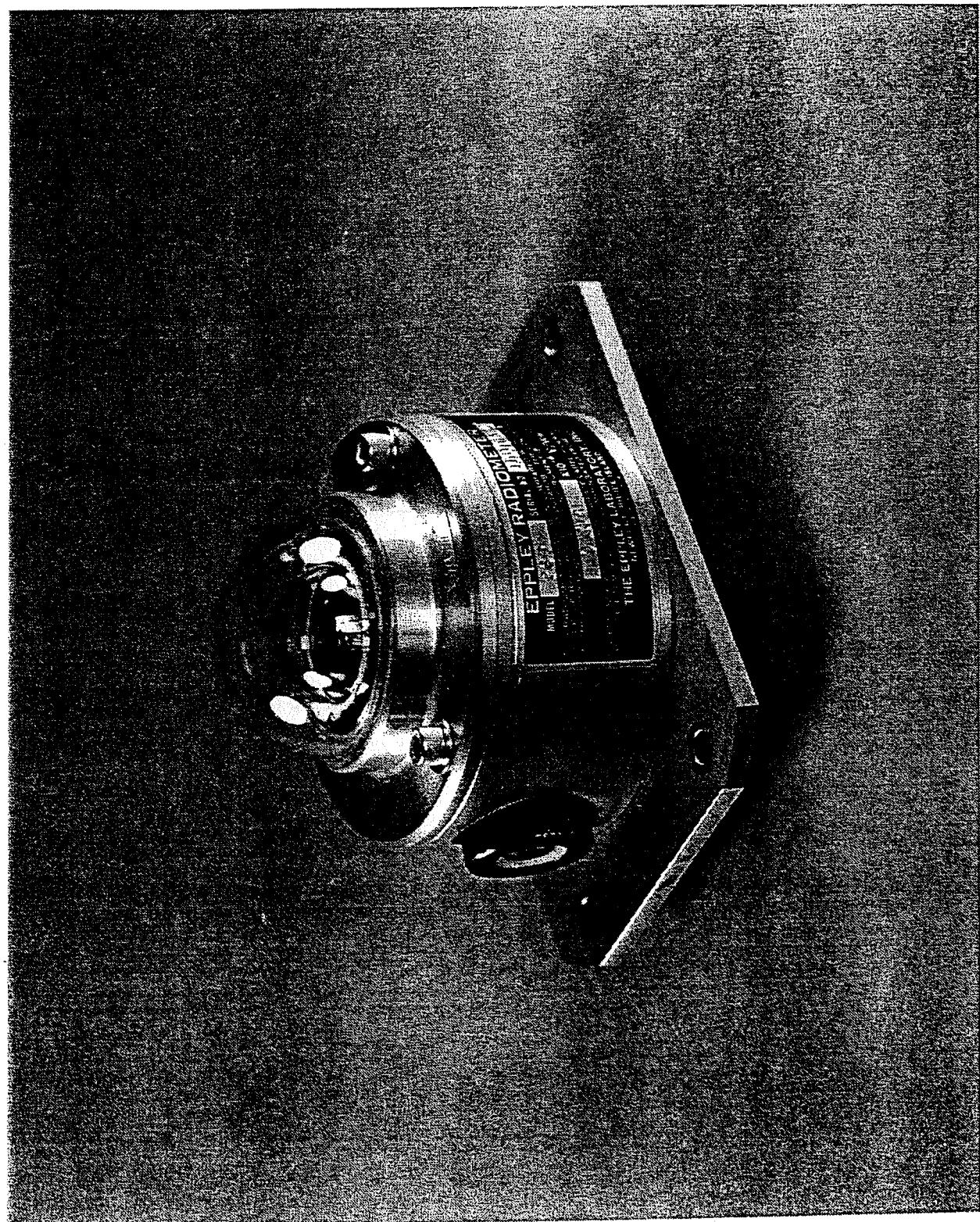
The aircraft's orientation and the angle of the sun relative to the aircraft's orientation are important factors in determining the irradiance measured by the pyranometer.

The aircraft's orientation and the angle of the sun relative to the aircraft's orientation are important factors in determining the irradiance measured by the pyranometer.

The aircraft's orientation and the angle of the sun relative to the aircraft's orientation are important factors in determining the irradiance measured by the pyranometer.

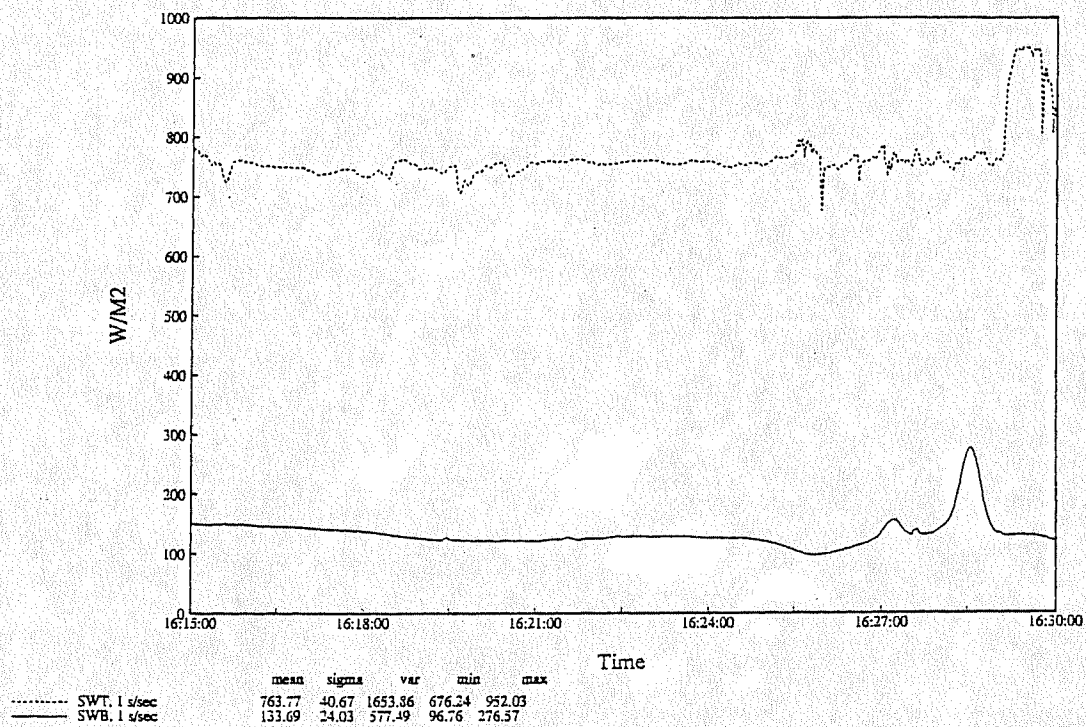
The aircraft's orientation and the angle of the sun relative to the aircraft's orientation are important factors in determining the irradiance measured by the pyranometer.

Figure 3.5 — Pyranometer



BOREAS - 818, Flight #13

8/1/1994, 16:15:00-16:30:00



Example of the instrument output from the pyranometer

Figure 3.6

Pyrgeometer

Introduction

Used for measuring hemispheric infrared (IR) radiation, the pyrgeometer operated at RAF is a repackaged version of the Eppley PIR pyrgeometer. Modifications made by RAF to the pyrgeometer are similar to those made to the pyranometer, except that temperature sensors have been added to the pyrgeometer for the purpose of measuring sink and dome temperatures needed for the correct determination of measured irradiance. As with the RAF pyranometer, the reflective collar added by Eppley to the pyrgeometer has been removed. An internal signal amplifier has also been added to the RAF pyrgeometer for the purpose of boosting the instrument's signal output.

The RAF pyrgeometer is shown in Figure 3.7, and an example of the instrument output is given in Figure 3.8.

Operating Principles

A silicon dome within the pyrgeometer provides the 3.5 to 50 μm passband filtering for this instrument. In determining the correct infrared irradiance measured by the pyrgeometer, the sink and dome temperatures of the radiometer must be taken into account. This is necessary because the sink and dome each emit energy that influence the energy incident on the pyrgeometer's sensing thermopile. The equation used to calculate the corrected IR irradiance is as follows:

$$\text{IRC} = \text{IR} + \epsilon_0 \sigma (\text{TS})^4 - k \sigma ((\text{TD})^4 - (\text{TS})^4),$$

where IRC is the corrected IR irradiance (W/m^2), IR the calibrated, amplified thermopile output (W/m^2), TD the dome temperature (K), TS the sink temperature (K), ϵ_0 the emissivity of the blackened thermopile surface, k the ratio of the dome material emissivity to transmissivity, and σ the Stefan-Boltzmann constant. In RAF processing, k is given a value of 4.3. (This is an average value from in-house calibrations.)

Sensor Output and Specifications

a) general information

Manufacturer:	RAF-modified Eppley instrument
RAF Resource Person(s):	Krista Laursen, Bruce Morley, and Julie Haggerty
Calibration Method:	Black body reference

b) primary output descriptions

RAF Parameter Names:	IRTC and IRBC (W/m^2)
Plain Language Names:	Infrared radiation, top & bottom, corrected
Range:	0-1 Volt
Directional Sensitivity:	Better than 5% from normalization, insignificant for a diffuse source
Orientation:	No effect on instrument performance
Linearity:	$\pm 1\%$ from - to 700 W/m^2
Temperature Dependence:	$\pm 1\%$, -20 to +40°C (nominal)
Response Time:	2 sec (63% response to step function)
Mechanical Vibration:	Capable of withstanding up to 20 g's

Measurement Problems

Due to atmospheric attenuation and scattering, a large portion of the solar radiation in the pyrgeometer passband does not reach the surface of the earth. Because of this, there is no direct solar IR radiation reaching ground level. At some flight levels, however, the amount of direct solar IR radiation measured by the pyrgeometer can be significant. The user should, therefore, be aware of the pyrgeometer's sensitivity to direct solar IR radiation and also to the sensitivity of the instrument to the attitude of the aircraft with respect to the sun. These problems are reported in greater detail by Glover and McFarland (1991).

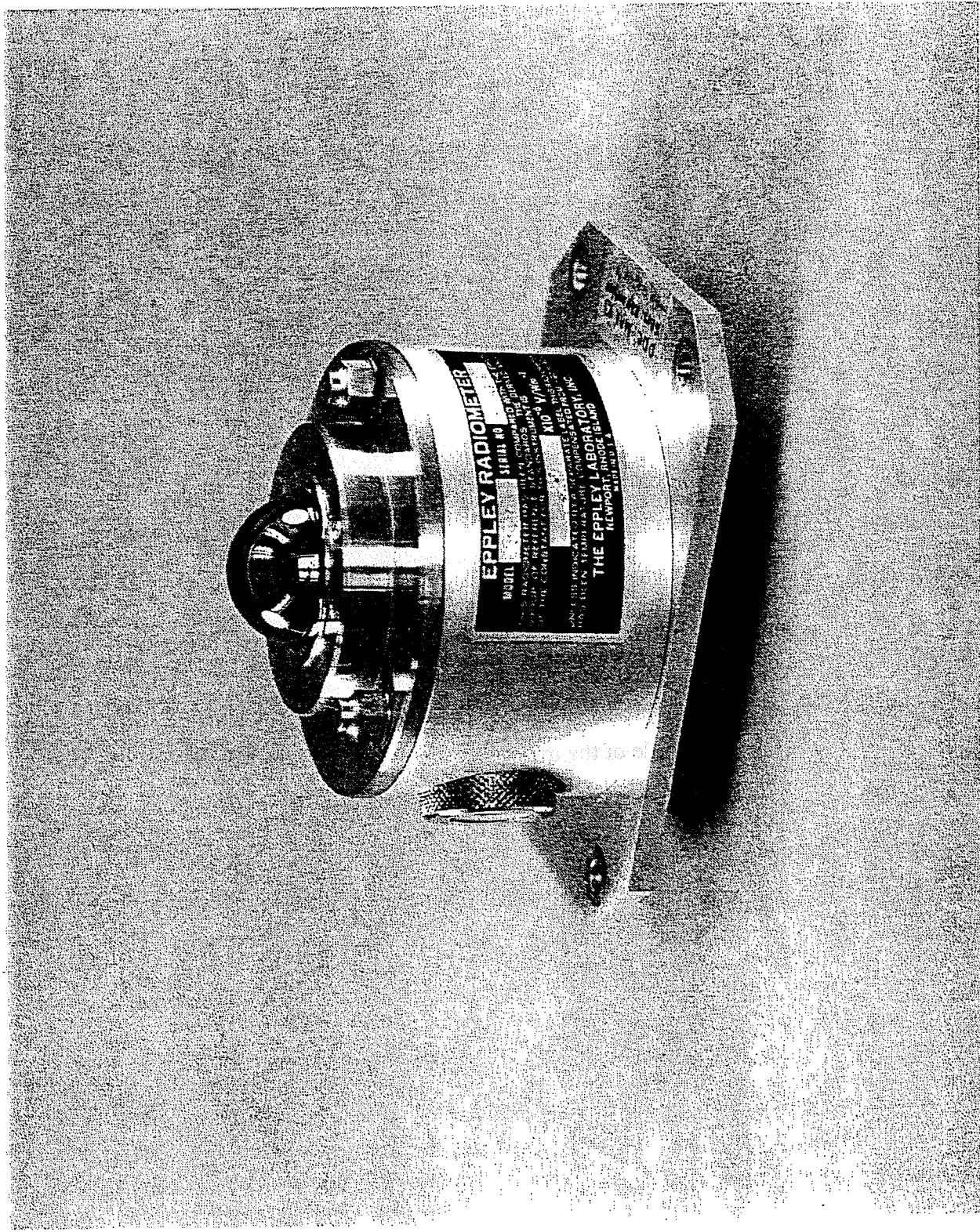
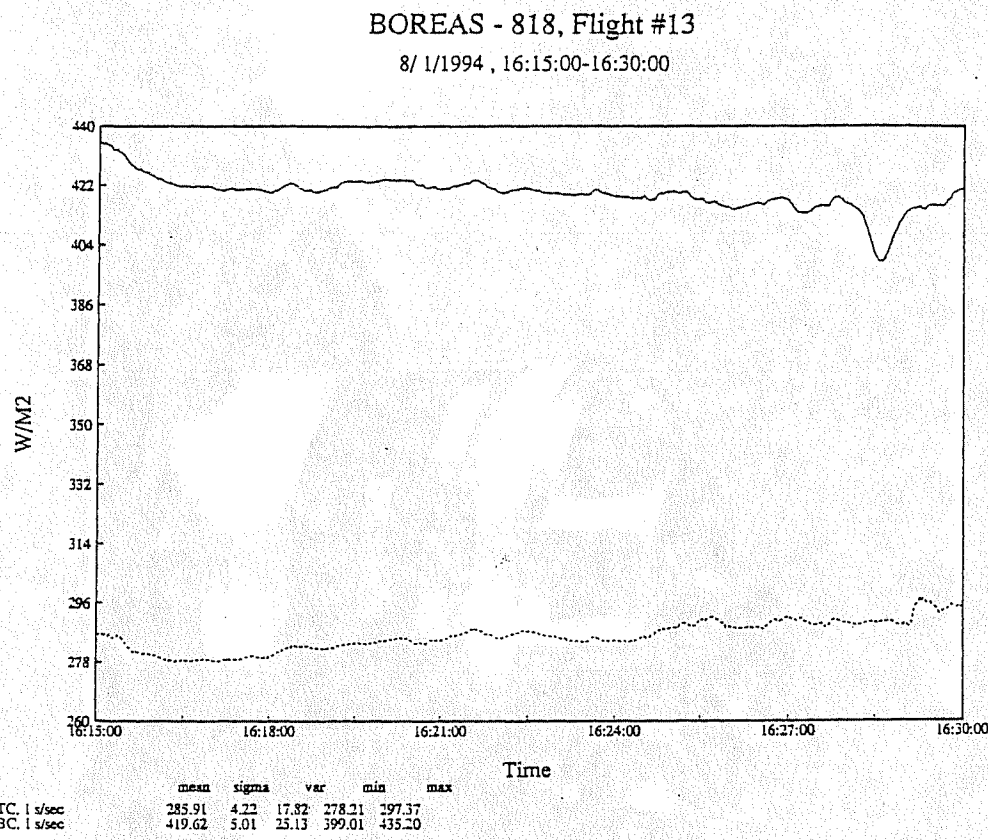


Figure 3.7 — Pyrgeometer



Example of the instrument output from the pyranometer

Figure 3.8

Precision Radiation Thermometer (PRT-5)

Introduction

This instrument is used to make airborne radiometric measurements at infrared wavelengths (see Figure 3.9). These measurements are used to derive surface temperature, where the surface in question may be water, land, or clouds. See Figure 3.10 for an example of output from this sensor.

Operating Principles

This device focuses the surface of interest on a detector contained within a temperature-controlled chamber. Before reaching the detector, radiation from the surface passes through a filter and focusing lens. Filters defining a spectral band of either 9.5-11 microns or 8-14 microns are available. A chopper blade outside the temperature-controlled chamber modulates the radiation coming from the surface before it reaches the detector. The blade, which is highly reflective in the infrared, presents the detector with a reflection of itself during the time when the target is obscured. Thus, the detector is alternately exposed to the target surface and a precision reference, so that surface temperature measurements can be made with respect to this reference. Electronic circuits process the difference between the detector output on alternate positions of the chopper to produce an indication of the surface temperature.

Periodic calibrations of the PRT-5 radiometers are performed with a blackbody source (Eppley Laboratories, Inc., Infrared Blackbody Source model BB16T). This blackbody has a temperature accuracy and uniformity of 0.1°C over the temperature range of -10 to 60°C . Its emissivity is 0.995.

Sensor Output and Specifications

a) general information

Manufacturer: Barnes Engineering Co.
RAF Resource Person(s): Krista Laursen, Bruce Morley, Julie Haggerty

b) primary output

RAF Parameter Names:	RSTT, RSTB
Plain Language Names:	radiometric sky temperature, radiometric surface temperature
Units:	$^{\circ}\text{C}$
Measurement range:	-20 to $+75^{\circ}\text{C}$
Accuracy:	$\pm 1.0^{\circ}\text{C}$
Response time:	0.5 s
Spectral range:	8 - 14 or 9.5 - 11.5 microns
Field of view:	2 degrees
Operating temperature range:	-20 to $+40^{\circ}\text{C}$

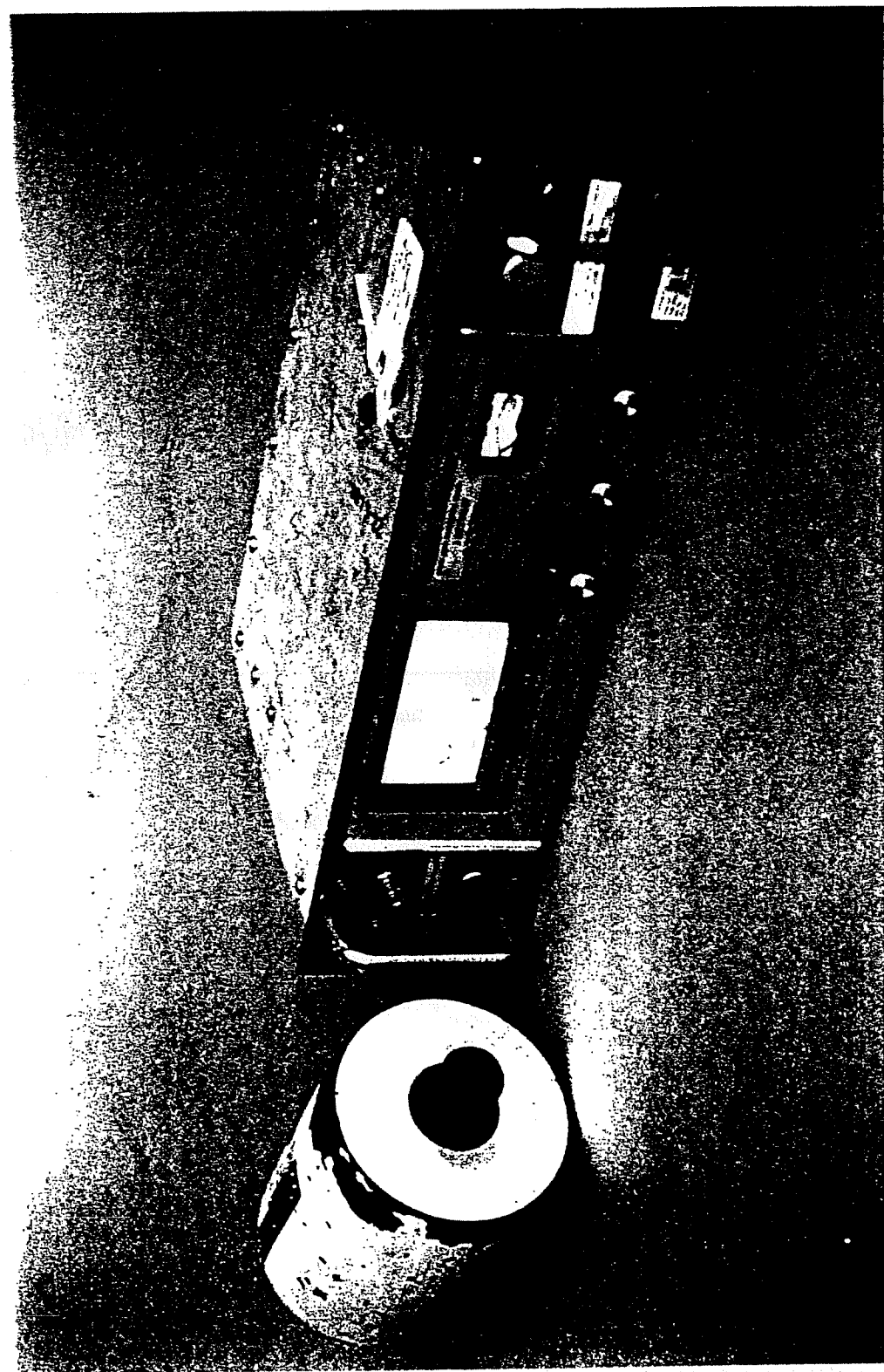
Data Interpretation

In some flight situations it is not possible to maintain temperature control of the reference due to heat losses which cannot be compensated. In this situation the reference temperature drops and the instrument no longer makes accurate measurements. To flag this condition, the RAF has modified the PRT-5 to include a measurement of the chamber temperature. This supplemental measurement does not correct the surface temperature measurement, but is provided only to alert users that chamber temperature control has been lost.

Although it is possible to accurately calibrate these radiometers, environmental effects of airborne usage degrade the accuracy of PRT-5 surface temperature measurements. In the final data processing, the RAF does not correct the raw PRT-5 output. The calibrated temperature output might be termed the "apparent surface temperature". Corrections can be made to account for water vapor effects, surface emissivity, and overhead sky conditions, but these sorts of modifications, at present, are left to the judgement and skill of the investigator.

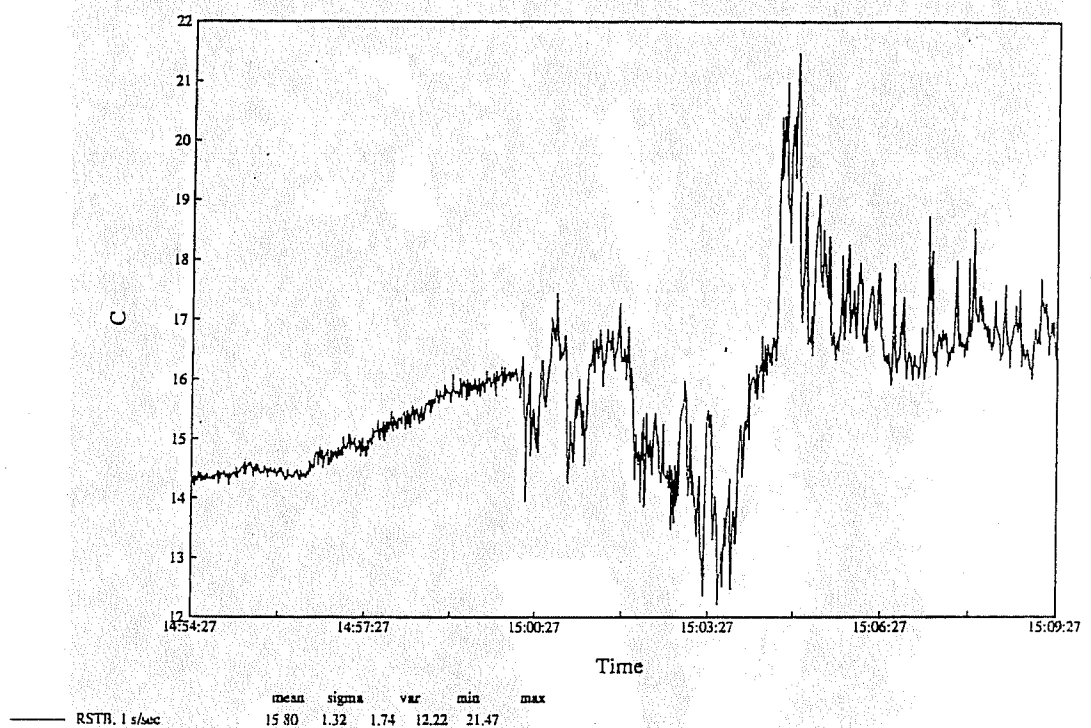
Should sources within your environment, such as windows, walls or doors, become hot enough to affect your chamber temperature, the PRT-5 will detect this change and provide you with information to determine if your chamber is still within acceptable limits. If your chamber is not within acceptable limits, you may want to take corrective action to bring your chamber back into acceptable limits.

Figure 3.9 — Precision Radiation Thermometer (PRT-5)



BOREAS - 818, Flight #20

9/3/1994 , 14:54:27-15:09:27



Example of output from the PRT-5

Figure 3.10

Heimann Radiation Pyrometer (KT19.85)

Introduction

The Heimann radiation pyrometers measure infrared radiation in the atmospheric window region (9.6 - 11.5 microns). Surface temperatures are derived from the radiation measurement. These instruments are intended to replace the aging Barnes PRT-5 radiometers. Figure 3.11 is a photograph of two Heimann KT19 units. An example of output from this sensor is shown in Figure 3.12.

Operating Principles

The radiation pyrometer is a measuring transducer which receives infrared radiation emitted by a surface and transforms it into a standardized output signal. The technology used is essentially the same as that used in the Barnes PRT-5 instrument. Radiation emitted from a water, land, or cloud surface passes through a filter which defines a spectral band from 9.6 to 11 microns. As with the PRT-5, the KT19.85 uses a reference target, which is highly reflective in the infrared portion of the spectrum, for comparison with radiation coming from the surface. Electronic circuits process the difference between the transducer output for the reference target and the surface to produce an indication of the surface temperature.

Sensor Output and Specifications

a) general information

Manufacturer: EG&G Heimann Optoelectronics
RAF Resource Person(s): Krista Laursen, Bruce Morley, Julie Haggerty

b) primary output

RAF parameter names:	XKT, XKT1
Plain language names:	surface temperature
Units:	C
Range:	-50 to 400 C
Temperature resolution:	~ 1C (depending on radiative temperature of surface)
Response time:	adjustable (RAF recommends 0.3 s to reduce noise)
Spectral band:	9.6 - 11.5 microns
Field of view:	2 degrees
Calibration:	blackbody target (EPLAB unit)

Data Interpretation

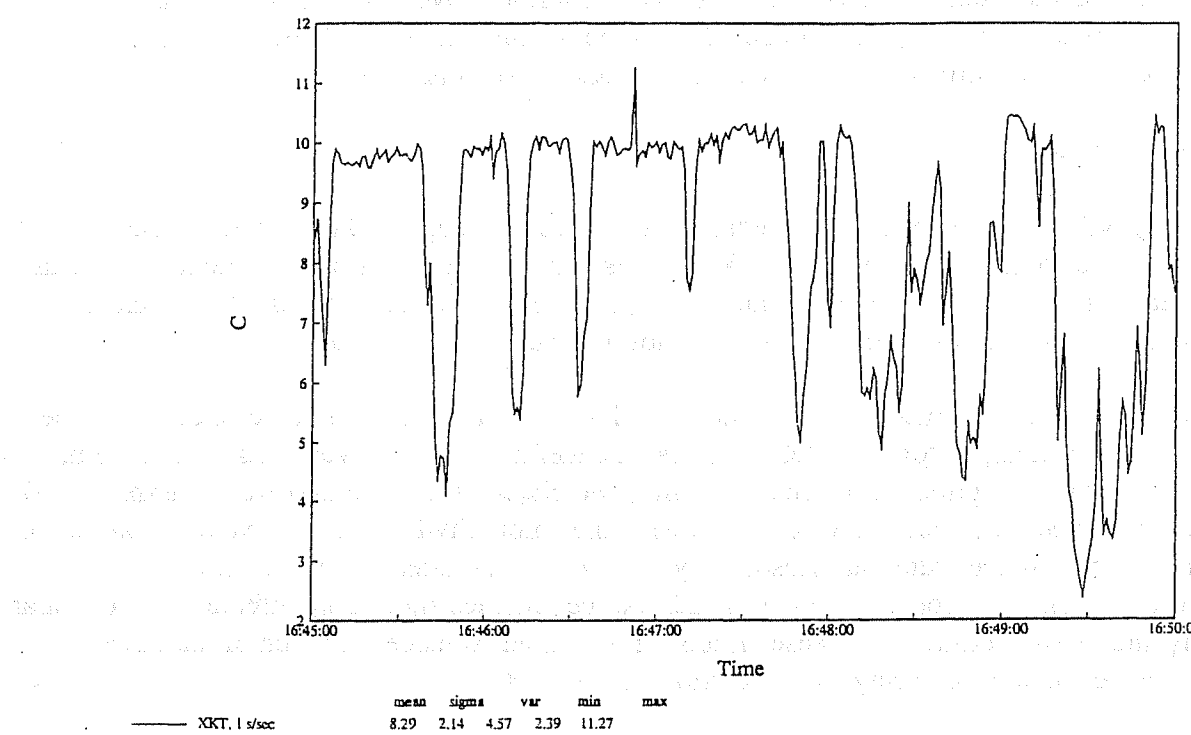
Response times for these instruments are programmable, but it has been demonstrated that response times faster than 0.3 s increase the noise level. Ambient temperature is another factor affecting the performance of the Heimann KT19. Tests conducted at RAF have shown that noise levels increase at operating temperatures colder than 15C and that calibration factors shift above 40C. RAF is currently taking action to rectify these problems.

Figure 3.11 — Heimann Radiation Pyrometer (KT19.85)



Telford - 127, Flight #8

12/09/1994 , 16:45:00-16:50:00



Example of output from the Heimann Radiation Pyrometer

Figure 3.12

Spectral Vegetation Radiometer (SVR)

Introduction

A spectral vegetation radiometer (SAR) has been developed at RAF for the purpose of examining the spectral characteristics of plants and other types of surface cover, providing a means of classifying ground cover using data collected from the instrument during research flights. Development of this instrument was based on the work of Bannehr (1990).

Operating Principles

The chlorophyll absorption band for vegetation lies within the range 400 to 680 nm in the visible section of the electromagnetic spectrum. Within this wavelength range, light incident on vegetation is absorbed and scattered by the photosynthetic pigment in the leaves. Beyond 680 nm and out to approximately 750 nm, this absorption by vegetation decreases significantly.

The above wavelength characteristics of chlorophyll absorption were used in the selection of the three channel wavelengths for the SVR. The first channel has a central wavelength of 650 nm, close to the chlorophyll absorption band. The remaining two channels have central wavelengths of 760 and 862 nm, respectively, both of which are outside the chlorophyll absorption band. It should be noted that at 650 nm, the radiation measured by the SVR is also affected by extinction due to molecules, aerosols and ozone. At 760 and 862 nm, the radiance signals are affected by molecular scattering and aerosol extinction. These effects on measured radiances for each of the three channels are accounted for during the calibration of the SVR.

The SVR is shown in Figure 3.13, and an example of the instrument output is given in Figure 3.14.

Sensor Output and Specifications

a) general information

Manufacturer:	RAF
RAF Resource person(s):	Krista Laursen
Calibration Method:	Ratio-Langley calibration technique [see Bannehr and Glover (1992) for details on this method]

b) primary output descriptions

RAF Parameter Names:	WV650, WV760 and WV862
Plain Language Names:	Voltages at 650nm, 760nm, 862nm
Range:	0-5 Volts for each channel
Units:	Volts
Response Time:	24 msec (from 0 to 99%)
Channel Bandwidth:	10 nm for each channel
Instrument Field of View:	2.3°; variable by changing apertures
Power Requirements:	+9 Volts, 30 mA; operable either from 110 Volts or from batteries

c) *derived output descriptions*

The normalized difference vegetation index (NDVI) can be calculated from the calibrated output from the SVR. This quantity is given by

$$\text{NDVI} = (\rho_2 - \rho_1) / (\rho_2 + \rho_1)$$

where ρ_1 and ρ_2 are the radiances measured by the 650 and 862 nm channels, respectively.

Users should note that the NDVI determined above is calculated from radiance signals and not reflectance values, as is typically done with satellite data.

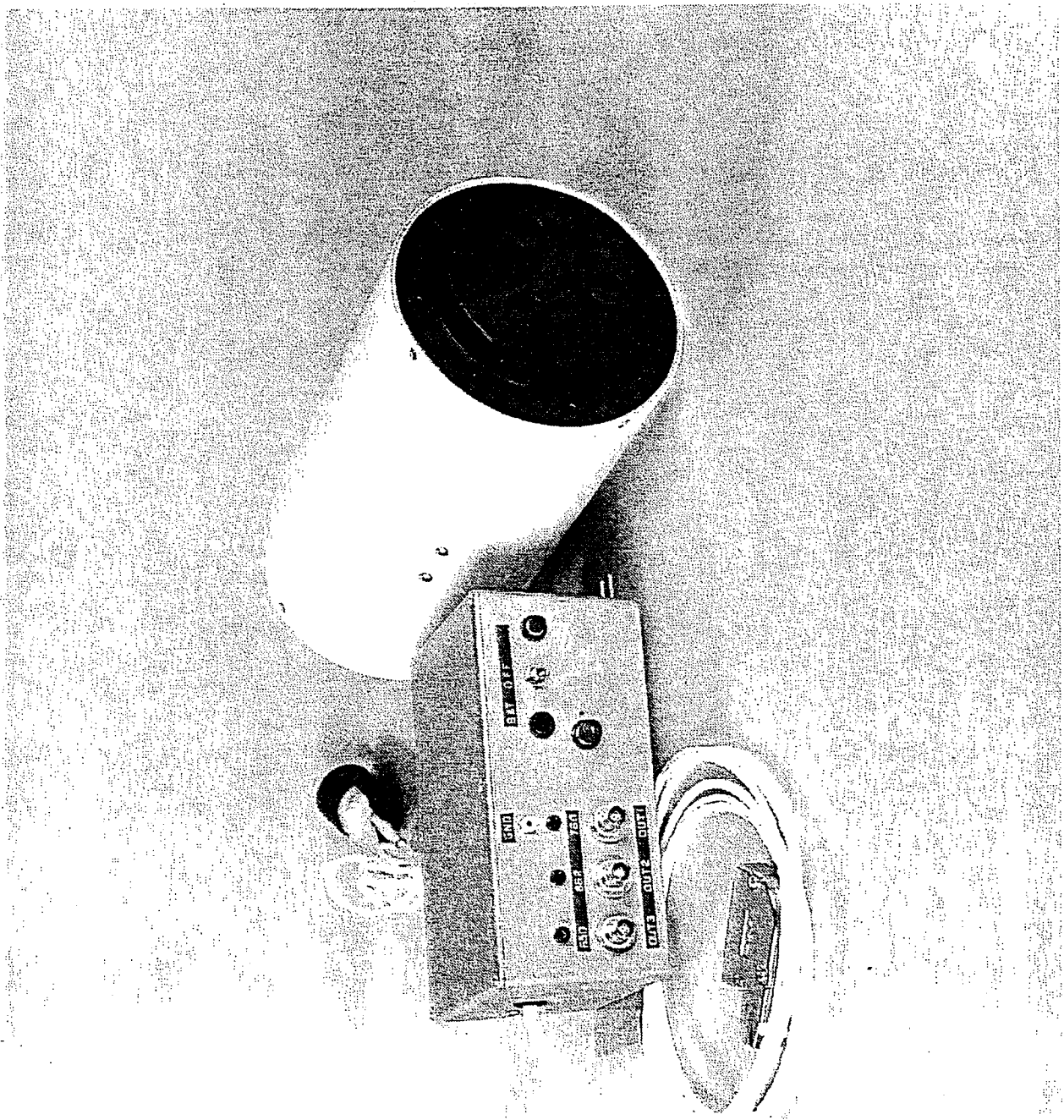
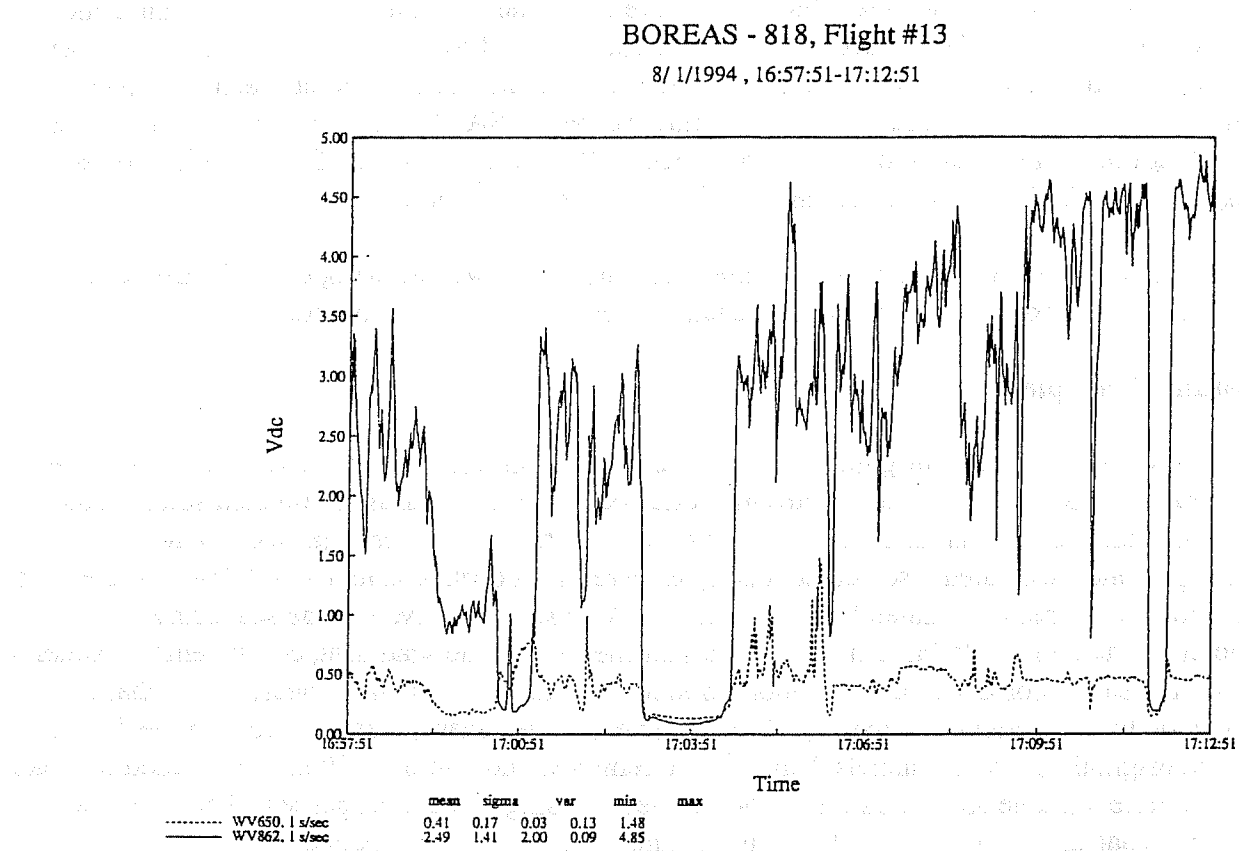


Figure 3.13 — Spectral Vegetation Radiometer (SVR)



Example of the output from the Spectral Vegetation Radiometer

Figure 3.14

Multichannel Cloud Radiometer (MCR)

Introduction

The multichannel cloud radiometer (MCR) is a seven-channel spectral radiometer designed and fabricated at NASA/Goddard Space Flight Center and acquired by RAF in 1993. This instrument is downward-looking and scans 45 degrees to either side of nadir. The MCR has been tested and flown on several different research aircraft, including the NASA Convair CV-990, a WB-57F (the same aircraft recently acquired by RAF), the NASA ER-2, and the NCAR C-130. In its present configuration at RAF, the MCR flies in one of the wing pods on the C-130.

A photograph of the MCR is shown in Figure 3.15, and a cut-away drawing of the instrument is shown in Figure 3.16. An example of one channel's output is shown in Figure 3.17.

Operating Principles

In the original instrument configuration, six of the MCR channels had central wavelengths in the near-infrared (NIR) portion of the electromagnetic spectrum and measured reflected solar radiation from clouds for the determination of various cloud properties. These original six channel wavelengths and associated research applications were as follows: channel 1 -- 0.754 μm (clear sky, cloud optical thickness); channel 2 -- 0.761 μm (O_2 A-band, altimetry, volume scattering coefficient); channel 3 -- 0.763 μm (O_2 A-band, altimetry, volume scattering coefficient); channel 4 -- 1.14 μm (H_2O vapor O-band, H_2O vapor amount); channel 5 -- 1.63 μm (clear, cloud phase, cloud/snow discriminator); channel 6 -- 2.16 μm (clear, cloud phase, particle size). In the fall of 1995, the original filters in channels 2 and 3 were removed and two new filters were added to make the MCR more suitable as an instrument for remotely sensing aerosol properties. The two new filters have central wavelengths of 0.55 μm (channel 2) and 0.63 μm (channel 3).

The seventh channel has a central wavelength of 10.76 μm (in the thermal infrared portion of the electromagnetic spectrum) and measures thermal emission from the tops of clouds to be used in the determination of cloud top temperature.

For more specific information on the MCR and the various channel applications, the user is referred to Curran *et al.* (1981).

Sensor Output and Specifications

a) general information

Manufacturer: NASA/Goddard Space Flight Center; modified in-house at RAF
RAF Resource Person(s): Krista Laursen and Dick Schillawski
Calibration Method: Channels 1 to 6 -- comparison with integrating sphere (standard source) output; channel 7 -- comparison with thermal calibration source in evacuated chamber. All calibrations previously performed at NASA/GSFC; calibrations cannot presently be performed at RAF.

b) primary output descriptions

RAF Parameter Names: MCR1, MCR2, MCR3, MCR4, MCR5, MCR6, and MCR7 (all in Volts)
Range: ± 10 Volts
Instrument Field of View: 0.007 radians
Clear Aperture: 12.38 cm
Instrument Scan Rate: 3.47 sec^{-1}
Data Sampling Rate (As of 9/94): 1000 Hz

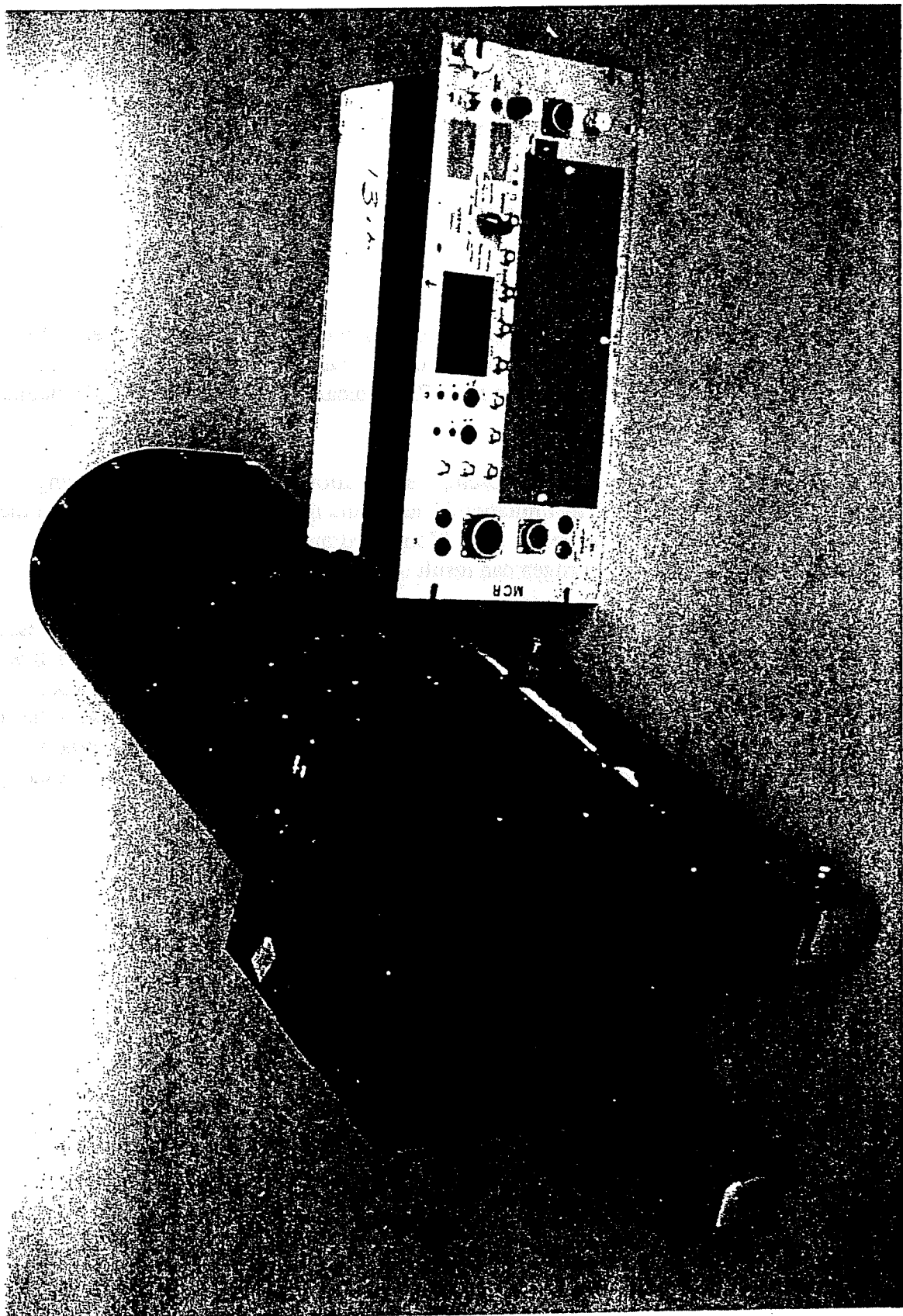
Special Issues

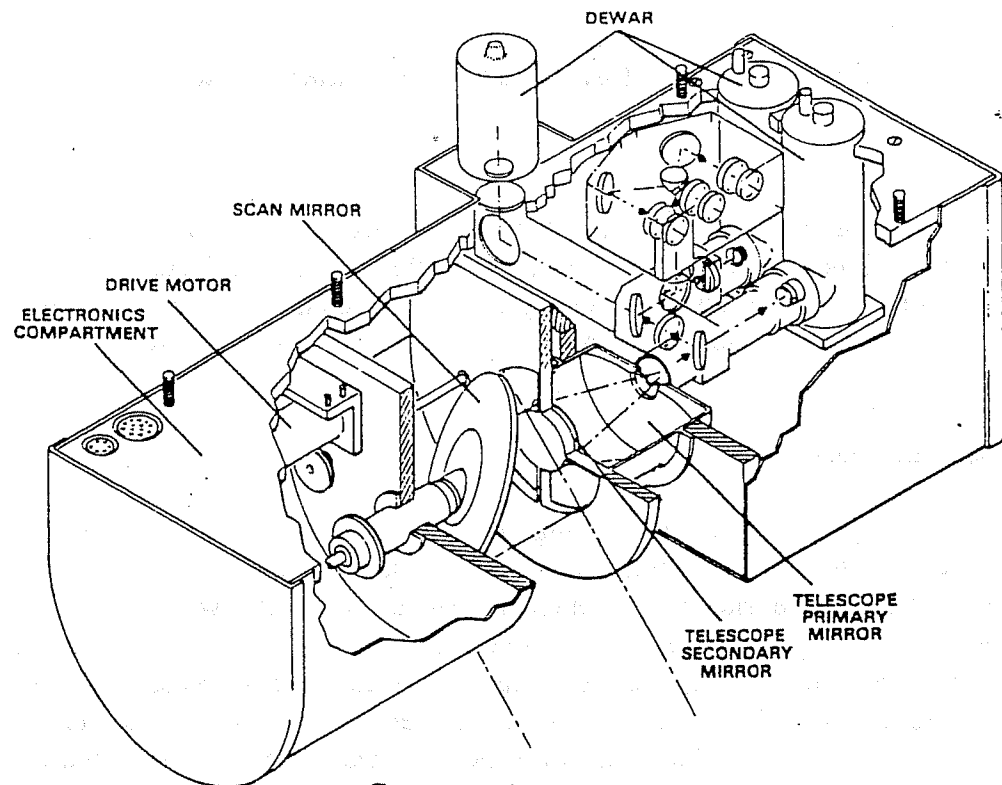
At present, the MCR is not operated as part of the standard and routinely-operated RAF suite of instruments. Consequently, a special request must be made for use of the MCR during a research project. A dedicated RAF operator for the MCR is typically needed to oversee the maintenance and operation of the MCR during a project.

The user should also be aware that, at present, the operational time of the MCR during a research flight is limited to six hours. This limitation is due to the lifetime of liquid nitrogen in the dewars containing the detectors for channels 4 to 7. (Continued operation of the MCR after the three dewars have run out of liquid nitrogen can result in permanent damage to the detectors.)

Finally, given the high volume of data that is generated by the MCR, data will be processed for the user on an "as requested" basis only. In other words, data will only be processed for those days and specific time intervals that are requested by the user. While no specific MCR data processing protocol has yet been established, it is anticipated that the user will be supplied with the active scan voltage (i.e. raw) data for the channels of interest along with the appropriate calibration information. It will be left to the user to develop and apply algorithms for retrieving specific physical quantities (e.g. optical thickness, particle size, etc.).

Figure 3.15 — Multichannel Cloud Radiometer (MCR)





Cut-away drawing of the MCR

Figure 3.16 — [from Curran, et al. (1981)]

BASE - 120, Flight #8
00/00/1900, 17:00:03-17:00:04

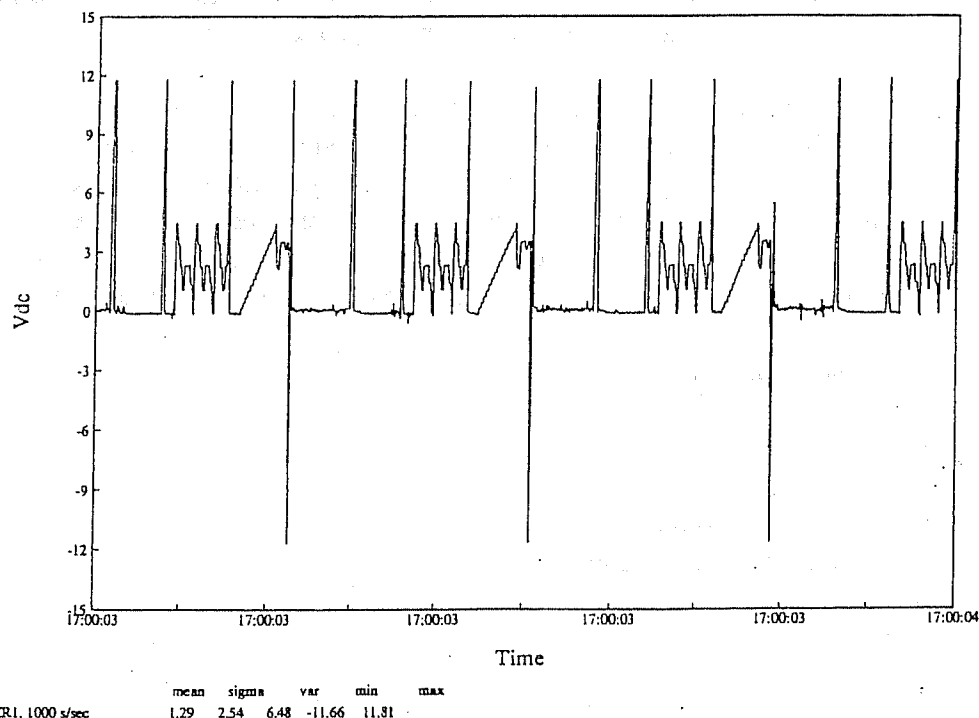


Figure 3.17 — Example of one channel's output from the MC

Airborne Imaging Microwave Radiometer (AIMR)

Introduction

The AIMR is a passive remote sensing system which measures microwave emission at 37 and 90 GHz to produce images of terrain and clouds below the aircraft (see Figure 3.18). It was originally built to observe the distribution of sea ice types, but it is potentially useful for measuring cloud liquid water, precipitation rate, sea surface roughness and windspeed, soil moisture, and oil spill extent.

Operating Principles

Data is collected by the AIMR via a rotating mirror which scans over a range of ± 60 degrees normal to the aircraft track. The beam is directed by the reflector into a four-channel gaussian optical lens antenna. The antenna is oriented so that, at each of the two frequencies, it receives polarization at ± 45 degrees to the vertical. The outputs from the antenna go through a series of mixers, oscillators, and amplifiers before being directed to a microprocessor which converts the signals into digital form. The data is then sent via fiber optic link to the main data system in the aircraft cabin. Figure 3.19 is a block diagram showing relationships between the AIMR components.

After completing each scan, the mirror views an ambient temperature load for calibration purposes. Before beginning the next scan, it passes over a hot (80 C) load. Each load has an emissivity close to unity and a known temperature, so the radiometric readings of the loads can be used to determine the relationship between radiance and brightness temperature. The scanning mirror is rotated by a stepping motor, so both the scan rate and the mirror position are controlled by the microprocessor (which receives commands from the operator-controlled data system).

The radiance measurements and calibration information are received by the cabin-mounted data system (note: the AIMR currently functions with a data system which is separate from ADS, the primary RAF data acquisition system). Information about aircraft position, including latitude, longitude, heading, altitude, roll angle, and drift angle, are received from ADS. With this information, the processor derives the ground position for each pixel, corrected for velocity, altitude, and aircraft drift and roll. It also converts the radiometer output to brightness temperature.

Sensor Output and Specifications

a) general information

Manufacturer: MPB Technologies

RAF Resource Person(s): Julie Haggerty, Bruce Morley

b) primary output

Parameter names: TB37-1, TB37-2, TB90-1, TB90-2

Plain language names: orthogonal components of brightness temperatures at 37 and 90 GHz

Units: degrees Kelvin

Sensitivity: 1 K at 37 GHz

Beam width: 2.7 degrees at 37 GHz, 1 degree at 90 GHz

Resolution: 50 m at 90 GHz when aircraft at 3000 m altitude

Scan angles: ± 60 nominally (RAF installation reduces field of view to ± 54.5 degrees)

d) derived output

RAF parameter name: TB37A, TB90A, TB37H, TB37V, TB90H, TB90V

Plain language names: average brightness temperatures at 37 and 90 GHZ; vertically and

horizontally polarized components at 37 and 90 GHz

Dependencies: ALAT, ALON, PALT, ROLL, DRIFT

Data Processing

The primary effort involved in processing this data is the derivation of horizontally and vertically polarized components of the radiance (brightness temperature) measurements. Using the orthogonal components (e.g., TB37-1, TB37-2) together with measurements of scan angle, the horizontal and vertical components (TB37H, TB37V) can be derived from the relations,

$$P_H = \frac{P_2 \sin^2(\theta - 45) - P_1 \cos^2(\theta - 45)}{\sin^4(\theta - 45) - \cos^4(\theta - 45)}$$

and

$$P_V = \frac{P_1 \sin^2(\theta - 45) - P_2 \cos^2(\theta - 45)}{\sin^4(\theta - 45) - \cos^4(\theta - 45)}$$

where P_H and P_V are power levels for vertical and horizontal components, P_1 and P_2 are power levels on channels 1 and 2 of the AIMR, and θ is scan angle in degrees.

Corrections for aircraft pitch, roll, and drift are also made during post-flight processing.

Data Interpretation

Output is produced in the form of two-dimensional images of any of the parameters listed above.

Appearance of a given feature depends on its emissivity and physical temperature. For example, the emissivity of the ocean surface is very low, so open water surfaces will appear dark (cold) in AIMR images. Emissivity increases with roughness, so higher brightness temperatures are related to regions of high windspeed. Ice surfaces have higher emissivity than water and therefore appear warmer. New ice appears warmer than old ice. An example of a 90 GHz average brightness temperature (TB90A) image is shown in Figure 3.20. The strip of high brightness temperatures through the middle of the image is an Arctic lead which is beginning to freeze over.

This is a new instrument for RAF (as of this writing), so the applications and limitations of AIMR data have not been fully explored.

Figure 3.18 — Airborne Imaging Microwave Radiometer (AIMR)



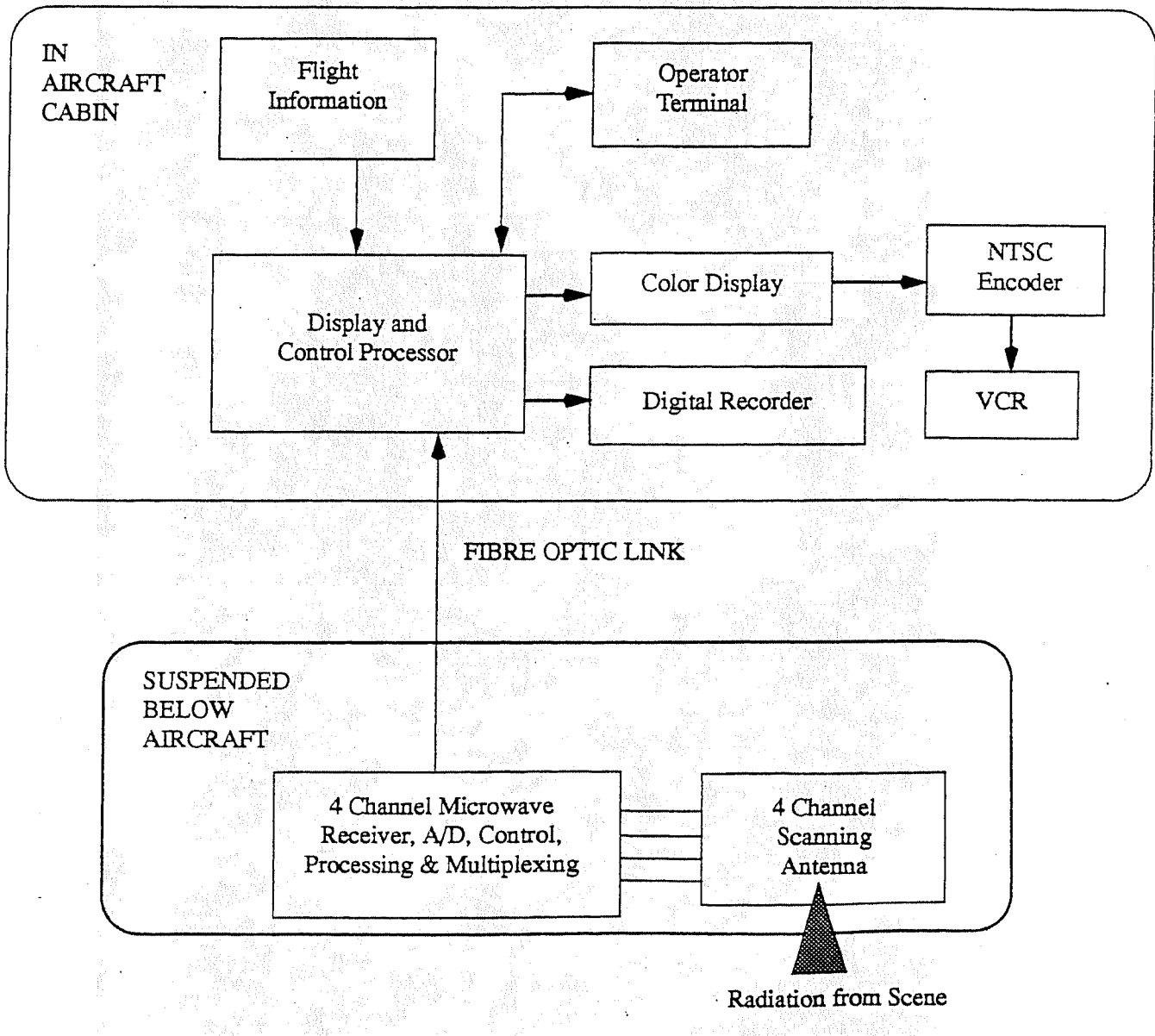


Figure 3.19 — Block diagram showing relationships between the AIMR components.



Figure 3.20 AIMR 90 GHz image of Arctic ice from BASE.
Bright areas represent leads in the ice.

Scanning Aerosol Backscatter Lidar (SABL)

Introduction

The Atmospheric Technology Division (ATD) of NCAR has developed an aerosol lidar for use from the Research Aviation Facility (RAF) aircraft and from Surface and Sounding Systems Facility (SSSF) Integrated Sounding System (ISS). The Scanning Aerosol Backscatter Lidar (SABL) was deployed for the first time during the Aerosol Characterization Experiment-1 (ACE-1) in late 1995. SABL was used as a nadir- and zenith-looking lidar system during ACE-1 and is expected to evolve over time into a cross track scanning volume imager. During ACE-1, SABL was used to map the vertical aerosol structure and illuminate the complex mixing processes of the marine boundary layer and the free troposphere over the southern oceans. These backscatter maps were used as a real-time guide for *in situ* sampling of air masses that had different backscatter properties and possibly different origins.

Operating Principles

The technical specifications for SABL are summarized in Table 1. The telescope is of Cassagrainian design with a 14-inch diameter and a speed of f/5. Some of our goals in the design of SABL were to maximize the signal-to-noise ratio and to build a stable instrument, one that would not require a lot of operator fine tuning to perform well. The critical components of the telescope are built of low expansion materials so that the optical performance will not change with large temperature changes. The receiver is built on an optical plate that is rigidly mounted to the base plate of the telescope. This was done to minimize the effect of vibration on system performance. To maximize the signal-to-noise ratio we have done several things in component selection. In the infrared channel we control the temperature of the silicon avalanche photodiode (APD) with a thermoelectric cooler. This does two things; it reduces the dark current noise of the detector and it keeps the gain of the detector stable. We also control the temperature of the photomultiplier tube (PMT) used to detect the green signal. The main benefit of cooling the PMT is not in reduced dark current but in gain stability. To reduce the background noise in the system we use narrow band interference filters. We have filters of less than 1.0 nm at this time and will obtain filters of less than 0.2 nm in the future. The system will then be dark current noise limited except under high background light level conditions. An example of high background conditions is found when looking at the top of a sunlit cloud.

A two-channel 12-bit, 40-MHZ digitizer is used in the receiver. Using these high dynamic range digitizers enables us to record the signals from the detectors without using logarithmic amplifiers. Removing the logamps from the receiver has made the analysis for quantitative aerosol properties easier and more accurate. For the operator and scientist displays, we have the option of displaying logarithmic/range corrected return signals or linear lidar data. Either the scientist or the lidar operator can save any interesting display image to a disk file by clicking on a button on the display screen. This image can be displayed or printed out at a later time to show colleagues.

Data Examples and Analysis

Figures 3.21(a) and 3.21(b) are examples of lidar scattering ratio data taken during a research flight to look at the Kilauea volcano plume. The scattering ratio is defined as the ratio of total backscatter to Rayleigh or molecular backscatter. The backscatter profiles are a one second average of 20 laser pulses. The C-130 is at an altitude of four kilometers above sea level and the lidar is nadir pointing. Both the 532nm and 1064nm return signals show a 'clean' atmosphere down to about 1700 meters above the surface where the Kilauea volcano plume is encountered. The plume is about 1100 meters thick and is above the marine boundary layer. The marine boundary layer extends from the surface to 600 meters. The scattering ratios at 532nm and 1064nm are at levels that are appropriate for naturally occurring aerosols. The 532nm scattering ratios are less than those at 1064nm because the scattering processes in the atmosphere at 532 nm are dominated by Rayleigh or molecular scattering. At 1064 nm atmospheric scattering is dominated by aerosols.

If you take the ratio of scattering ratios, it is possible to obtain some size information about the aerosols. Figure 3.22 is the ratio of 1064nm scattering ratio to the 532nm scattering ratio. In the clear air region of the atmosphere where Rayleigh scattering is dominate this ratio is close to one. The scattering processes are dominated by "large" particles in the marine boundary layer. This is evident by the large values in the ratio of scattering ratios from the surface to 600m. In the Kilauea plume the values are between those of the Rayleigh atmosphere and the marine boundary layer. This indicates that the aerosols are larger than molecules but smaller than marine aerosols. This is consistent with the evolution of aerosols from volcanoes.

The RAF resource people for SABL are Bruce Morley, Julie Haggerty and Larry Radke.

Table 1. SABL Specifications

Wavelength/energy	1064 nm/75 mJ - 532 nm/50 mJ
Pulse length	15 nsec
Pulse rate	Up to 60/second
Beam divergence	1 mrad to 4 mrad adjustable
Telescope diameter - speed	14 inch - f/5.
Telescope field-of-view	1 mrad to 5 mrad adjustable
Background filter bandwidths	0.92 nm @ 1064 nm/0.16 nm @ 532 nm
Detectors	Avalanche photo diode @ 1064 nm. Photomultiplier tube @ 532 nm
Digitizer - 2 channel - bits/speed	12 bits / up to 40 MHZ
Number of range gates per channel	Up to 2500
Recording media	Exabyte tape
Transmitter/Receiver Size - Weight	15 x 15 x 32 inches - 110 lbs
Computer/Operating System	VME Bus/VxWorks for data acquisition. Sun Sparc-5 for display and control

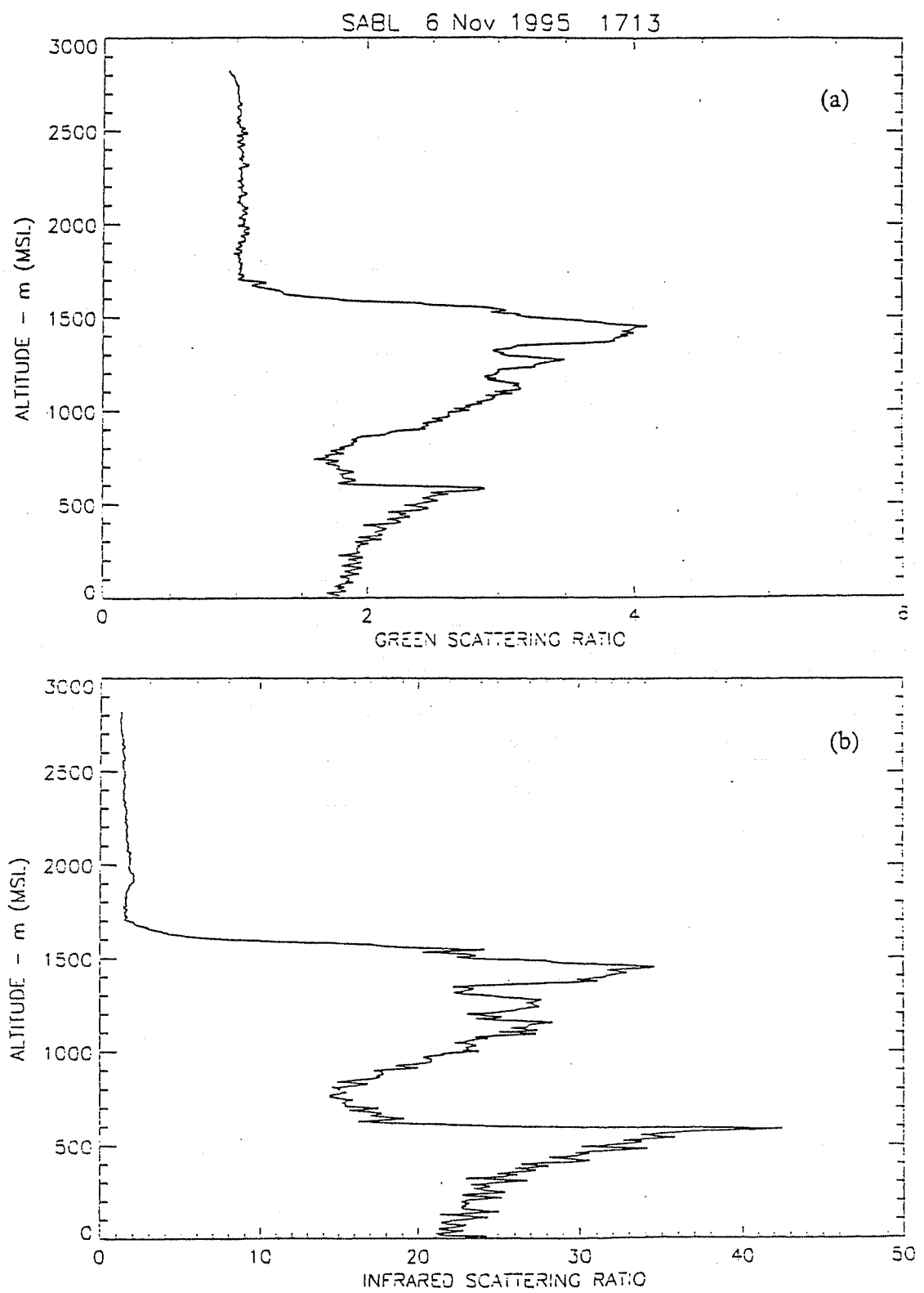


Figure 3.21. Scattering ratios at 532 nm (a) and 1064 nm (b).

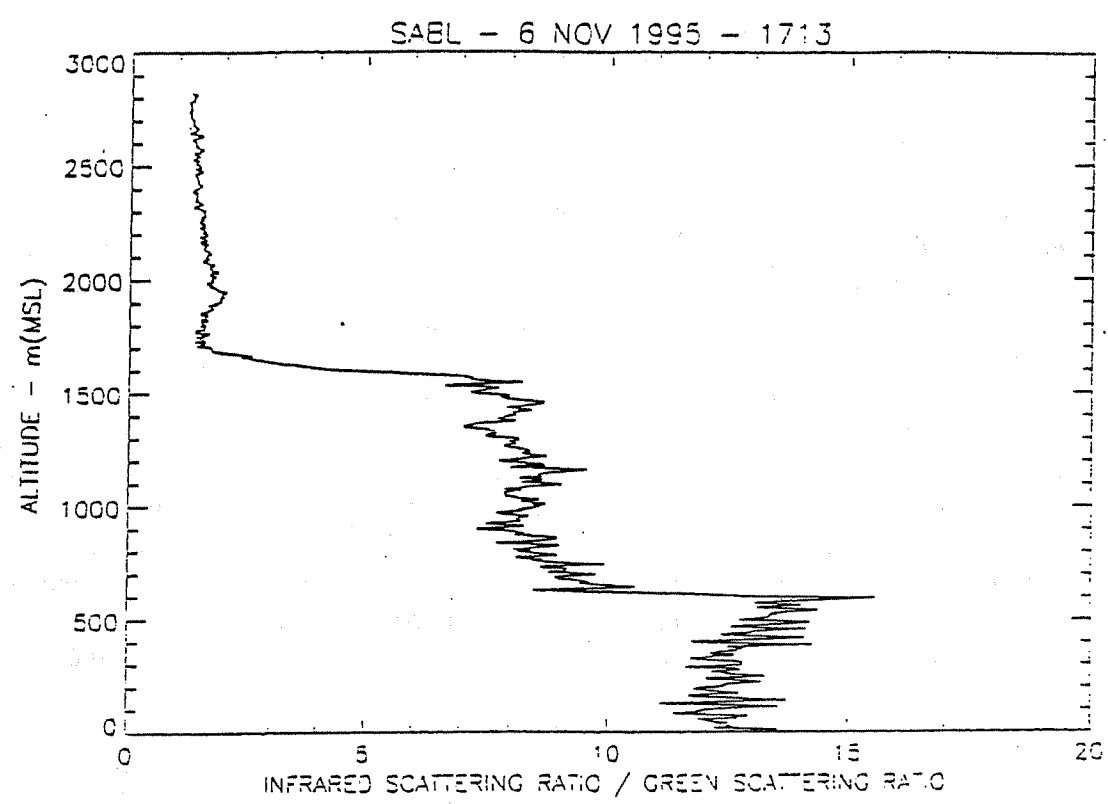


Figure 3.22. Ratio of scattering ratios.

SECTION 4—Chemical Sensors

Nitrogen Oxide Analytical System

Introduction

The nitrogen oxide analytical system at RAF can be configured to measure either NO (nitric oxide), NO_y (total reactive nitrogen oxides) or both. A photograph of this instrument is shown in Figure 4.1. The instrument is laboratory constructed. It is a joint development between the NOAA Aeronomy Laboratory and RAF.

Operating Principles

The fundamental analysis is the chemiluminescent reaction of NO with high concentrations of ozone, 3-5%. This produces NO₂ in an excited electronic state. The NO₂ chemiluminesces with emission in the red and infrared region. This is detected using a cooled photomultiplier. The analysis of both NO and NO_y utilize the same chemiluminescent analytical reaction. For the measurement of NO_y, an inlet is used, that converts the reactive nitrogen species to NO. This is accomplished by mixing the inlet air with CO to give a final concentration of 0.3%, and then passing the air stream over a gold tube heated to 325 C. NO_y is comprised of a number of different species, some which are very susceptible to loss on surfaces. To minimize this loss, a special inlet system has been designed, which mounts the converter partially outside of the aircraft. The air inlet utilizes a Rosemount temperature housing as the head. This takes the center core of the airstream and brings it directly to the heated inlet of the converter. Studies are presently underway to define the aerosol cut point of this inlet, and it appears to be about 2 microns. The inlet is heated to 200 C, and the CO added directly. This minimizes the loss of reactive nitrogen compounds on the inlet surfaces.

This system can also be used in conjunction with the one second ozone instrument. The instrument needs to be located on the aircraft where there is a fuselage aperture available to accommodate the 3.5 inch diameter converter unit in undisturbed air flow, and space for the rear facing NO inlet. These inlets should be located within about 1 meter of the analytical instruments. For the installation of the analytical instrumentation and supporting equipment, one full large aircraft rack is needed or two King Air racks. The totally configured instrument package weighs about 400 pounds.

The instrument is calibrated using a standard cylinder of NO cal gas. This is either used in a standard addition mode on top of ambient air or on zero air. The standard cylinder is referenced to a NIST NO SRM. For additional checking on the conversion efficiency of the NO_y inlet, a back titration system is implemented to convert the NO to NO₂, which is then run through the converter.

Sensor Output and Specifications

The detection limit of the NO/NO_y analytical system is better than 50 pptv for a one second average. The detection limit can be enhanced by optimization of the instrument. The uncertainty is ± 15%.

The instrument requires 9 analog channels, 2 digital counting channels and one digital parallel channel for full operation with the data system. Some of the housekeeping analog channels do not need to be recorded if there is a shortage of channels on the data system.

a) general information

Manufacturer: NCAR and NOAA Aeronomy Lab
RAF Resource Person: Greg Kok

b) outputs

XNMBT, temperature of the gold NO_y converter, in deg C. This is a 0-10V analog channel.

XNCLF and XNOCF are the calibration flows for the NO_y and NO instruments respectively. These are 0-5 V output.

XNZAF and XNOZA are the zero air flows to back flush the NO_y and NO inlets respectively, typically at takeoff and landing. These flows are used to give a yes/no indication if the instrument is sampling ambient air or zero air. The output of each channel is 0-5 V.

XNSAF and XNOSF are the sample flows through the NO_y and NO instruments respectively. These flows are typically 1 SLPM. The signal output is 0-5 V.

XNBTF is the back titration flow through the NO_y instrument. This is a 0-5 V signal.

XNCOF is the CO flow to the NO_y inlet. This is typically set at 3 sccm. The signal output is 0-5 V.

XNOY and XNO are the raw data counts from the NO_y and NO instruments respectively. These are TTL pulses of about 50 ns wide.

XNST is the parallel digital line for the status of the NO_y and NO instruments. For XNST of zero the instrument is in the measure mode. Typically the instruments are operated simultaneously with both in zero or calibrate at the same time. For XNST of 5, the instruments are in the zero mode, for XNST of 10, the instruments are in the calibrate mode.

The data processing is a two pass process using the spline program. Each parameter needs to be baseline corrected separately. The selected variable is XNOY or XNO and the status is XNST. Four seconds are allotted for settling time during the transition. The counts are averaged during the zero operations, and this forms the zero baseline when these values are fit to a cubic spline. These parameters are XNOYZRO and XNOZRO for NO_y and NO respectively. These zero values are subtracted from the signals XNOY and XNO to give the baseline corrected data, XNOYCOR and XNOCOR. Linear calibrations are applied to this data to give the corrected data XNOYCAL and XNOCAL for corrected NO_y and NO concentrations respectively.

Data Interpretation

The instrument requires a long warmup time to reach optimum performance. No less than 1.5 hours of full operation before a flight should be allocated. For the best stability, a minimum of 3 hours of warmup is recommended. The NO_x analytical system has spikes in the data when operating in cloud. This is potentially due to cloud water evaporation on the heated inlet and the resultant aspiration of the nitrogen aerosols into the inlet.

Plots of NO and NO_x concentrations are shown in Figures 4.2 and 4.3.

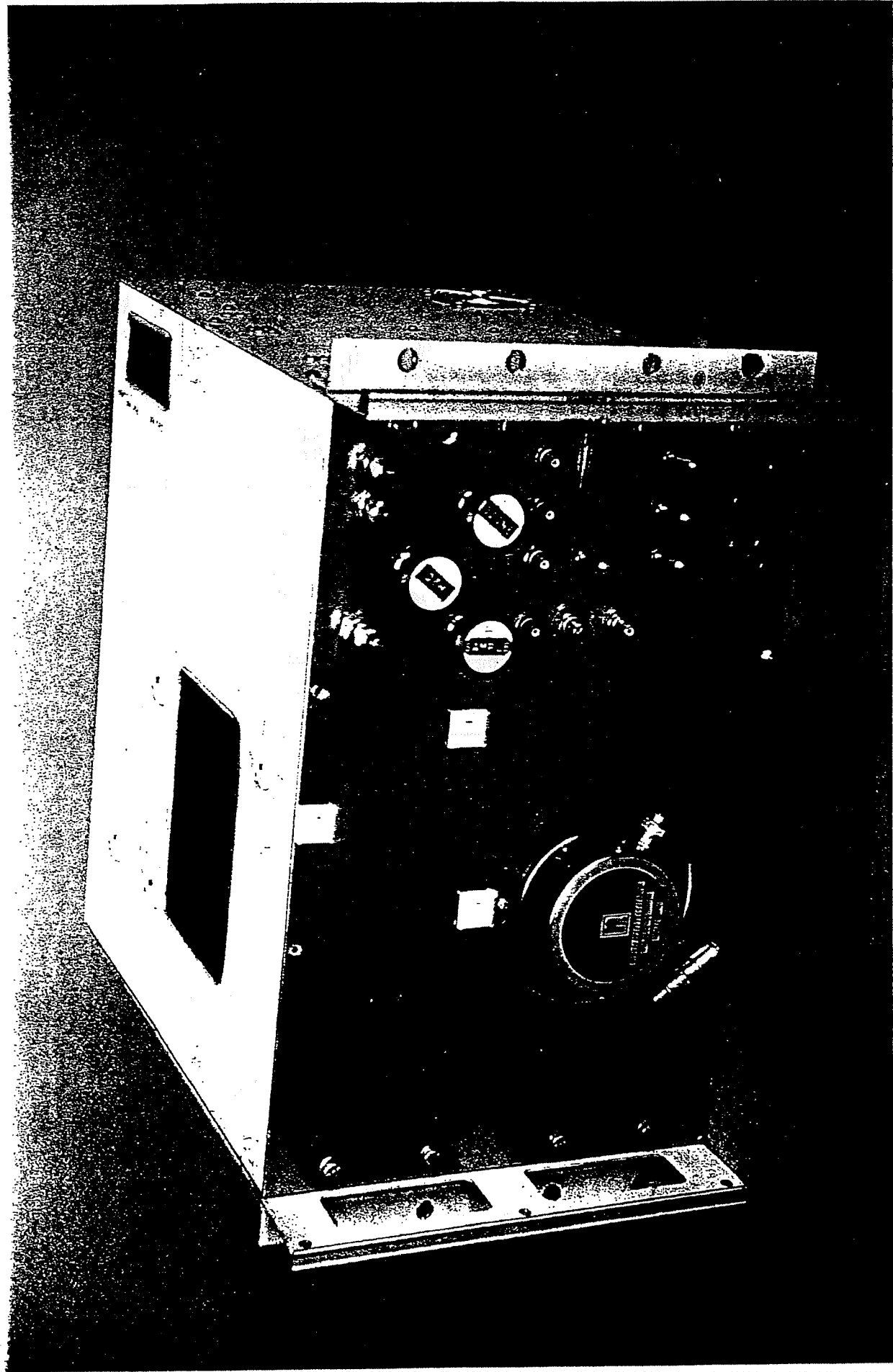


Figure 4.1 — Nitrogen Oxide Analytical System

Hong Kong - 201, Flight #91

11/16/1994, 07:00:00-08:00:00

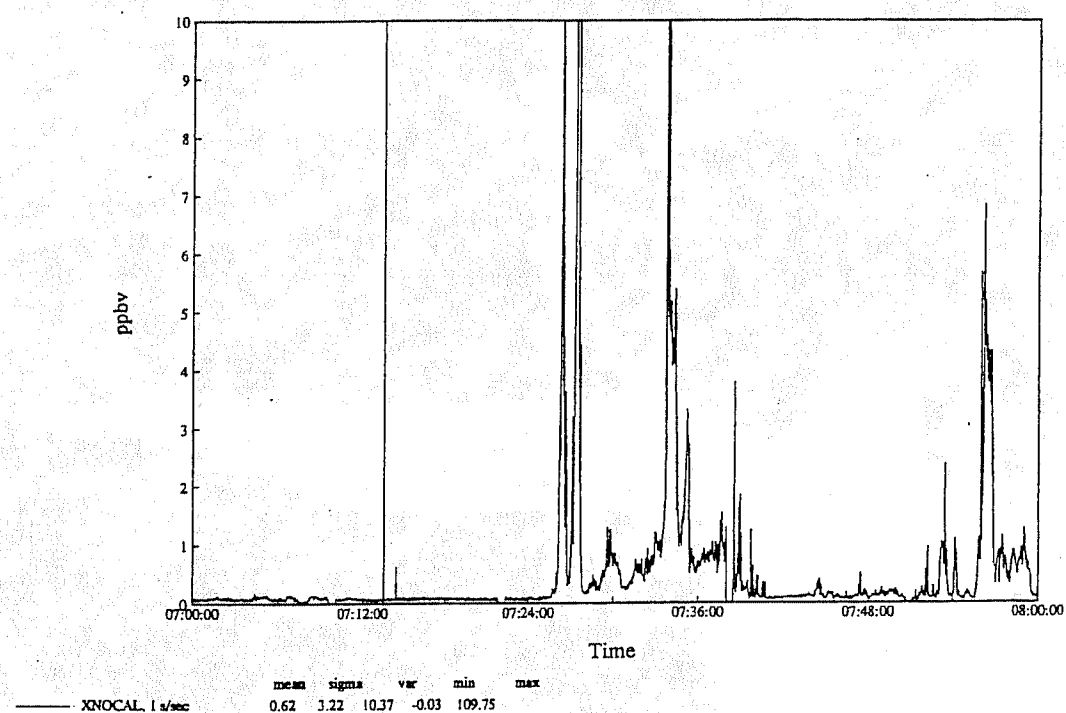


Figure 4.2 — Plots of NO and NO_y concentrations

Hong Kong - 201, Flight #91

11/16/1994, 07:00:00-08:00:00

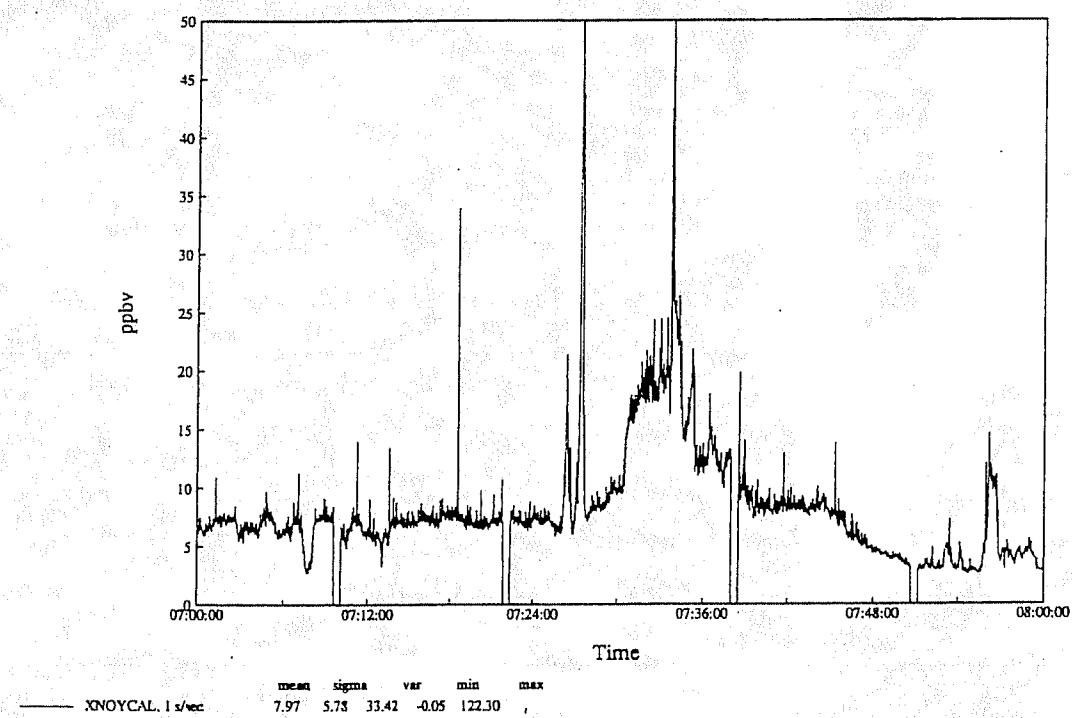


Figure 4.3 — Plots of NO and NO_y concentrations

RAF "Fast" Ozone Analyzer

Introduction

The RAF fast ozone analyzers determine ozone concentrations by measuring some of the chemiluminescent light generated by ozone's reaction with nitric oxide (NO). This is the reverse of the method commonly used to measure various odd-nitrogen species in air. The RAF instrument draws upon earlier instruments used by Stedman and Pearson. Figure 4.4 is a photograph of this instrument.

Operating Principles

The ozone-nitric oxide reaction produces light mainly in the near infrared. A small fraction of the light produced overlaps the 600-900 nm wavelength range at the long wavelength end of the light detectible by a cooled, red-sensitive photomultiplier tube (PMT). The RAF chemistry group has deployed a number of variants of this instrument, depending upon the objectives and constraints of the particular project. Two PMT-cooling options are available, a Freon refrigerated system and a dry-ice cooled system. The dry-ice cooled system tends to produce a signal with less noise, and is generally preferred if dry ice is readily available. The tray containing the dry-ice cooler is also considerably lighter than that containing the refrigerated unit (about 28 lb versus 66 lb). The other major variation, which has been used when weight was a constraint and the fast response needed for eddy-correlation flux estimates has not been a goal, is to reduce the sample flow and reactor size from 300+ LPM and ~330 ml, respectively, to about 250 cc/m and 20 ml. This variant, called "semi-fast" ozone, has been used in several air pollution studies in the King Air, in which avoiding the ~70 lb. weight of the pump used in the large-flow version was important. A smaller NO bottle was used in these King Air projects to avoid most of the 50 lb weight of the usual bottle and containment box.

The NO reagent used in these instruments is 99 percent pure, and is a toxic gas. A containment box vented through one inch diameter tubing to the outside of the aircraft is used to avoid the potential danger from a regulator failure. An NO detector and alarm are in operation during flight to minimize any danger from leaks which may develop in the small diameter, low pressure plumbing outside the containment box.

Installation of the fast ozone instruments involves a rear-facing inlet, CLEAN PFA Teflon tubing between that inlet and the reactor, and a preferably short, one inch diameter or larger dump of the material flowing from the reactor through the sample pump. The NO bottle and plumbing must be done with care to ensure safety; it is usual practice that a member of the RAF chemistry group install these and operate the instrument in flight.

Sensor Output and Specifications

a) general information

Manufacturer: NCAR/RAF
RAF Resource Persons: Dick Schillawski and Greg Kok

b) primary outputs

<u>Parameter Name</u>	<u>Plain Language Name</u>	<u>Units</u>
03FS	voltage from PMT	V
03FN	NO flow	sccm
03FP	reactor pressure	mb
03FF	sample flow	slpm
03FT	reactor temperature	C
03FV	PMT high voltage	V

c) derived output

<u>Parameter Name</u>	<u>Plain Language Name</u>	<u>Units</u>
03FC	calibration ozone conc.	ppbv

Usually not all of these outputs are recorded because of data-system limitations. The units shown are valid after calibration factors are applied by the RAF data system. The output of the fast ozone instrument increases very linearly with ozone concentration increases, and the baseline zero is very stable. Ideally, all that should be required to produce a calibrated output is a single proportionality factor. In practice, the situation is not quite that simple. The reactor reflectivity tends to decrease over the course of a project, and sometimes other adjustments need to be made. Usually a different calibration factor has been derived for each research flight based upon preflight calibration against the TECO 49 analyzer sampling ozonized bottled air (to avoid the aerosol interference in the TECO 49) and/or comparisons of the in-flight results produced by the two different analyzers. The calibrated output is O3FC, or some variation thereof, in ppbv.

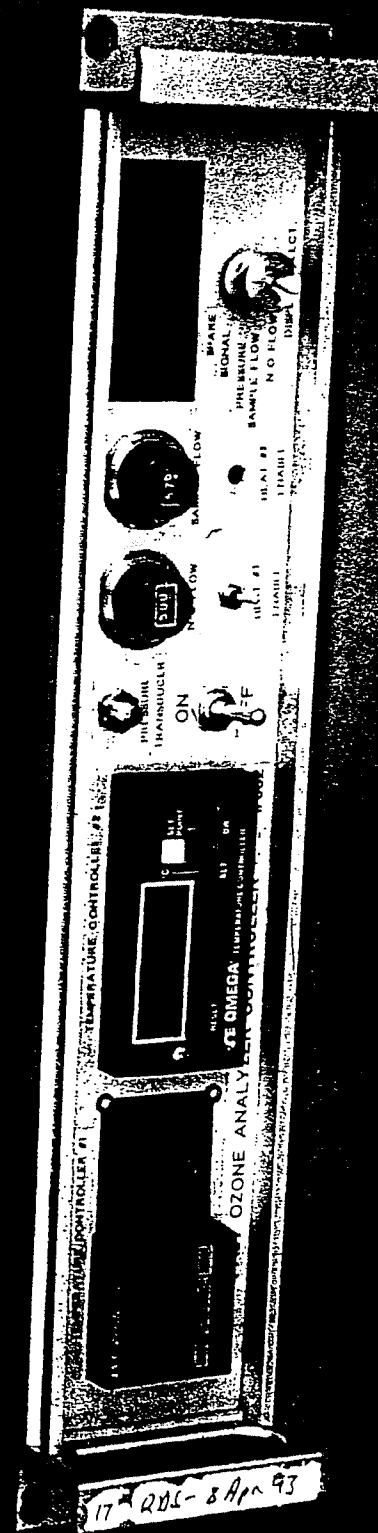
Data Interpretation

Typical ozone concentrations encountered are included in the discussion of the TECO 49 ozone analyzer. The accuracy of the fast ozone results is dependent upon that of the TECO 49 used for calibration; a multipoint calibration is capable of reducing the quantization problem of the TECO 49 and producing a statistically reliable proportionality factor. The fast ozone results do not share the TECO 49's problem of roundoff error, and interference by aerosols is negligible. The data do require a correction for humidity because collisions with the water molecule are very efficient quenchers of excited nitrogen dioxide; these corrections are applied in data processing and are not large in magnitude. A major use of the fast ozone data is estimating ozone fluxes based upon the eddy-correlation method. This method requires fast response which is taken into account in design of the system. To date, frequency spectrums of fast-ozone data collected in the marine boundary layer, where turbulence is usually minor compared to over land, display shot noise at their high-frequency ends; the eddy-correlation method is believed to be tolerant of reasonable levels of uncorrelated noise.

The RAF instruments are still undergoing some development. The instrument used in the ACE-1 project will probably be operated at lower pressures than in the past to allow easier in-flight calibration checks. Improved reactor temperature control is also on the list of planned modifications.

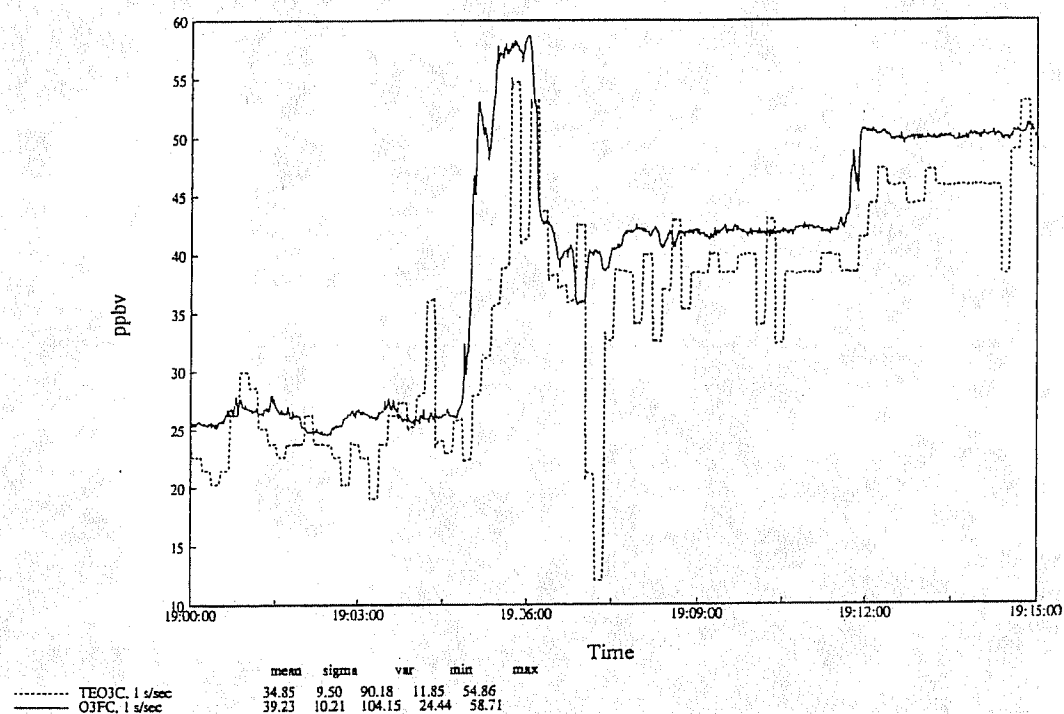
Figure 4.5 shows an example of output from this instrument.

Figure 4.4 — RAF "Fast" Ozone Analyzer



BOREAS - 818, Flight #5

6/6/1994, 19:00:00-19:15:00



Example of output from the "Fast" Ozone Analyzer

Figure 4.5

TECO 49 Ozone Analyzer

Introduction

This instrument measures ozone concentrations in air using the ultraviolet (UV) absorption method. It weighs about 50 pounds, and is usually rack mounted inside the aircraft. Ozone concentrations are of interest in many projects, but the TECO 49 has limitations in speed and resolution which make it unsuitable for some programs; in some cases interferences from aerosols and water can also be a problem. The instrument's calibration is extremely stable, requiring no adjustment over periods of years, which makes it very useful for calibration of other ozone measuring instruments. RAF's chemistry group maintains a dedicated transfer-standard instrument which is periodically checked against a NIST reference photometer. Figure 4.6 is a photograph of the instrument.

Operating Principles

Internally the TECO 49 has two measurement cells, which are tubes about 0.5 inch in diameter by 14 inches long. These are operated in a cycle 20 s long, with one cell measuring the reduction in UV light intensity caused by both ozone and all other species, while the other cell is measuring the reduction in intensity in essentially the same air from which the ozone has been removed by an ozone-destroying catalyst. The cells' functions are reversed half way through the cycle, with the measuring cell changing to the "zeroing" or reference function, and vice versa. The UV light used is confined to the 254 nm line at which ozone strongly absorbs. The ozone concentration is determined by the difference between the sample-side UV absorption and the reference-side absorption using Beer's law. This calculation is performed by the internal microprocessor, which also controls the cycle timing.

The aircraft inlet for the TECO 49 should be rear-facing and preferably located near the front of the aircraft. Installation includes a CLEAN, and preferably short, length of 1/4 in PFA Teflon tubing between the aircraft inlet and the instrument's inlet, plus a dump line of generic material between the instrument's output and outside the aircraft. The purpose of the dump is to reduce the workload of the TECO 49's internal sample pump, especially at high altitudes where it may be unable to overcome the pressure difference between the cabin and the ambient pressure. Clean inlet tubing is essential since ozone is easily destroyed; cleaning even new tubing with a flow of air with a relatively high ozone concentration overnight is highly recommended before installation aboard the aircraft.

Sensor Output and Specifications

a) general information

Manufacturer: TECO
RAF Resource Person(s): Dick Schillawski and Greg Kok

b) primary output

Parameter Name	Plain Language Name	Units
TEO3	voltage proportional to ozone conc.	V
TET	digital signal representing cell temp.	C
TEP	digital signal representing cell pres.	mb

c) derived output

<u>Parameter Name</u>	<u>Plain Language Name</u>	<u>Units</u>
TEO3C	corrected ozone concentration	ppbv

The RAF data system applies calibration factors to change these raw signals into units of ppb, C, and mb, respectively. The cell pressure and temperature are then applied to TEO3 using the ideal gas equation to calculate TEO3C, the corrected ozone concentration in ppbv.

Data Interpretation

Generally, TET should be 20-45 C, and TEP should be slightly below the ambient pressure outside the airplane (PSFDC). Reasonable corrected ozone numbers are 30-70 ppbv in "clean" continental air and 5-20 ppbv in "very clean" marine air; values above 200 ppbv are sometimes encountered in polluted air and are usual in the lower stratosphere. The detection limit of the TECO 49 is about 2 ppbv with an accuracy of 4 ppbv or three percent, whichever is greater. TEO3 is output in 1 ppbv "quanta" every half cycle (10 s); averaging over a full cycle produces the best results. It should be noted that at $\frac{1}{2}$ atmosphere (~ 18 kft) the ideal gas correction converts the 1 ppbv quanta of TEO3 into about 2 ppbv quanta in TEO3C, and the phenomenon gets worse with increasing altitude.

The TECO 49 has three problems which limit its usefulness. The first is that TEO3 is output rounded to the nearest ppb, which means that little information about the fine structure of the ozone concentration can be resolved, especially in clean air. This is compounded by its slow response speed, which is much too slow for such calculations as eddy-correlation flux estimates. The slow update speed also limits the usefulness of sounding data from the instrument.

The third problem is mainly caused by the ozone-destroying catalyst through which the air flowing to the reference cell flows. This acts to some extent as a filter, and aerosols tend to be slowed down, if not stopped, by it. This results in more UV light-scattering or light-absorption by aerosols in the sampling cell than in the reference cell, and an over-estimation of the ozone concentration. After passage into relatively cleaner air, the process can be reversed with aerosols delayed by the catalyst progressing into the reference cell and an under-estimate of ozone occurring. This under-estimate can continue for periods of $\frac{1}{2}$ hour or more. On a much shorter time scale of a few minutes, the same behavior can be seen in data from soundings; moisture tends to be delayed by the catalyst causing underestimates of ozone concentration on the ascents as the moisture concentration decreases, and overestimation on the descents. Using a filter in the incoming sample air has been attempted to remedy the aerosol problem but proved ineffective; the material collecting on the filter turned it into an ozone destroyer.

In summary, the TECO 49 has an extremely stable calibration. Its results are reliable within the limits quoted above, but it is not capable of producing data suitable for all purposes, particularly in air where high aerosol concentrations are also present. In these latter cases, it is best used to calibrate other ozone-measuring instruments, which in general do not share its stable calibration.

Figure 4.5 is an example of output from this sensor.

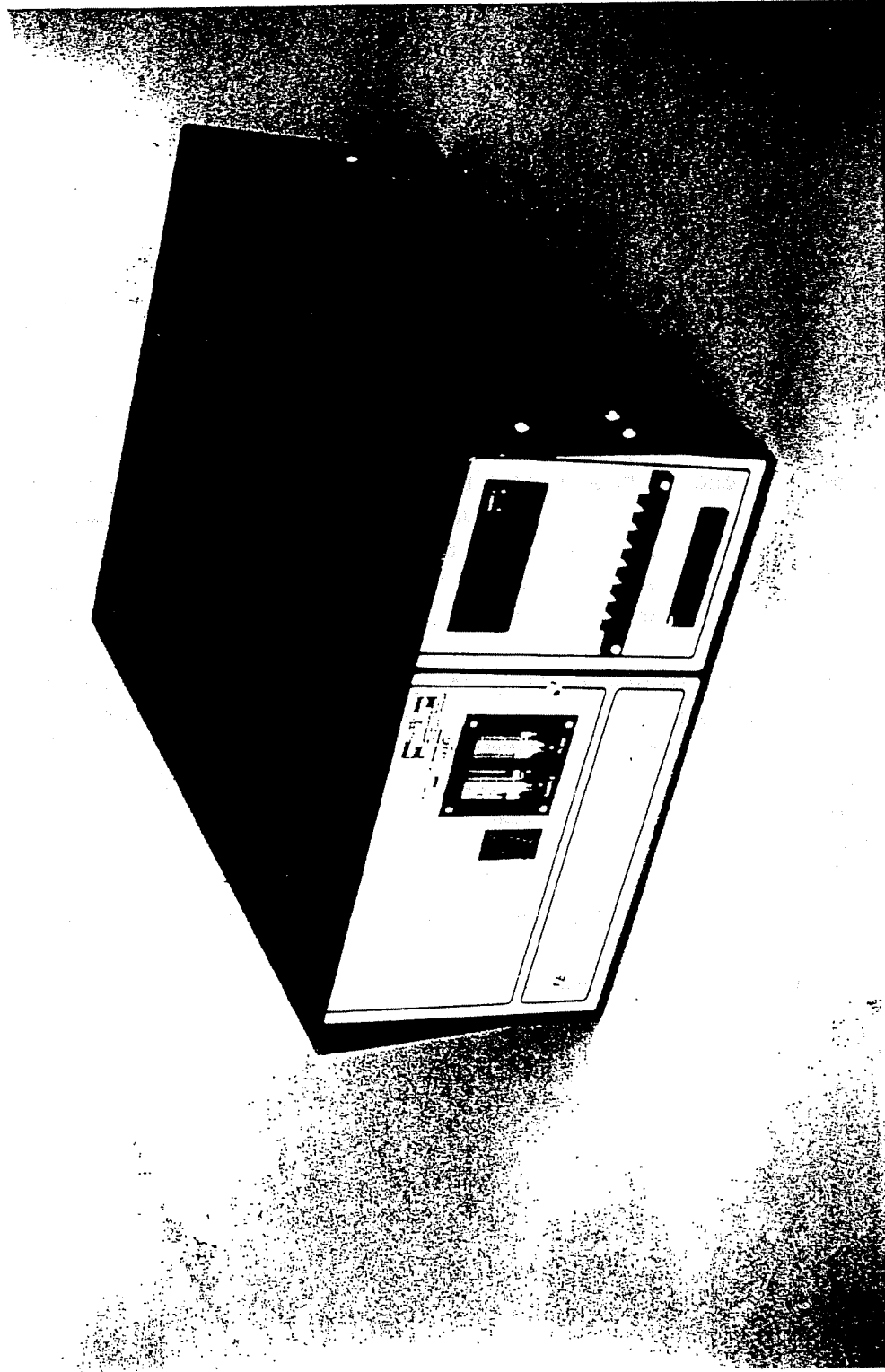


Figure 4.6 — TECO 49 Ozone Analyzer

TECO 48 Carbon Monoxide Analyzer

Introduction

Carbon monoxide is determined using a modified TECO 48 gas correlation analyzer. A photograph of this instrument is shown in Figure 4.7.

Operating Principles

The analytical technique is based on the gas filter correlation principle. The infrared absorbance of the gas in the sample cell is compared to that of pure CO gas in the reference cell. This offers a high degree of specificity in the analysis. The instrument is highly modified from the original TECO design. A diagram of the optics and electronics is given in Figure 4.8.

The optical system has been enhanced with the addition of a lens just ahead of the detector. This increases the amount of light reaching the detector. This modification follows the paper of Dickerson and Delany (1988). A major problem with the instrument is a baseline drift that is temperature dependent. With an increase in operating temperature, the baseline will drift negative. The exact source of this problem is unknown. To compensate for this, a heated palladium zero trap has been added, and the instrument is operated in a mode of two minutes zero, and five minutes measure. The data is then fit to this baseline for correction. Additional temperature control has been added to the optical bench to increase stability.

A rear facing inlet is recommended using 3/8 or 1/2 inch Teflon tubing. The ambient air is brought up to cabin pressure using a KNF diaphragm pump. Most of this flow is over vented to the cabin. The CO instrument samples at cabin pressure using the internal pump. To eliminate the interference of water vapor on the instrument, all sampling is done through a CaSO₄ (Dririte) trap. To maintain a stable sample flow through the instrument, a mass flow controller is used to control the sample flow at 3 SLPM.

The instrument is calibrated using standard span gas. This cylinder is compared to a NIST SRM.

Sensor Output and Specifications

a) general information

Manufacturer: TECO
RAF Resource Person(s): Dick Schillawski and Greg Kok

b) primary output

<u>RAF Parameter Name</u>	<u>Plain Language Name</u>
CO	raw carbon monoxide concentration
CMODE	status parameter

The signal output is 0-10 volts, parameter CO on the data system, units VDC. The CO range that this corresponds to can be set on the front panel of the instrument. It is imperative that the person responsible for the instrument keep track of the front panel switch settings. Changes in these will influence the span of the final data set. The standard instrument output averages the data to 10 seconds. The EPROM in the instrument has been replaced with a one second update version, however the factory diagnostics are not enabled. A second analog channel is needed to record the status parameter, CMODE, units VDC. This is also a 0-10 V output, and a one second recording is adequate.

c) derived output

<u>RAF Parameter Name</u>	<u>Plain Language Name</u>
COZRO	baseline zero signal
COCOR	corrected baseline carbon monoxide
COCAL	calibrated carbon monoxide

The data processing is a two pass process, that utilizes the program spline. This program selects the times when the instrument is in the zero mode, indicated when the CMODE parameter is at 8.0 volts or greater. Typically 20 seconds is allowed for the signal to reach the stable zero value, and the program averages the data for the rest of the zero, to obtain the zero baseline point. These values are fit to a cubic spline to generate the baseline zero signal, COZRO. This parameter is subtracted point by point from the raw signal, CO, to obtain the zero corrected baseline, COCOR. A linear calibration is applied to this value to obtain the zero corrected and calibrated signal, COCAL. The spline program asks for both an intercept and a slope value to be applied to generate the COCAL value. Since the spline program generates a new zero for the data, the intercept will generally be zero for these applications.

Data Interpretation

The instrument is sensitive to turbulence, and in the boundary layer, the signal can have considerable noise. It is recommended that the data be averaged to 10 seconds for best results. The detection limit of the instrument is 10 ppbv, with an uncertainty of 20% for data averaged to 30 seconds. The response time is approximately 30 seconds considering both the inlet system and the instrument itself.

Figure 4.9 is an example of data from this sensor. (See previous page for Figure 4.9)

No Photograph Available

Figure 4.7 — TECO 48 Carbon Monoxide Analyzer

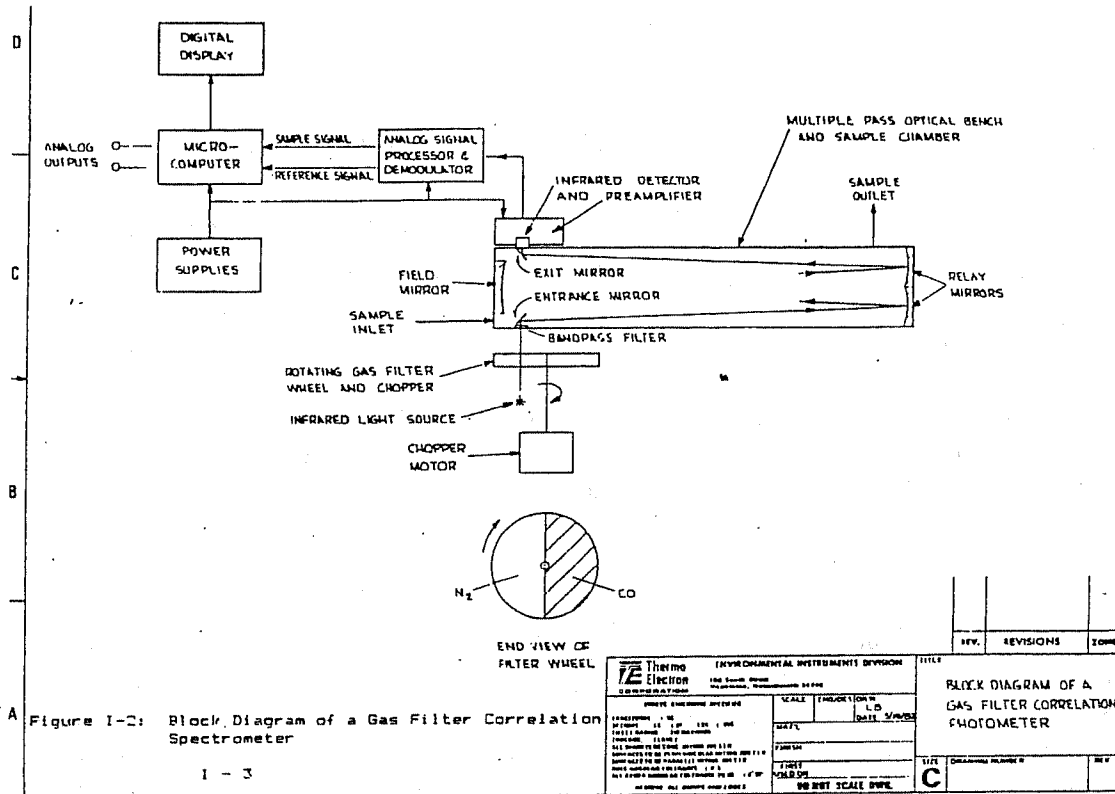


Figure 4.8 —Diagram of the TECO 48 optics and electronics

Hong Kong - 201, Flight #91

11/16/1994, 07:00:00-08:00:00

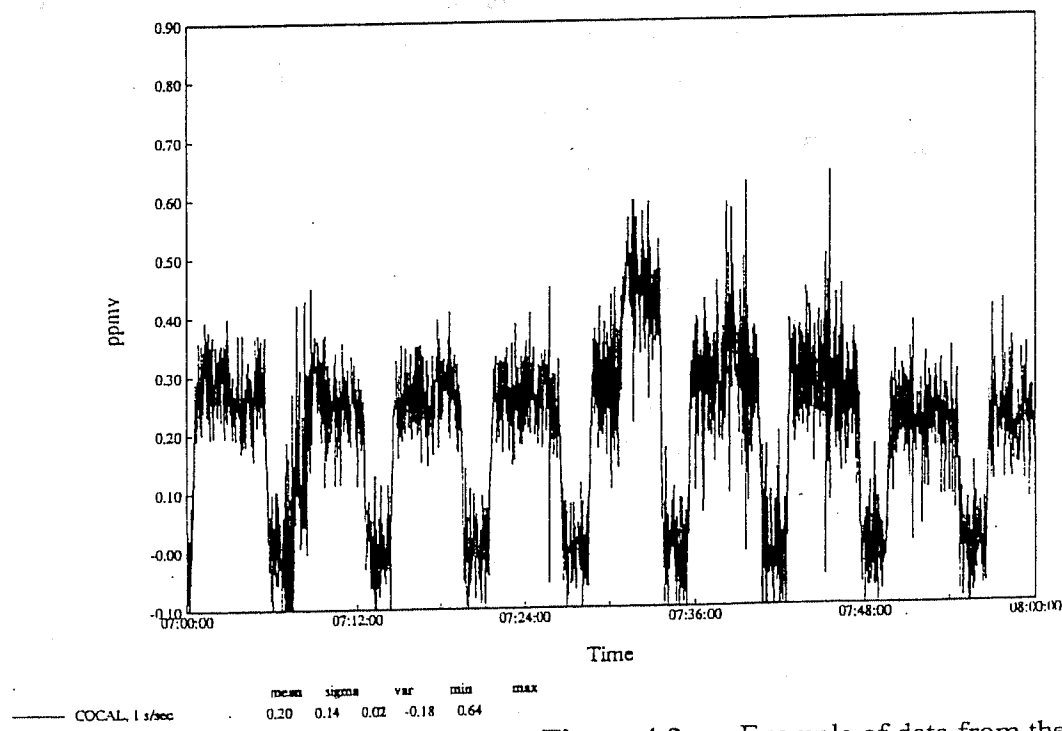


Figure 4.9 — Example of data from the TECO 48 Carbon Monoxide Analyzer

SECTION 5—Aerosol Sensors

Passive Cavity Aerosol Spectrometer Probe PCASP-100 Aerosol Probe

Introduction

The Passive Cavity Aerosol Spectrometer Probe (PCASP) Model 100 is an instrument developed by Particle Measuring Systems (PMS, Inc., Boulder, Co) for the measurement of aerosol particle size distributions. This sensor is utilized in studies of tropospheric chemistry and aerosol physics.

Operating Principles

The PCASP is of that general class of instruments called optical particle counters (OPCs) that detect single particles and size them by measuring the intensity of light that the particle scatters when passing through a light beam. The schematic diagram shown in Figure 5.1 illustrates the optical path of this instrument. A Helium Neon laser beam is focused to a small diameter at the center of an aerodynamically focused particle laden air stream. Particles that encounter this beam scatter light in all directions and some of this light is collected by a mangin mirror over angles from about 35° - 135°. This collected light is focussed onto a photodetector and then amplified, conditioned, digitized and classified into one of fifteen size channels. The size of the particle is determined by measuring the light scattering peak intensity and using Mie scattering theory to relate this intensity to the particle size. The size information is sent to the data system where the number of particles in each channel is accumulated over a preselected time period. Figure 5.2 shows a typical size distribution where the number, surface area, and volume concentration of particles in each size category is shown, normalized by the width of the size channel. Figure 5.3 is a photograph of the PCASP inside a canister that is normally mounted on an aircraft pylon.

Sensor Output and Specifications

a) general information

Manufacturer:	Particle Measuring Systems, Inc., Boulder, Co.
RAF Resource Person(s):	Darrel Baumgardner
Calibration Method:	Monodispersed polystyrene latex beads
Range:	0.1 μm - 3.0 μm
Accuracy:	$\pm 20\%$ (Diameter) $\pm 16\%$ (Concentration)

b) primary output

RAF Parameter Name	Plain Language Name	Description
APC01-15	Channels 1-15	15 channels of accumulated counts

c. derived output

RAF Parameter Name	Plain Language Name	Description
CONCP	Concentration	# off particles per unit volume - number per cubic centimeter
SFCP	Surface Area	Total surface area - micrometers squared per cubic centimeter
VOLP	Volume	Total particle volume - Cubic micrometers per cubic centimeter
DBARP	Average Diameter	Arithmetic average of particle size - micrometers

$$CONCP = \sum_{i=1}^{i=15} \frac{n_i}{V}; SFCP = \pi \sum_{i=1}^{i=15} \frac{n_i d_i^2}{V}; VOLP = \frac{\pi}{6} \sum_{i=1}^{i=15} \frac{n_i d_i^3}{V}; DBARP = \frac{\sum_{i=1}^{i=15} n_i d_i}{\sum_{i=1}^{i=15} n_i}$$

where n_i is the number of particles detected in size channel I, d_i is the diameter represented by channel I, and V is the sample volume measured in a given sample period.

Data Interpretation

The PCASP was developed as an aerosol particle measurement instrument. The size that is determined by the PCASP assumes that the scattered light detected is from a spherical particle of refractive index 1.58. The size distributions produced from these measurements must be viewed with great caution when in mixed composition aerosols. Particles will not be correctly sized due to their different refractive indices and non-spherical shapes (Kim, 1995; Liu, et al, 1992). Volatile particles will also lose part of their mass because of heating in the inlet and sample cavity (Liu, et al, 1992).

The probability of more than a single particle coinciding in the beam or being missed during the electronic reset time increases with concentration. Corrections are applied to account for these losses but still lead to concentration uncertainties.

The PCASP is a particle sizing instrument, not a particle surface area or volume probe. Since the surface areas and volumes are derived by integrating the size distribution, uncertainties in the size measurement lead to root sum squared uncertainties in surface area and volume a factor of two and three times higher, respectively.

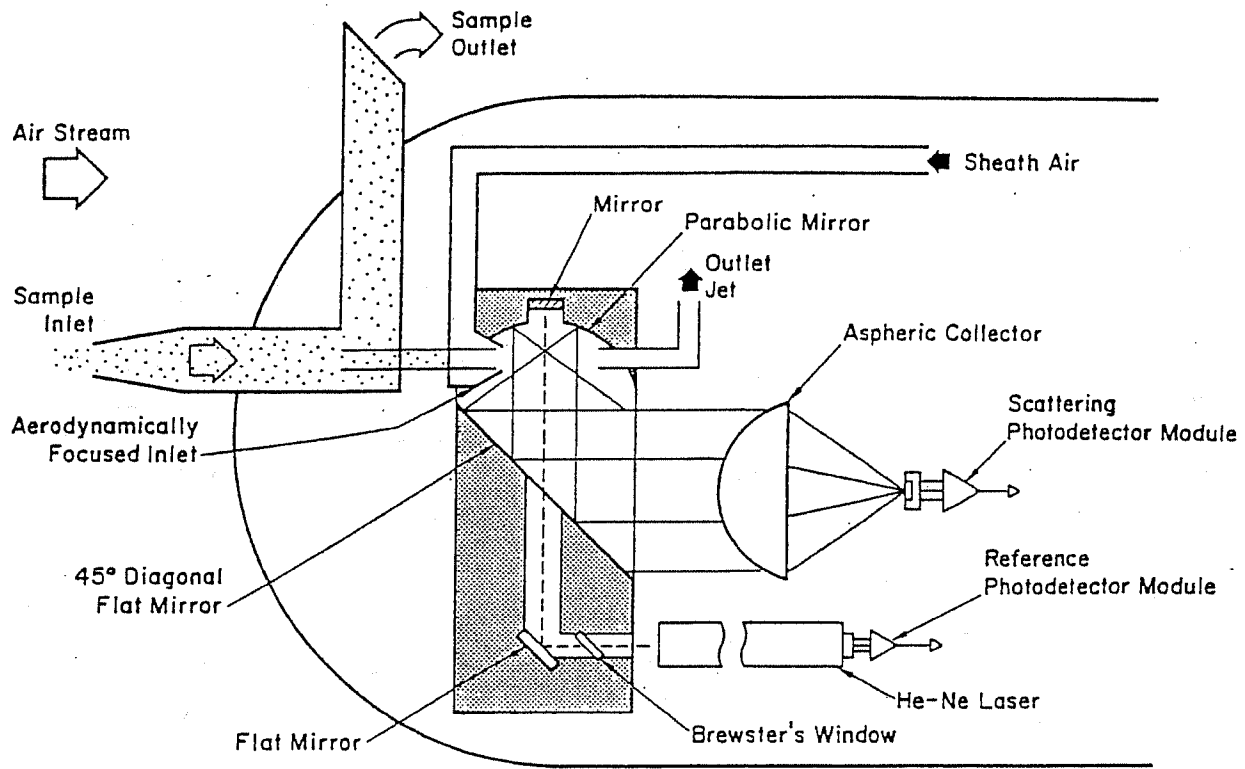


Figure 5.1 - Passive Cavity Aerosol Spectrometer Probe (PCASP) optical path

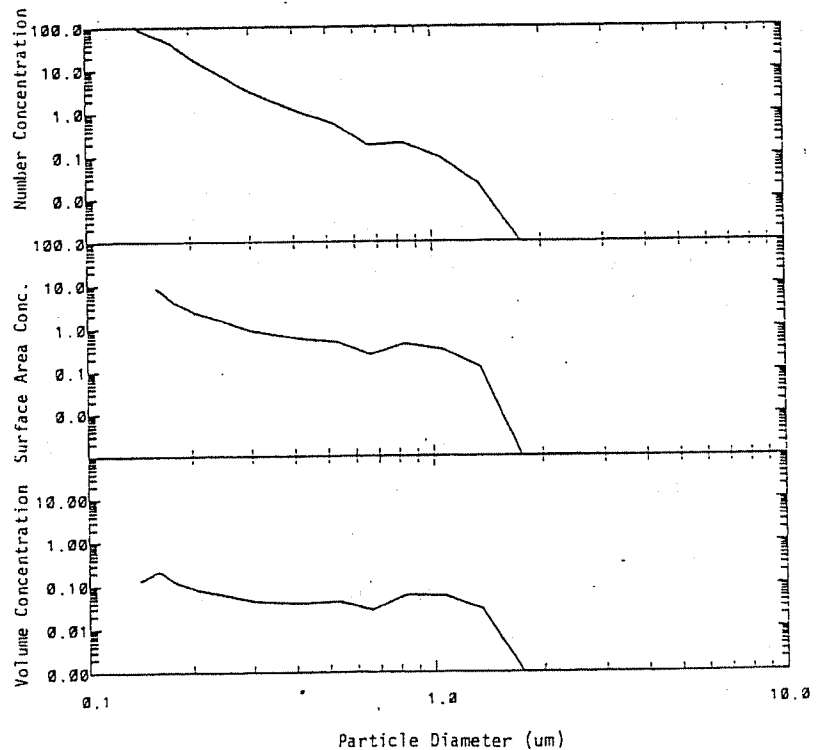


Figure 5.2 - Typical size distribution where the number, surface area, and volume concentration of particles in each size category is shown, normalized by the width of the size channel from the PCASP

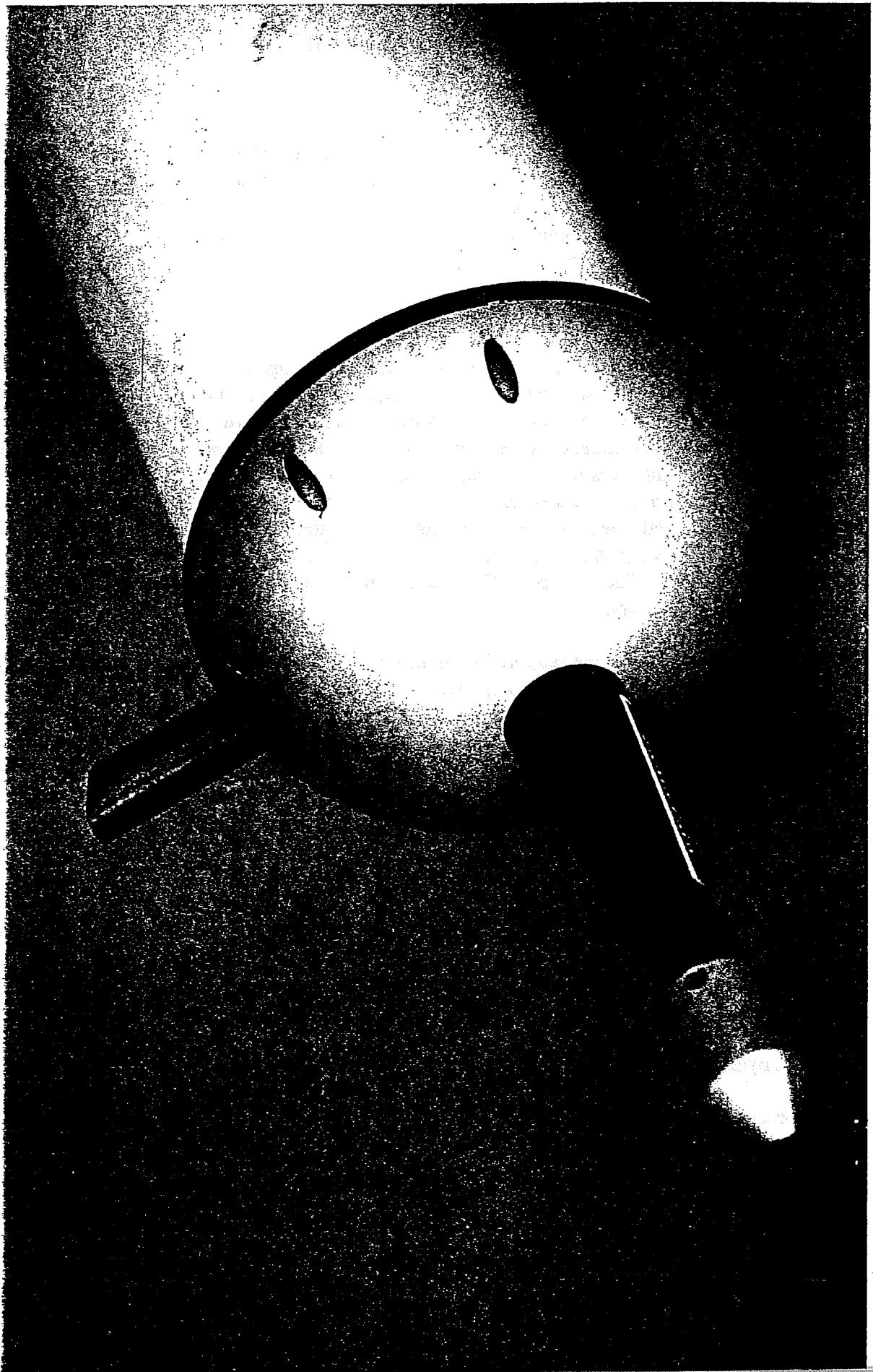


Figure 5.3 — Passive Cavity Aerosol Spectrometer Probe

Forward Scattering Spectrometer Probe

FSSP-300 Aerosol Probe

Introduction

The Forward Scattering Spectrometer Probe (FSSP) Model 300 is an instrument developed by Particle Measuring Systems (PMS, Inc., Boulder, Co) for the measurement of aerosol particle size distributions. The sensor was originally developed for the study of stratospheric aerosol distributions and polar stratospheric clouds but is now widely utilized in studies of tropospheric chemistry and aerosol physics.

Operating Principles

The FSSP-300 is of that general class of instruments called optical particle counters (OPCs) that detect single particles and size them by measuring the intensity of light that the particle scatters when passing through a light beam. The schematic diagram shown in Figure 5.4 illustrates the optical path of this instrument. A Helium Neon laser beam is focused to a small diameter at the center of an inlet that faces into the oncoming airstream. This laser beam is blocked on the opposite side of the inlet with an optical stop, a "dump spot", to prevent the beam from entering the collection optics. Particles that encounter this beam scatter light in all directions and some of that scattered in the forward direction is directed by a right angle prism through a condensing lens and onto a beam splitter. The "dump spot" on the prism and aperture of the condensing lens define a collection angle from about 4° - 12°.

The beam splitter divides the scattered light into two components, each of which impinges on a photodetector. One of these detectors, however, is optically masked to receive only scattered light when the particles pass through the laser beam within a region 0.5 mm either side of the center of focus. Particles that fall outside that region are rejected when the signal from the unmasked detector exceeds that from the masked detector. This defines the sample volume that is needed in order to calculate particle concentrations.

The size of the particle is determined by measuring the light scattering intensity and using Mie scattering theory to relate this intensity to the particle size. Figure 5.5 illustrates how the scattered light varies with particle diameter given that the particle is spherical and that the refractive index is known. The size is categorized into one of 31 channels and this information is sent to the data system where the number of particles in each channel is accumulated over a preselected time period. Figure 5.6 shows a typical size distribution where the number, surface area, and volume concentration of particles in each size category is shown, normalized by the width of the size channel. Figure 5.7 is a photograph of the FSSP-300 in the canister that is normally mounted on an aircraft pylon.

Sensor Output and Specifications

a) general information

Manufacturer: Particle Measuring Systems, Inc., Boulder, Co.
RAF Resource Person(s): Darrel Baumgardner
Calibration Method: Monodispersed polystyrene latex beads

Range: $0.3 \mu\text{m} - 20.0 \mu\text{m}$
 Accuracy: $\pm 20\%$ (Diameter)
 $\pm 16\%$ (Concentration)

b) primary output

RAF Parameter Name AFS301-31 FRST3	Plain Language Name Channels 1-31 Total Resets	Description 31 channels of accumulated counts Total Particles passing through the beam
--	--	--

c) derived output

RAF Parameter Name CONC3	Plain Language Name Concentration	Description $\#$ of particles per unit volume - number per cubic centimeter
SFC3	Surface Area	Total surface area - micrometers squared per cubic centimeter
VOL3	Volume	Total particle volume - Cubic micrometers per cubic meter
DBAR3	Average Diameter	Arithmetic average of particle size - micrometers

$$\text{CONC3} = \sum_{i=1}^{i=31} \frac{n_i}{V}; \text{SFC3} = \pi \sum_{i=1}^{i=31} \frac{n_i d_i^2}{V}; \text{VOL3} = \frac{\pi}{6} \sum_{i=1}^{i=31} \frac{n_i d_i^3}{V}; \text{DBAR3} = \frac{\sum_{i=1}^{i=31} n_i d_i}{\sum_{i=1}^{i=31} n_i}$$

where n_i is the number of particles detected in size channel I, d_i is the diameter represented by channel I, and V is the sample volume measured in a given sample period.

Data Interpretation

The FSSP-300 was developed as an aerosol particle measurement instrument (Baumgardner, et al, 1992). The size that is determined by the FSSP assumes that the scattered light detected is from a spherical particle of refractive index 1.58. The size distributions produced from these measurements must be viewed with great caution when in mixed composition aerosols. Particles will not be correctly sized due to their different refractive index and non-spherical shapes. The probability of more than a single particle coinciding in the beam or being missed during the electronic reset time increases with concentration from about 5% losses at 300 cm^{-3} to greater than 30% at 1000 cm^{-3} . Corrections are applied to account for these losses but still lead to concentration uncertainties.

The FSSP is a particle sizing instrument, not a particle surface area or volume probe. Since the surface areas and volumes are derived by integrating the size distribution, uncertainties in the size measurement lead to root sum squared accuracies in surface area and volume a factor of two and three higher, respectively.

CCN/IN Counter

Principle of Operation

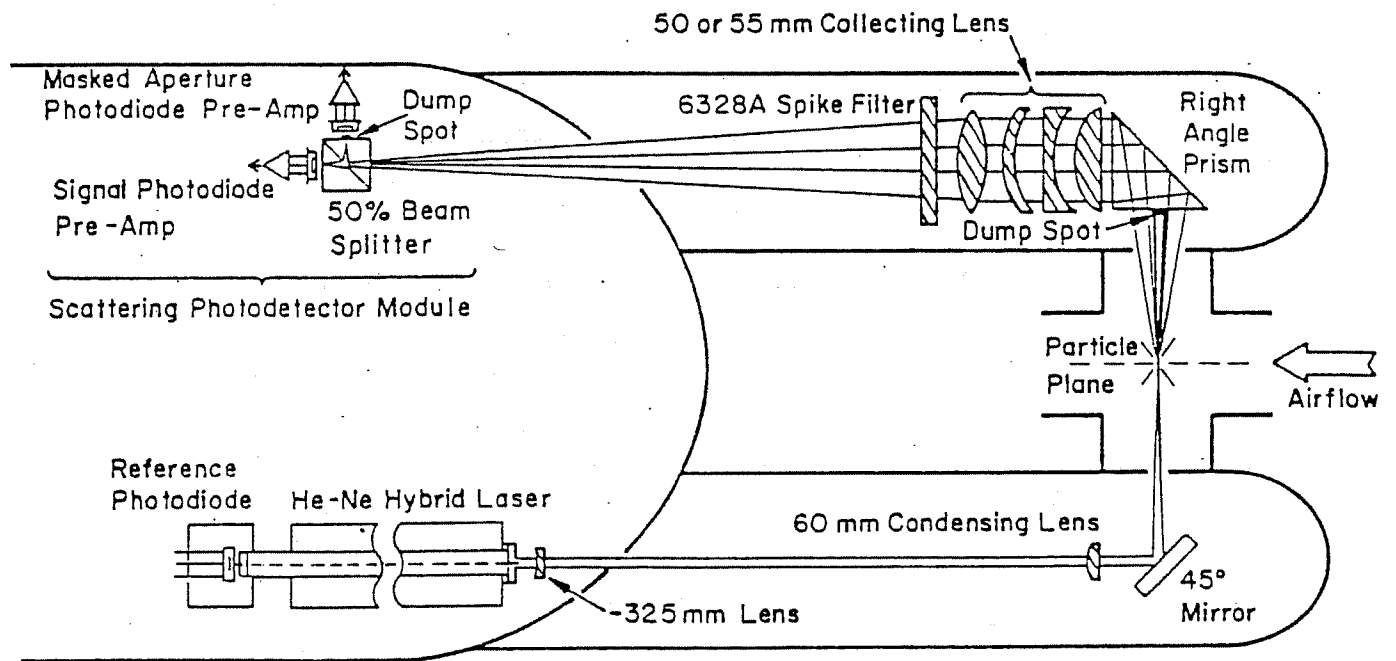
Soluble particles are exposed to controlled humidity in an isothermal chamber, grown to detectable sizes as either ice or water, and detected by an optical counter. Humidity is controlled by varying the pressure difference across a set of capillary tubes, one to supply the aerosol sample and others to provide sheath flow around the aerosol sample. Humidity can be maintained at small supersaturations with respect to water for activation of cloud condensation nuclei, or below water saturation at low temperature to detect ice nucleation from the freezing of solution droplets. Operation is continuous but provides a measurement at only one supersaturation; the instrument can change supersaturation to cover supersaturations in the range from 0.1-1% in less than 5s.

The instrument is under development, so characteristics are design targets rather than confirmed results. A schematic diagram of the CCN/IN counter is shown in Figure 5.8.

Sample volume: Typically $100 \text{ cm}^3 \text{s}^{-1}$ for CCN operation, 1 l s^{-1} for ice detection.

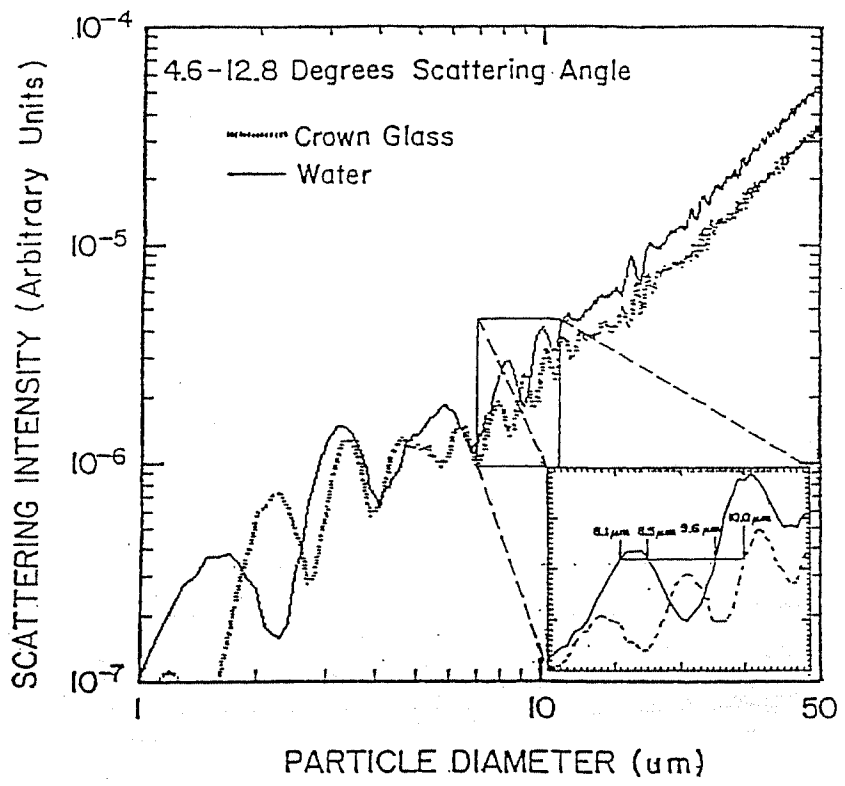
Supersaturation range: 0.1-5% for CCN operation; from ice saturation to water saturation for IN detection.

RAF Resource Person: Cindy Twohy, Bruce Gandrud



The optical path of the Forward Scattering Spectrometer Probe (FSSP) Model 300

Figure 5.4



Variation of scattered light with particle diameter for the FSSP

Figure 5.5

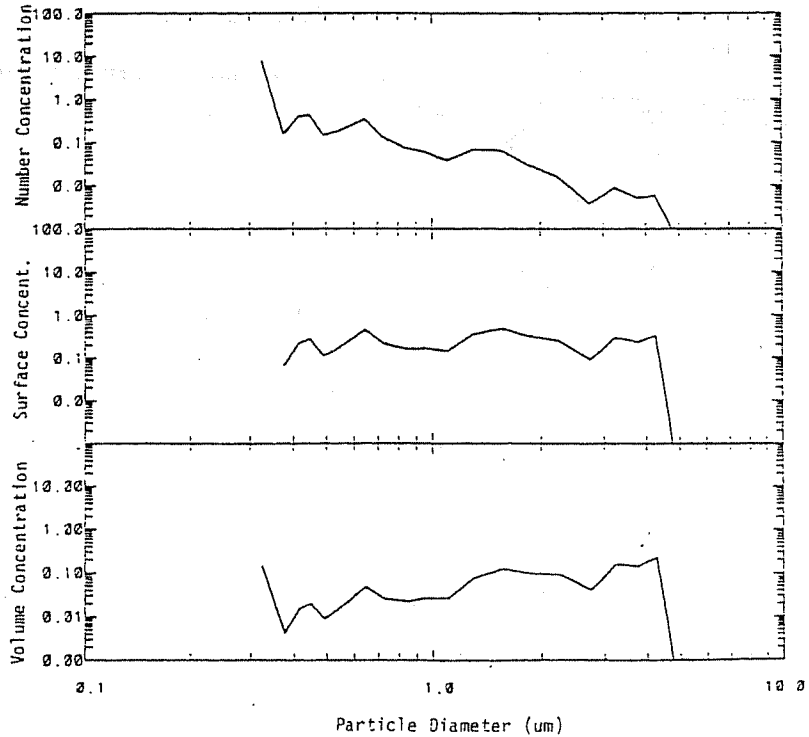


Figure 5.6 - Typical size distribution along with the number, surface area, and volume concentration of particles in each size category

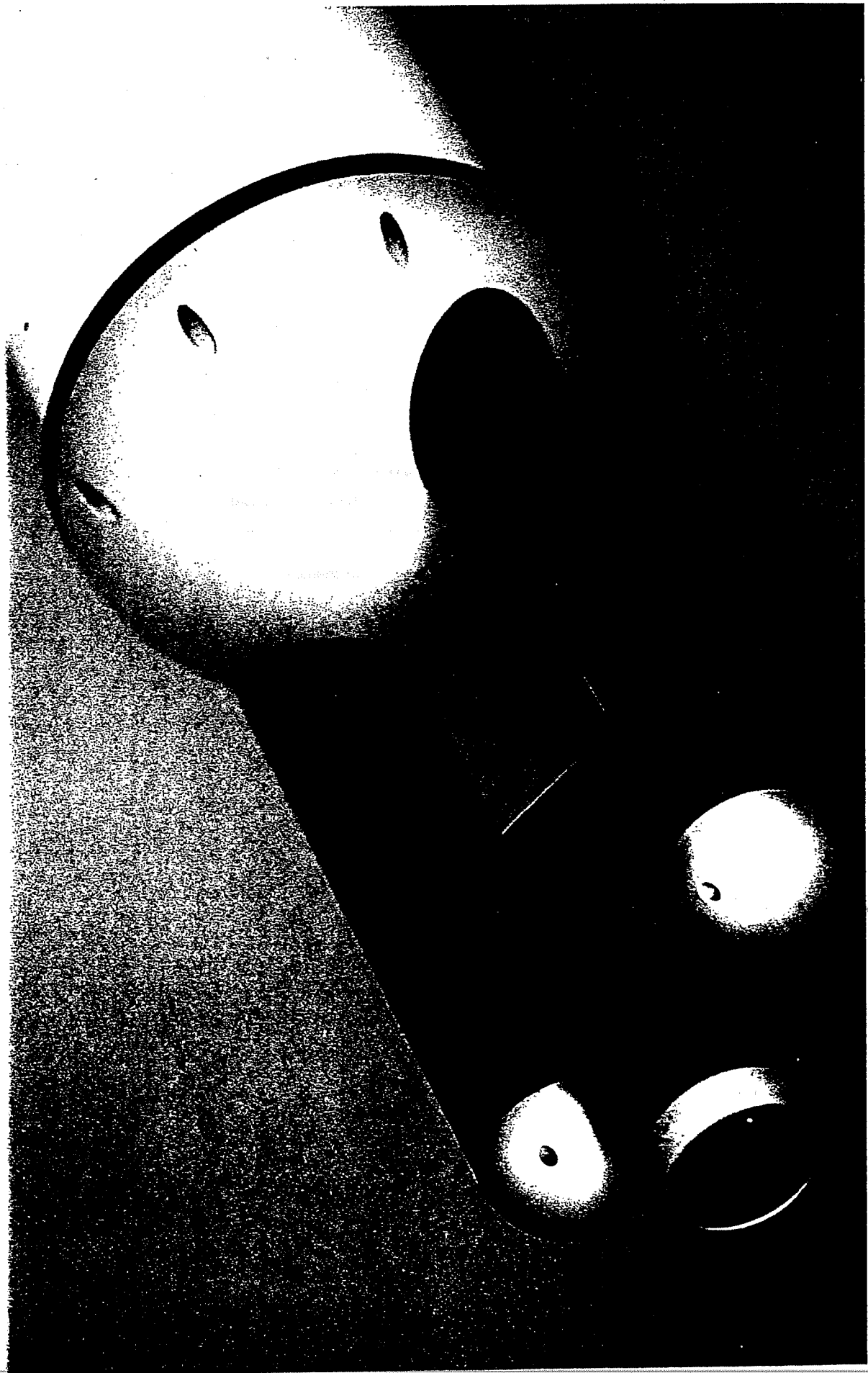
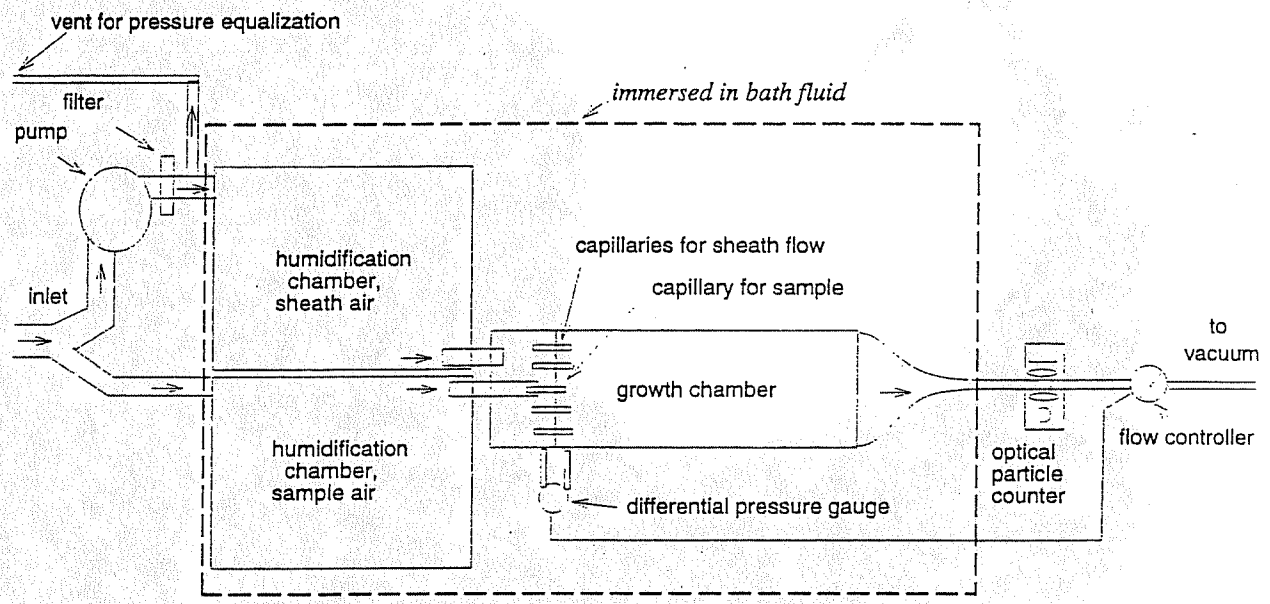


Figure 5.7 — Forward Scattering Spectrometer Probe



Schematic diagram of the CCN/IN counter

Figure 5.8

Airborne Condensation Nucleus Counter

Introduction

In response to an increased interest in aerosol and chemical measurements, RAF has modified a TSI, Inc., Model 3760 condensation nucleus (CN) counter in order to measure particle concentrations throughout the troposphere. The counter has been flown successfully on the Electra and C-130 as a stand-alone device, but may also be used downstream of various instruments (e.g., a counterflow virtual impactor or differential mobility analyzer) to measure particle concentrations. More details can be found in NCAR Tech Note NCAR/TN-356+EDD.

Principles of Operation

The TSI CN counter measures the number concentration of particles larger than about 0.01 micrometers in diameter. The particles are detected by condensing n-butyl alcohol (butanol) on the particles, which allows them to grow to a size that can be detected by a single particle optical detector. The sample flow is drawn into a sponge-like alcohol reservoir where it is saturated with butanol vapor. The sample is then cooled in a condenser tube, where the vapor supersaturates and condenses on the particles. After the particles have grown, they are passed through a laser-diode optical detector which counts them. Since all particles are grown to about the same size in the condenser, the CN counter does not resolve particle concentration by size.

Several modifications or additions have been made to the factory instrument (Figure 5.9) for operation on NCAR aircraft (Figure 5.10). The following have been added: an isokinetic sampling inlet, a charcoal filter to trap butanol vapor, two flowmeters, a vacuum pump, and an external exhaust port. Inside the instrument, the "purge" airflow (only necessary for clean room operation) has been capped off. The filter between the inlet and saturator has been replaced with one with a smaller pressure drop, which allows the internal pressure to equalize more easily at high altitudes.

Flow through the CN counter is maintained by an external vacuum source, and controlled by a critical orifice inside the instrument. The sample flow (FCN) is monitored by a Sierra mass flowmeter, which measures in standard liters per minute (slpm). Since the conditions at the CN inlet are generally not standard (1013 mb and 21 °C in this case), the flowmeter output must be corrected to volumetric liters per minute (vlpm). This flow rate (FCNC) is calculated by the onboard software from flow, temperature, and pressure inputs. The exhaust line is dumped outside the aircraft for two reasons: to remove any excess butanol vapor from the cabin, and to improve the pump efficiency at low ambient pressures.

The CN counter inlet is designed to be "isokinetic", meaning that the flow velocity just inside the inlet equals the airstream velocity. A sideflow (XICN, corrected volumetric value XICNC) supplements the CN sample flow in order to bring the TOTAL flow at the inlet approximately up to the required isokinetic flow rate. The sideflow valve is adjusted during project test flights to bring the total flow to within 10% of isokinetic at the typical research airspeed and altitude for each project.

Sensor Output and Specifications

a) general information

Manufacturer: TSI, Inc.
RAF Resource Person(s): Cindy Twohy

b) primary output

<u>Parameter Name</u>	<u>Plain Language Name</u>	<u>Units</u>
CNTS	counts	s ⁻¹
FCN	CN flow rate	slpm

c) derived output

<u>Parameter Name</u>	<u>Plain Language Name</u>	<u>Units</u>
CONCN	concentration	cm ⁻³
FCNC	corrected CN flow rate	vlpm

CN concentration (CONCN, cm⁻³) is calculated by dividing the digital count output (CNTS, s⁻¹) by the sample flow rate (FCNC, vlpm), with an additional correction for coincidence. The volumetric flow rates FCNC and XICNC are calculated from the mass flow rates FCN and XICN (slpm), respectively, and the input pressure (PCN) and temperature (CNTEMP). Normal values for CONCN range from less than a few hundred per cubic centimeter in clean air (high altitude or marine environments) to 10^4 cm⁻³ or more in polluted air.

At high concentrations, two or more particles may be present in the viewing volume at once and produce a single pulse. This "coincidence" error is statistically corrected in post-processing, and increases from about 0.6% at 10^3 cm⁻³ to 6% at 10^4 cm⁻³. At concentrations higher than about 2×10^4 cm⁻³, data should be used qualitatively, rather than quantitatively, due to the large coincidence errors. There is approximately a two second delay between when particles enter the inlet and are recorded on the data system. The instrument responds to changes faster than this, however, requiring less than 1/6 second to shift from 10% to 90% of the maximum concentration.

No direct calibration of the CNC is required, since one pulse is well above the electronic noise level and corresponds to exactly one particle (except at very high concentrations, as discussed before). The pressure transducer and flowmeters are calibrated before each project, and the data system outputs, especially CNTS, are verified with other methods. The CNC optics are also cleaned occasionally if necessary.

Data Interpretation

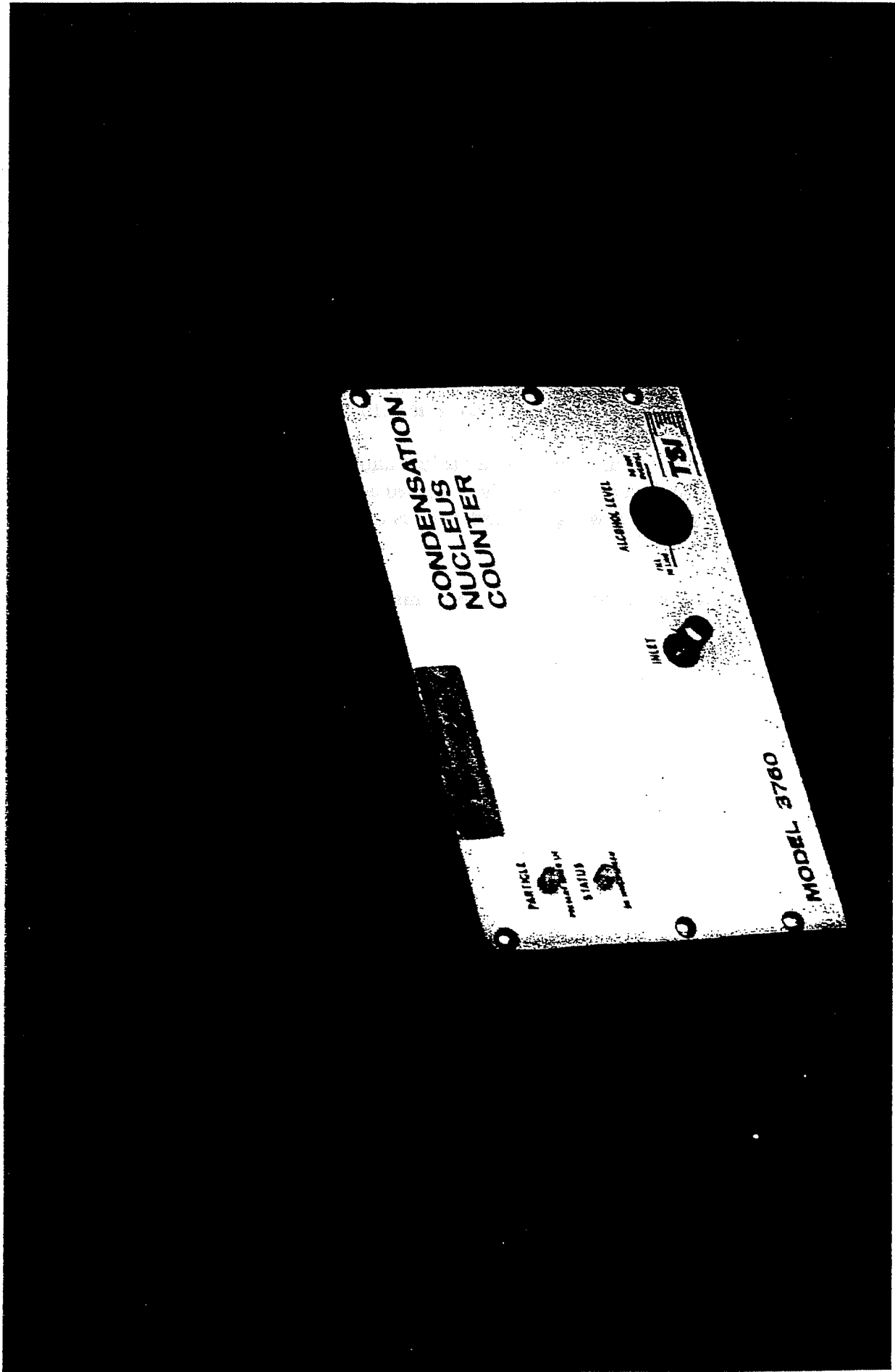
The CN inlet is small and unheated; therefore this instrument is not recommended for use under icing conditions. Also, measurements within cloud may not be accurate as droplet/crystal shattering can occur upstream of the instrument. With prolonged operation in humid environments, water may be ingested into the butanol reservoir, lowering the instrument's efficiency. Under such circumstances, the butanol should be drained and replaced after about every ten hours of operation.

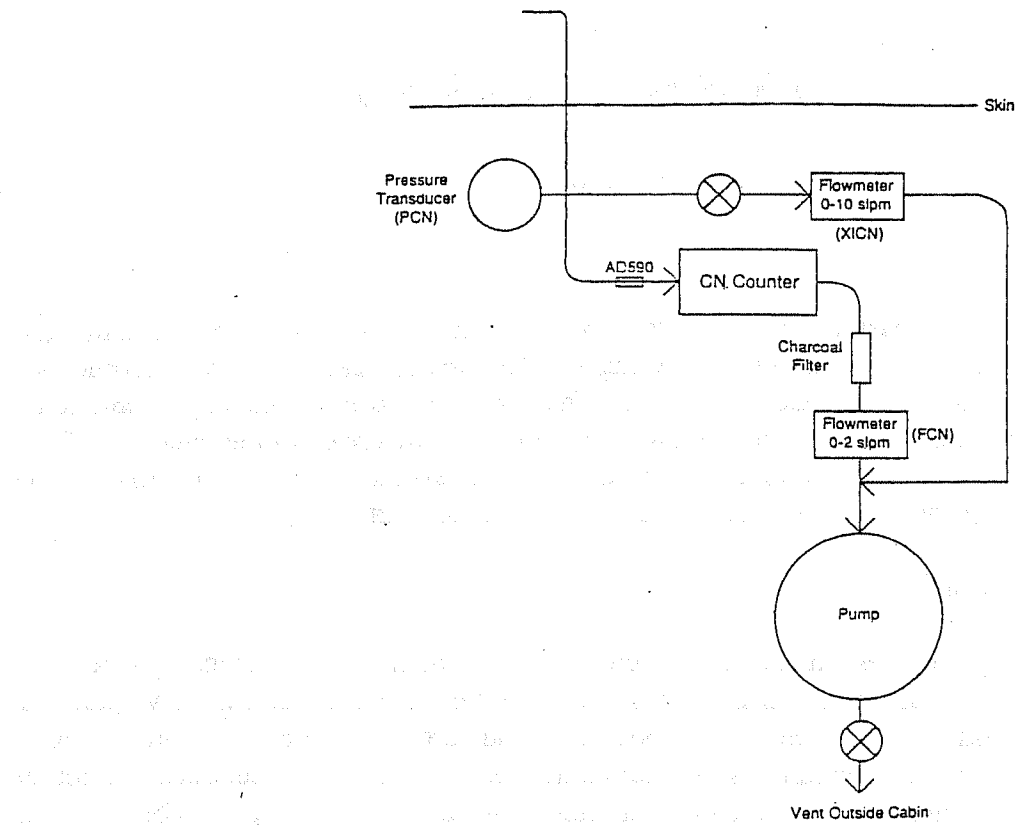
Flow into the inlet is also affected by attack and yaw angle; therefore particle concentrations will not be as accurate during climbs, descents, and turns. Even during straight and level flight, some particle losses will inevitably occur inside the inlet and sample line due to turbulence, particle impaction, and deviations from isokineticity and isoaxiality (alignment with air streamlines). Neglecting the above sources of error, which are difficult to quantify and variable, uncertainty in CONCN has been calculated to be about 6% at $3 \times 10^3 \text{ cm}^{-3}$.

When evaluating the data, keep in mind the limitations at high concentrations, in cloud, and during deviations from straight and level flight discussed above. Since particle concentration is derived in part from pressure and flow signals, disturbances in these measurements may affect particle concentration.

Figure 5.11 gives an example of output from this sensor. (See previous page for Figure 5.11)

Figure 5.9 — Airborne Condensation Nucleus Counter





Operation of the CCN Counter on NCAR aircraft

Figure 5.10

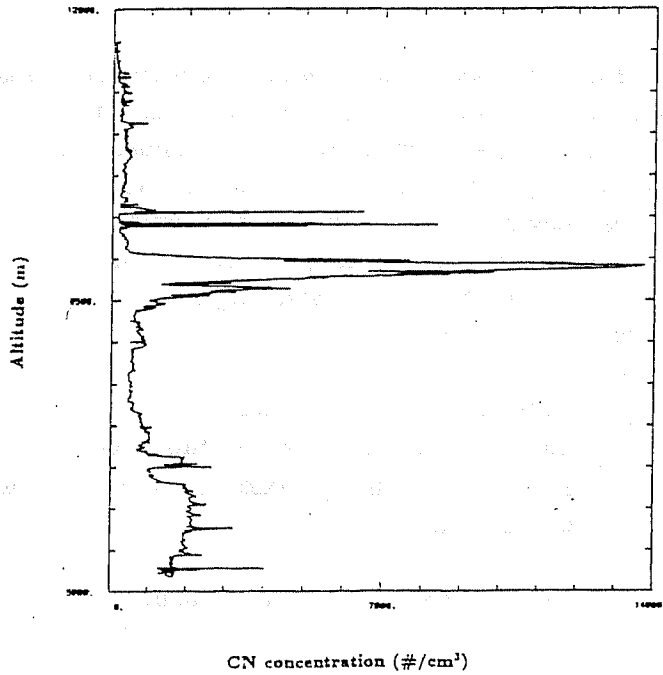


Figure 5.11 — CN variation with height in summer near Denver, Colorado. Note the maximum in particle concentration near the tropopause.

SECTION 6—Cloud Sensors

Counterflow Virtual Impactor

Introduction

The counterflow virtual impactor (CVI) impacts only cloud particles with aerodynamic diameters greater than about $5 \mu\text{m}$ into dry air, while rejecting smaller particles and gas-phase constituents. Once cloud particles are collected and heated within the CVI inlet, volatile components and non-volatile particles (the residual nuclei) are measured by sensors downstream of the inlet. The CVI has been flown on the NCAR King Air and Electra, as well as several non-NSF platforms. Figure 6.1 shows the CVI inlet flown on the Electra and CSIRO F-27 aircraft.

Principles of Operation

The CVI collects large particles via inertial impaction, while a small air flow out the tip (the counterflow) prevents smaller particles and interstitial gases from being collected. Low detection limits for various cloud properties are possible because cloud particles are impacted into initially dried, particle-free air and the sampling is sub-isokinetic; i.e., particles are concentrated within the sample airstream. The minimum size of cloud particles sampled ("cut size") can also be varied in order to resolve cloud properties by particle size. The current version of the CVI requires an RAF operator. Figure 6.2 is a schematic diagram of the CVI.

Sensor Output and Specifications

a) general information

Condensed water content is obtained from the water vapor content measured after evaporation. In the past, this has been measured with a chilled-mirror/Lyman-alpha combination, but it may be obtained using an ultraviolet hygrometer in the future. Residual nuclei number concentration is measured using a TSI 3760 condensation nucleus counter, and cloud particle number and the diameter of average mass may be derived from this measurement. Special arrangements can be made to analyze the residual nuclei or volatile gases from cloud particles by various techniques, such as electron microscopy, ion chromatography, single-particle mass spectroscopy, or ice or cloud condensation nuclei methods.

Specifications:	5-30 μm (aerodynamic particle diameters)
	2 cm^{-3} (lower limit of particle concentration)
	1 mg m^{-3} (lower limit of condensed water content)
	1 s response time

Cindy Twohy is the RAF resource person for this instrument.

b) *primary output*

The primary CVI raw variables include various flow rates (CVF1, CVF2, CVFCN, CVFH, and CVFX) in standard lit min^{-1} , the inlet temperature and pressure (CVTEMP and PCN), and inlet tip temperature (CVTT).

c) *derived output*

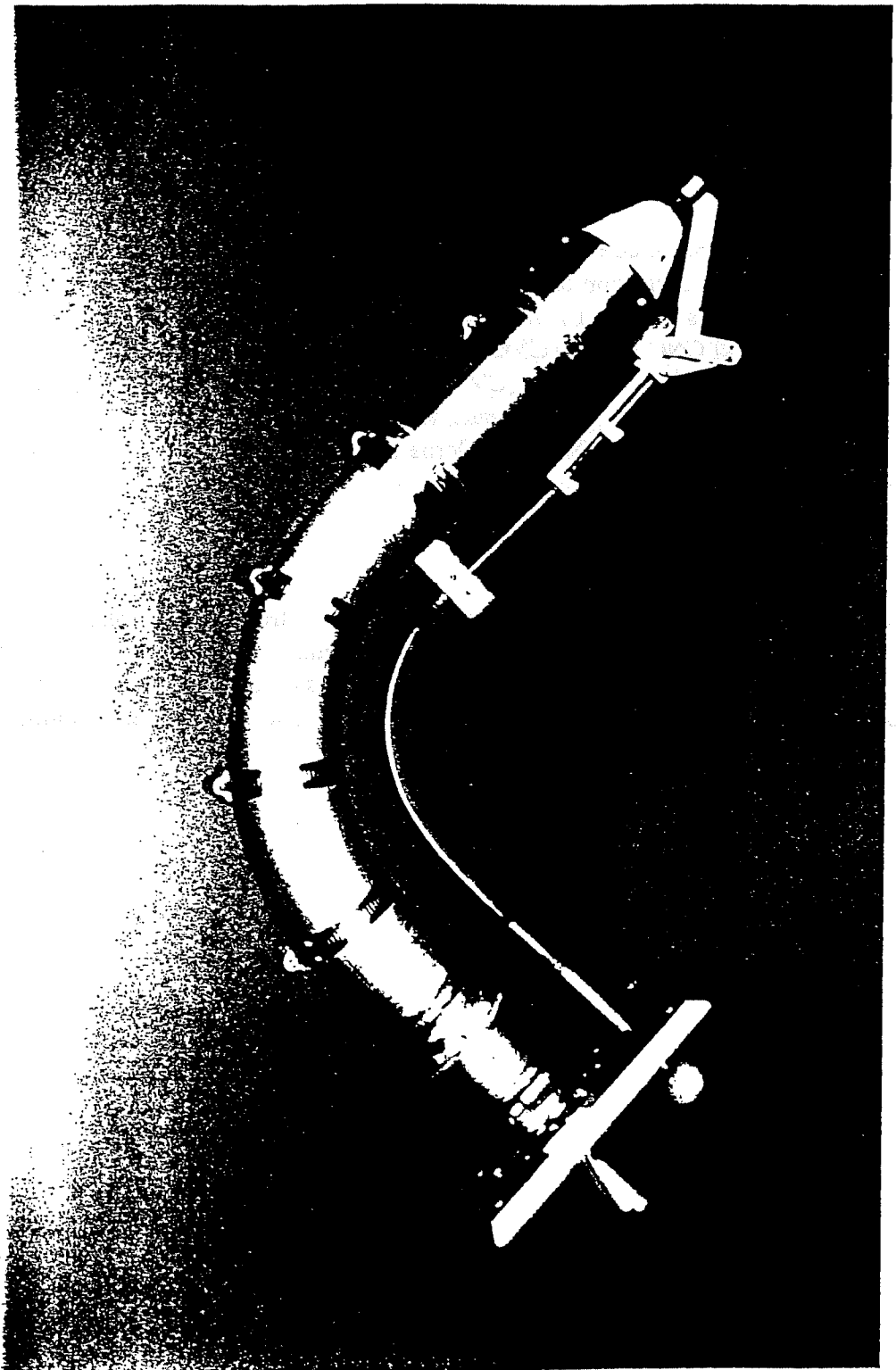
Calculated parameters include flow rates corrected to volumetric units (CVF2C, CVFCC, CVFHC, and CVFXC), the concentration factor (CFACT), the distance to the inlet stagnation plane (CVL), and stopping distances for 4 and 7 μm radius droplets (CVS4 and CVS7). Other calculations convert the raw CVI CNC counts (CVCNT) to particle concentration inside the CVI (CVCNC) and to the effective outside concentration (CVCNO). Condensed water content processing converts the raw CVI Lyman- α voltage (VLA1) to water vapor density inside the CVI (RHOLA1), using the CVI dewpoint (CVDP, RHCV) as a baseline. Some of these variables have an "X" prefix to indicate a non-standard RAF instrument.

Data Interpretation

Due to the complexity of the instrument and its non-standard mode of operation, RAF staff will work closely with the user in data analysis and interpretation. Data must be stratified for cut size and cloud characteristics for effective use. Cloud periods containing large drops or ice crystals (> approx. 50 μm in diameter) should be used with caution due to inefficient sampling or potential breakup of these particles.

An example of output from this sensor is shown in Figure 6.3.

Figure 6.1 — Counterflow Virtual Impactor



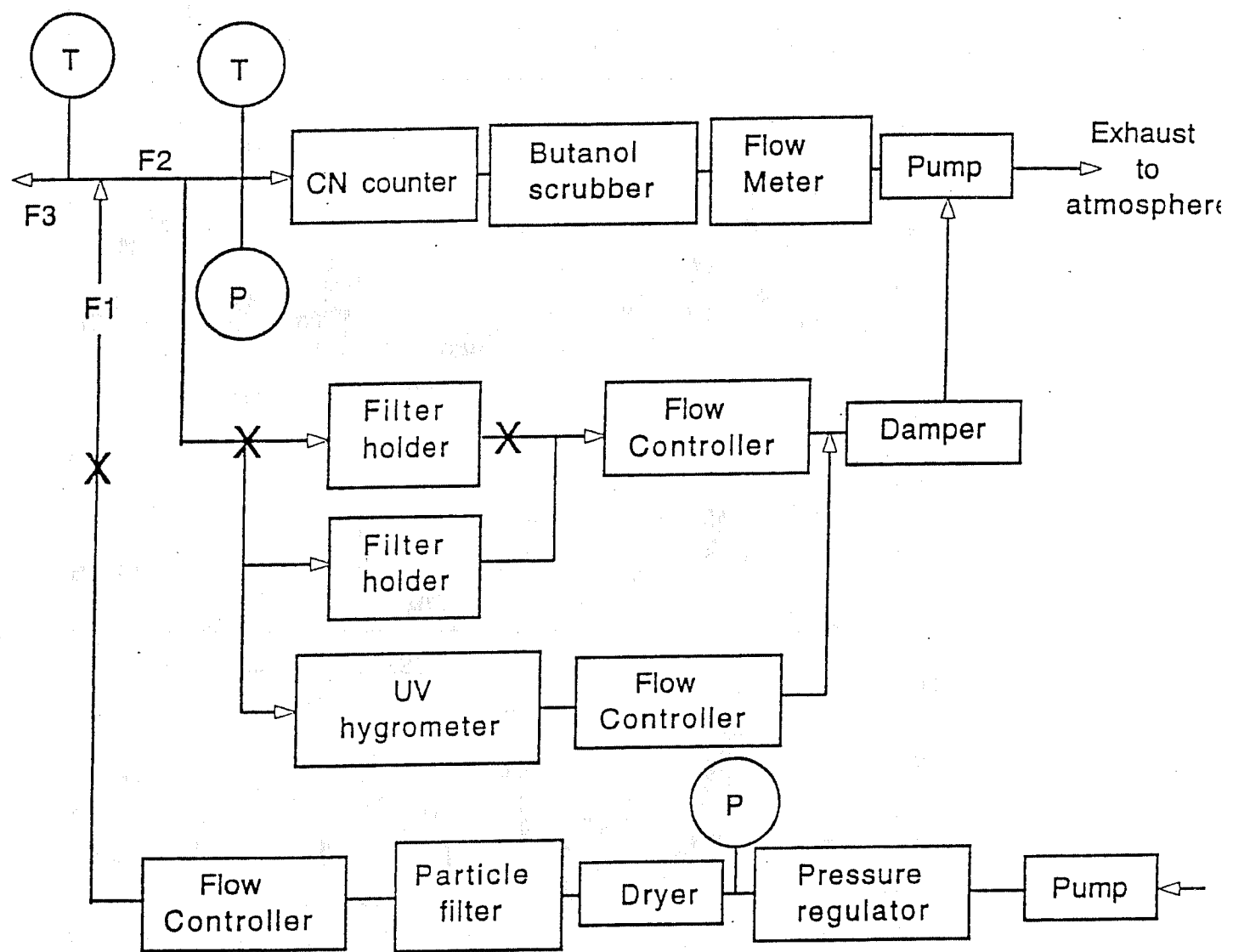


Figure 6.2 CVI Schematic

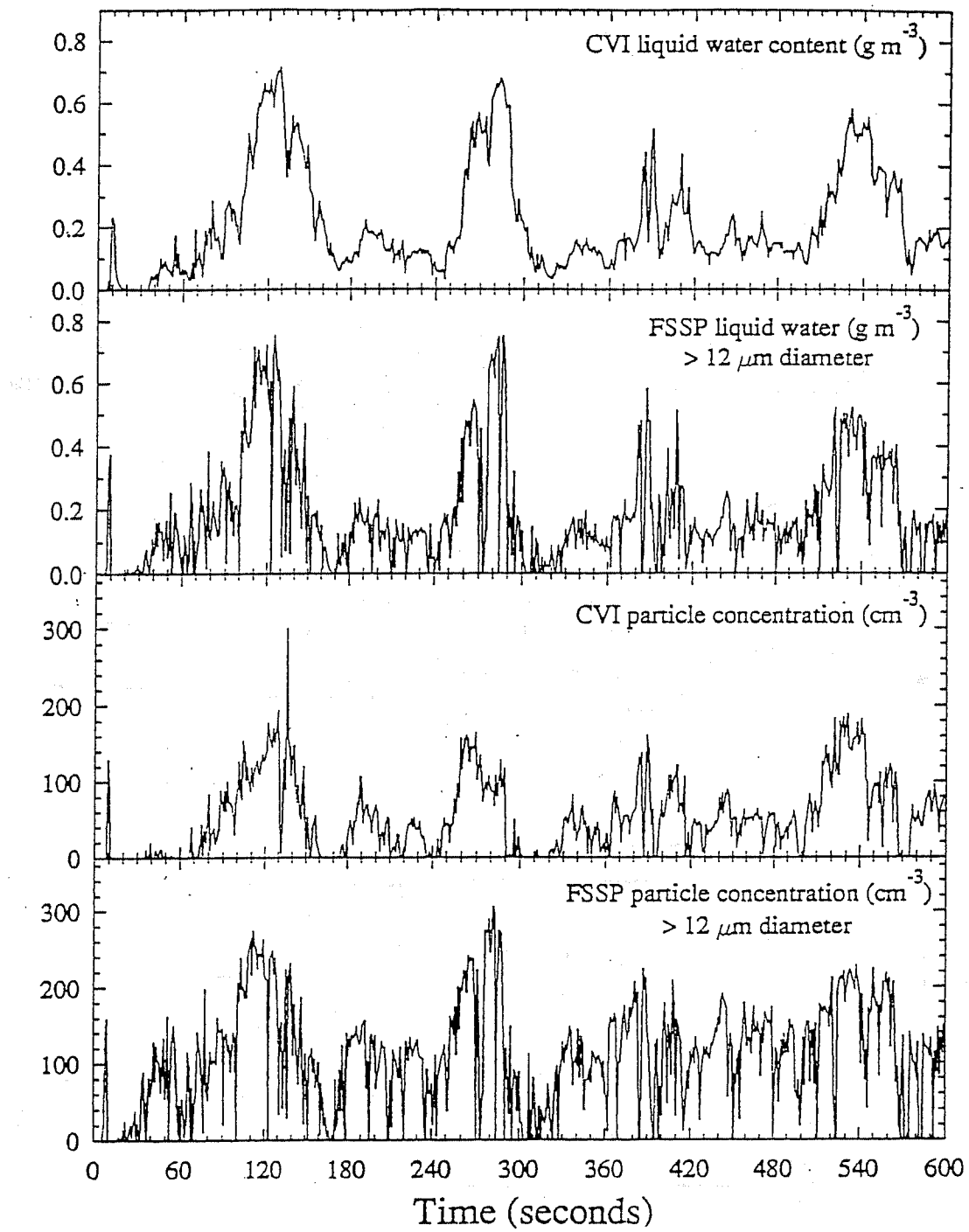


Figure 6.3 — Time series of microphysical data taken with the NCAR King Air in California coastal stratus. The first plot is liquid water content derived from water vapor content inside the CVI, the second is liquid water content derived from the FSSP-100, the third is droplet concentration derived from the CVI particle concentration, and the fourth is droplet concentration measured by the FSSP. Because the CVI cut size was $12 \mu\text{m}$ diameter, only droplets larger than $12 \mu\text{m}$ are included in the FSSP traces.

One Dimensional Optical Array Probe 260X OAP Cloud Probe

Introduction

The one dimensional optical array probe (1D-OAP), model 260X, is an instrument developed by Particle Measuring Systems (PMS, Inc., Boulder, Co) for the measurement of cloud droplet size distributions. The sensor is used primarily for the study of cloud microphysical processes, for example, the growth of cloud droplets through condensation and coalescence into drizzle and precipitation drops.

Operating Principles

The 260X measures the size of hydrometeors from the maximum width of their shadow as they pass through a focussed He-Ne laser beam (Figure 6.4). The shadow is cast onto a linear diode array and the total number of occulted diodes during the particle's passage represents its size. The diodes at each end of the array act as a mechanism for rejecting those particles that would be undersized when they do not pass entirely within the bounds of the array.

The size is categorized into one of 62 channels and this information is sent to the data system where the number of particles in each channel is accumulated over a preselected time period. Figure 6.5 shows a typical size distribution where the concentration of droplets in each size category is shown, normalized by the width of the size channel. Figure 6.6 is a photograph of the 260X in the canister that is normally mounted on an aircraft pylon.

Sensor Output and Specifications

a) general information

Manufacturer:	Particle Measuring Systems, Inc., Boulder, Co.
RAF Resource Person(s):	Darrel Baumgardner
Calibration Method:	Monodispersed glass beads, etched spinning disk
Range:	40 μm - 620 μm
Accuracy (Diameter):	Function of particle size, shape and orientation
Accuracy (Concentration):	Function of particle size

b) primary output

RAF Parameter Name	Plain Language Name	Description
A26X01-62 counts	Channels 1-62	62 channels of accumulated

c) derived output

RAF Parameter Name	Plain Language Name	Description
CONC6	Concentration	# of particles per unit volume - number per cubic liter
PLWC6	Liquid Water Content	Total droplet mass (assuming spherical water drops) - grams per cubic meter
DBAR6	Average Diameter	Arithmetic average of droplet size - micrometers

$$CONC6 = \sum_{i=1}^{i=62} \frac{n_i}{V}; PLWC6 = \frac{\pi}{6} \rho \sum_{i=1}^{i=62} \frac{n_i d_i^3}{V}; DBAR6 = \frac{\sum_{i=1}^{i=62} n_i d_i}{\sum_{i=1}^{i=15} n_i}$$

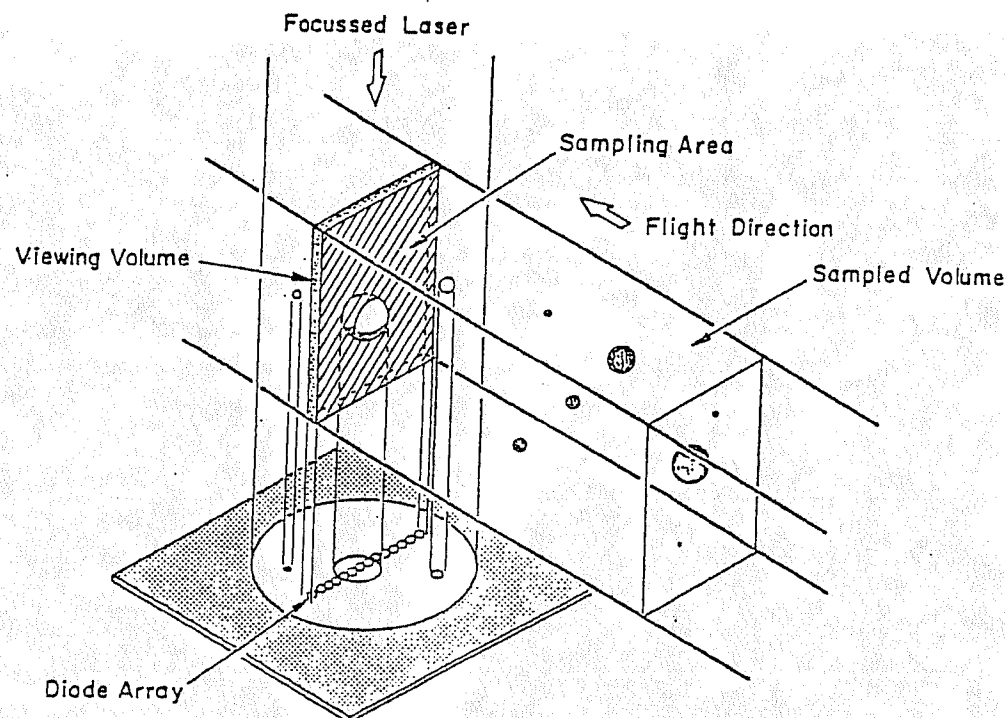
where n_i is the number of droplets detected in size channel i , d_i is the diameter represented by channel i , and V is the sample volume measured in a given sample period.

Data Interpretation

The electronic response time of the 260X imposes some limitations on the minimum detectable size (Baumgardner, 1987). A photodiode is registered as shadowed when its output is sensed as decreasing by at least 50% and at least one diode must change by 67%. The edges of particles will oftentimes be missed and particles in the lower end of the size range can pass undetected when the velocity of a particle through the beam exceeds the response of the probe. At 100 ms^{-1} this imposes a lower size threshold of $30-40 \mu\text{m}$ on the 260X.

The 260X is a particle sizing instrument, not a liquid water content probe. The 260X detects any particles that cause the diode array to be occulted; however, these probes cannot differentiate shapes or particle orientation. If liquid water content information is desired, some fairly loose assumptions must be made with regard to the phase, habit, and density of the particles. These assumptions may lead to significant errors in derived liquid water content.

The sample volume of this instrument is relatively small, and varies with particle size. This imposes a limitation on the minimum sampling time if a statistically significant measurement is to be made, particularly of large sizes.



Schematic diagram of the 260X OAP Cloud Probe

Figure 6.4

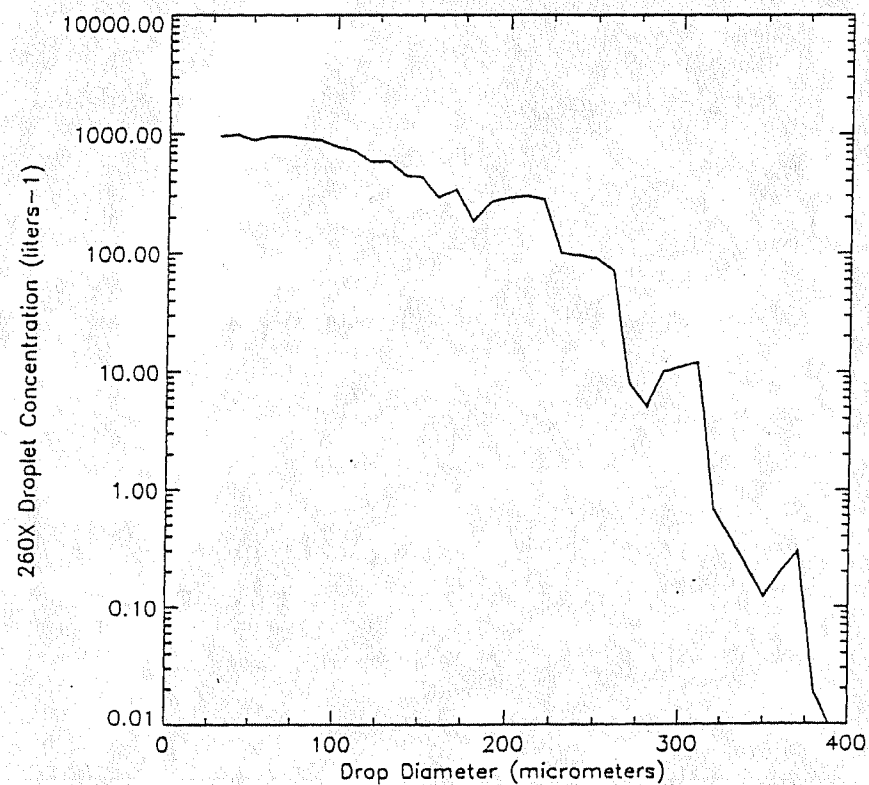
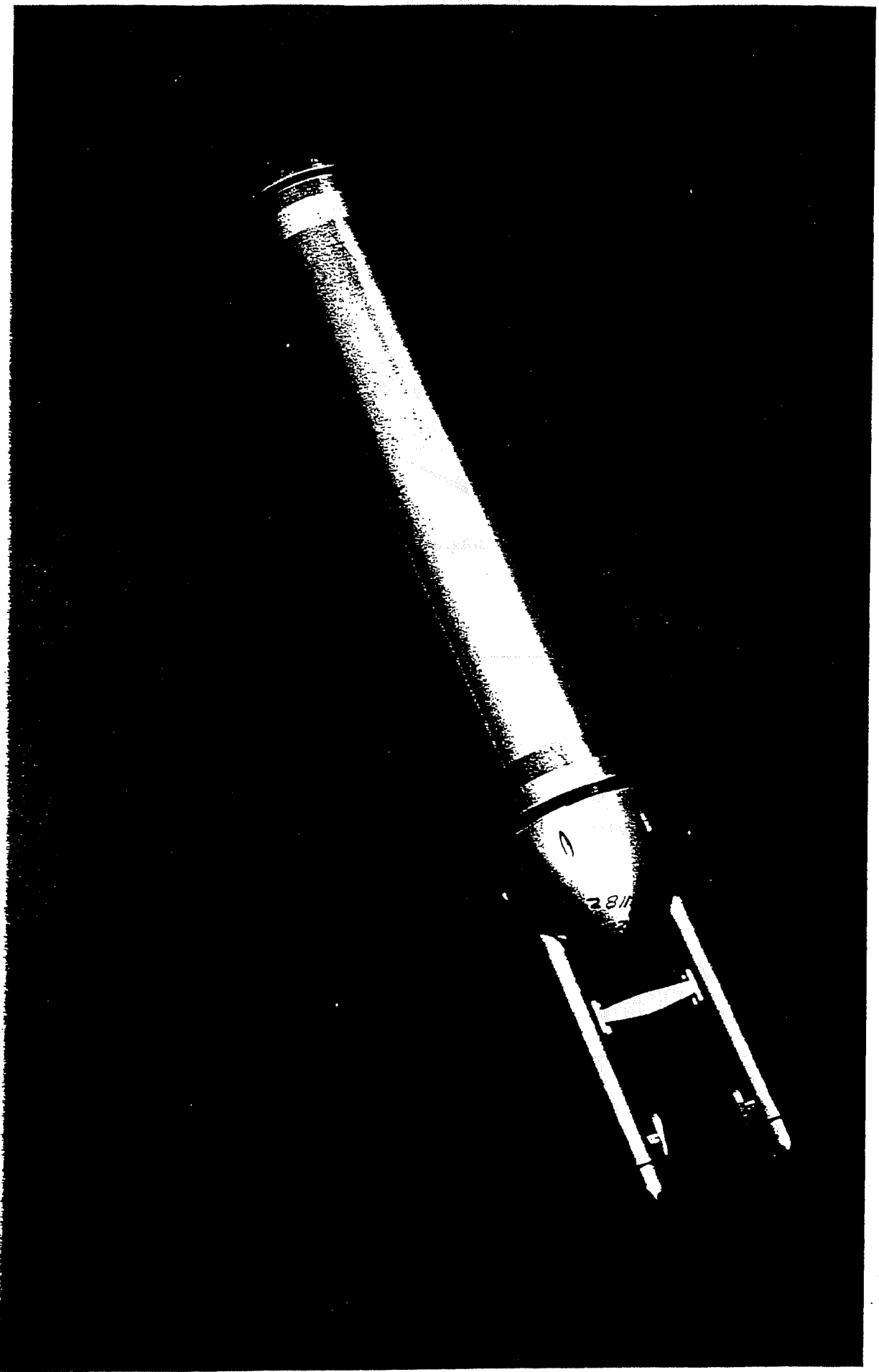


Figure 6.5 - A size distribution of droplets as measured by the 260X OAP Cloud Probe

Figure 6.6 — One Dimensional Optical Array Probe



Two Dimensional Optical Array Probes 2D Cloud and Precipitation Probes

Introduction

The Two dimensional optical array probes (2D-OAP), models 2D-C and 2D-P, are instruments developed by Particle Measuring Systems (PMS, Inc., Boulder, Co) for the measurement of cloud and precipitation drop size distributions. These sensors are used primarily for the study of cloud microphysical processes, for example, the growth of cloud drops and ice crystals through aggregation, riming and coalescence into drizzle, rain drops, graupel or other forms of precipitation.

Operating Principles

The 2Ds record the two dimensional shadows of hydrometeors as they pass through a focussed He-Ne laser beam (Figure 6.7). The shadow is cast onto a linear diode array and the on/off state of these diodes is stored during the particle's passage through the laser beam. This information, along with the time that has passed since the previous particle, is sent to the data system and recorded for post-flight analysis.

Information about a particle's shape and size is deduced from analysis of the recorded shadow with a variety of pattern recognition algorithms. Figure 6.8 illustrates some measurements by the 2D probe in several different types of ice particles, ranging from rain drops to pristine ice crystals to more complex heavily rimed ice particles. Figure 6.9 is a photograph of the 2D-C in the canister that is mounted on an aircraft pylon. A pair of 2Ds is normally flown during a project to cover the size range of interest. The 2D cloud probe (2D-C) measures in the range from 25 μm to 800 μm and the 2D precipitation probe (2D-P) measures in the large size range from 200 μm to 6400 μm .

Sensor Output and Specifications

a) general information

Manufacturer:	Particle Measuring Systems, Inc., Boulder, Co.
RAF Resource Person(s):	Darrel Baumgardner
Calibration Method:	Monodispersed glass beads and spinning disk with etched dots
Range:	25 μm - 800 μm (2D-C) 200 μm - 6400 μm (2D-P)
Accuracy (Diameter):	Function of particle size, shape and orientation
Accuracy (Concentration):	Function of particle size

b) primary output

RAF Parameter Name	Plain Language Name	Description
SDWC1	2D-C Shadow Or	Total count of all particles passing through the laser beam of the 2D-C
SDWP1	2D-P Shadow Or	Total count of all particles passing through the laser beam of the 2D-P

The raw shadow information is maintained in a compressed format and is left to the user to analyze at their own discretion. Software is available from the RAF to assist in this processing but is not a routine option.

c) derived output

RAF Parameter Name	Plain Language Name	Description
CON2C1	Concentration	# of particles per unit volume from the 2D-C probe - number per liter
CON2P1	Concentration	# of particles per unit volume from the 2D-P probe - number per liter

$$CON2C = \frac{SDWC1}{V_c} ; CON2P = \frac{SDWP1}{V_p} ; V_c = DOF \cdot A \cdot v \cdot t ; DOF = 9482r^2 ; A = W + 4r$$

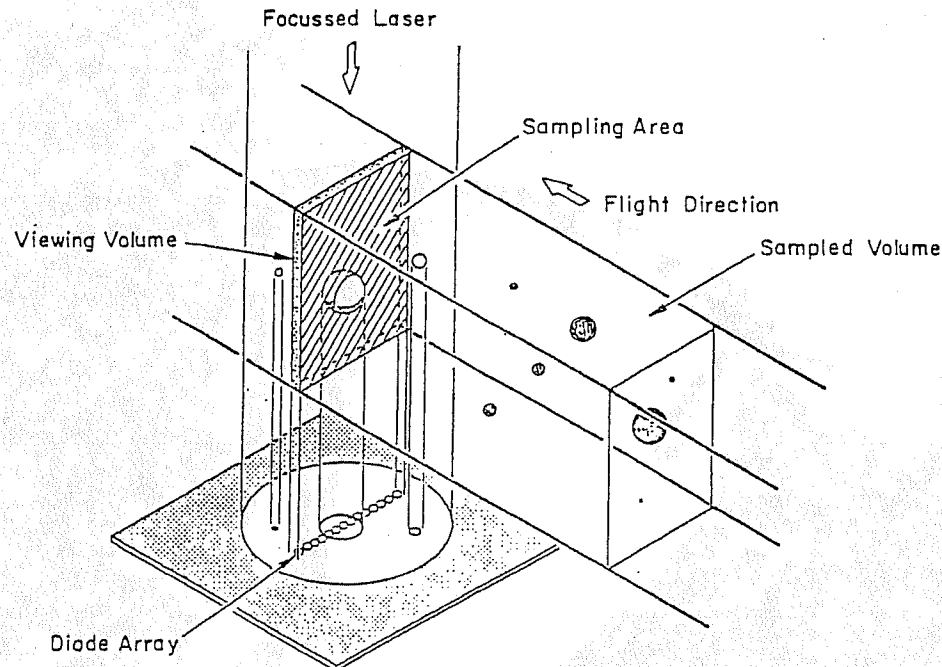
where r is the particle radius, W is the diode array width (800 μm and 6400 μm for the 2D-C and 2D-P, respectively), v is the particle velocity and t is the sample period.

Data Interpretation

The electronic response time of the 2Ds imposes some limitations on the minimum detectable size (Baumgardner, 1987). A photodiode is registered as shadowed when its output is sensed as changing by at least 50%. The edges of particles will oftentimes be missed and particles in the lower end of the size range can pass undetected when the velocity of a particle through the beam exceeds the response of the probe. At 100 ms^{-1} this imposes a lower size threshold of 30-40 μm on the 2D.

The 2Ds are particle imaging instruments, not liquid water content probes. The 2Ds are able to capture a lot of information about a particle just from its shadow; however, if the water content of ice particles is desired, some fairly loose assumptions must be made with regard to the phase, habit, and density of the particles. These assumptions may lead to significant errors in derived liquid water content. A number of pattern recognition algorithms have been developed for analyzing 2D data; however, none of them work very efficiently for any but the most simple of particle shapes (Heymsfield and Baumgardner, 1985).

The sample volume of these instrument is relatively small with respect to the normally low concentrations typically encountered in clouds. This imposes a limitation on the minimum sampling time if a statistically significant measurement is to be made, especially of large particles.



Schematic diagram of the 2D Optical Array Probes

Figure 6.7

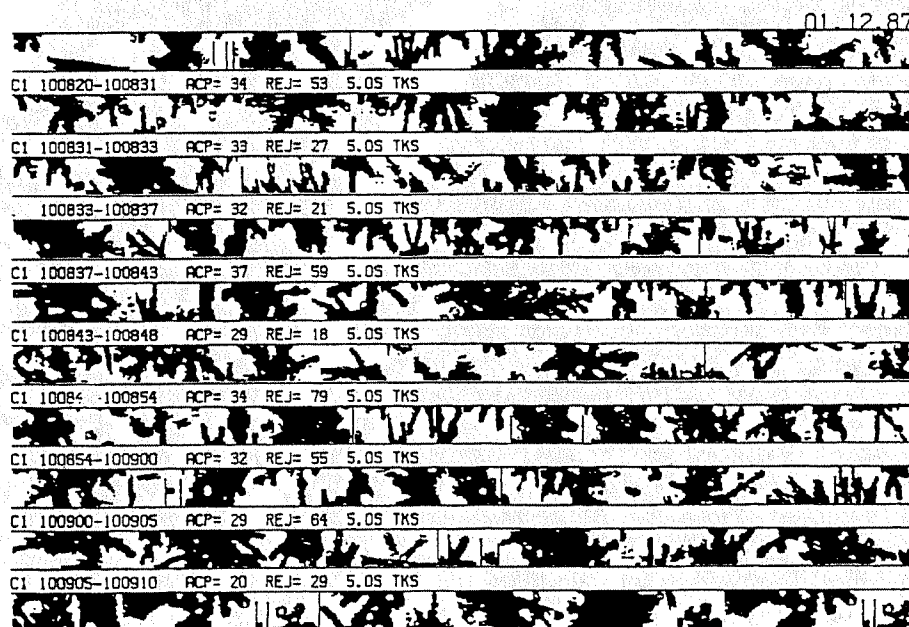


Figure 6.8 - Images from the 2D probe in several different types of ice particles ranging from rain drops to pristine ice crystals to more complex heavily rimed ice particles

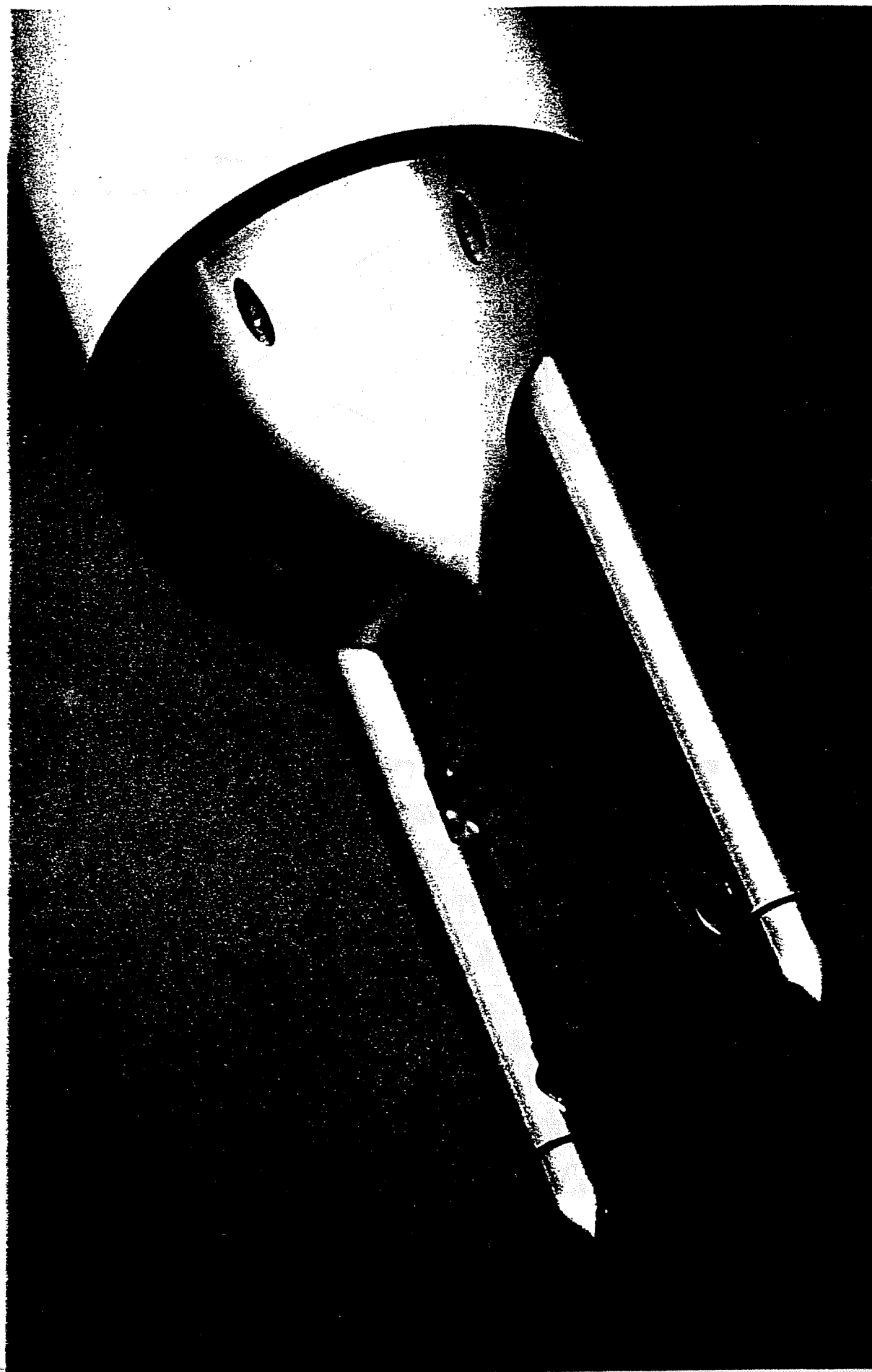


Figure 6.9 — Two Dimensional Optical Array Probes

Forward Scattering Spectrometer Probe FSSP-100 Cloud Probe

Introduction

The Forward Scattering Spectrometer Probe (FSSP), model 100, is an instrument developed by Particle Measuring Systems (PMS, Inc., Boulder, Co) for the measurement of cloud droplet size distributions. The sensor is used primarily for the study of cloud microphysical processes, particularly the nucleation and growth of cloud droplets through condensation and coalescence.

Operating Principles

The FSSP is of that general class of instruments called optical particle counters (OPCs) that detect single particles and size them by measuring the intensity of light that the particle scatters when passing through a light beam. The schematic diagram shown in Figure 6.10 illustrates the optical path of this instrument. A Helium Neon laser beam is focused to a diameter of 0.2 mm at the center of an inlet that faces into the oncoming airstream. This laser beam is blocked on the opposite side of the inlet with an optical stop, a "dump spot" to prevent the beam from entering the collection optics. Particles that encounter this beam scatter light in all directions and some of that scattered in the forward direction is directed by a right angle prism though a condensing lens and onto a beam splitter. The "dump spot" on the prism and aperture of the condensing lens define a collection angle from about $4^\circ - 12^\circ$.

The beam splitter divides the scattered light into two components, each of which impinges on a photodetector. One of these detectors, however, is optically masked to receive only scattered light when the particles pass through the laser beam displaced greater than approximately 1.5 mm either side of the center of focus. Particles that fall in that region are rejected when the signal from the masked detector exceeds that from the unmasked detector. This defines the sample volume needed to calculate particle concentrations.

The size of the particle is determined by measuring the light scattering intensity and using Mie scattering theory to relate this intensity to the particle size. Figure 6.11 illustrates how the scattered light varies with particle diameter given that the particle is spherical and that the refractive index is known.

The size is categorized into one of 15 channels and this information sent to the data system where the number of particles in each channel is accumulated over a preselected time period. Figure 6.12 shows a typical size distribution where the concentration of droplets in each size category is shown, normalized by the width of the size channel. Figure 6.13 is a photograph of the FSSP in the canister that is normally mounted on an aircraft pylon.

Sensor Output and Specifications

a) general information

Manufacturer:	Particle Measuring Systems, Inc., Boulder, Co.
RAF Resource Person(s):	Darrel Baumgardner
Calibration Method:	Monodispersed glass beads
Range:	2.0 μm - 47.0 μm
Accuracy:	$\pm 20\%$ (Diameter) $\pm 16\%$ (Concentration)

b) primary output

RAF Parameter Name	Plain Language Name	Description
AFSP01-15	Channels 1-15	15 channels of accumulated counts
FSTRB	Total Strobes	Total Particles in depth of field
FRESET	Fast Resets	Total Particles outside depth of field
FACT	Activity	Fraction of sample period that probe was active

c) derived output

RAF Parameter Name	Plain Language Name	Description
CONCF	Concentration	# of droplets per unit volume - number per cubic centimeter
PLWCF	Liquid Water Content	Total droplet mass - grams per cubic meter
DBARF	Average Diameter	Arithmetic average of droplet size - micrometers

$$\text{CONCF} = \sum_{i=1}^{i=15} \frac{n_i}{V}; \text{PLWCF} = \frac{\pi}{6} \rho \sum_{i=1}^{i=15} \frac{n_i d_i^3}{V}; \text{DBARF} = \frac{\sum_{i=1}^{i=15} n_i d_i}{\sum_{i=1}^{i=15} n_i}$$

where n_i is the number of droplets detected in size channel i , d_i is the diameter represented by channel i , and V is the sample volume measured in a given sample period.

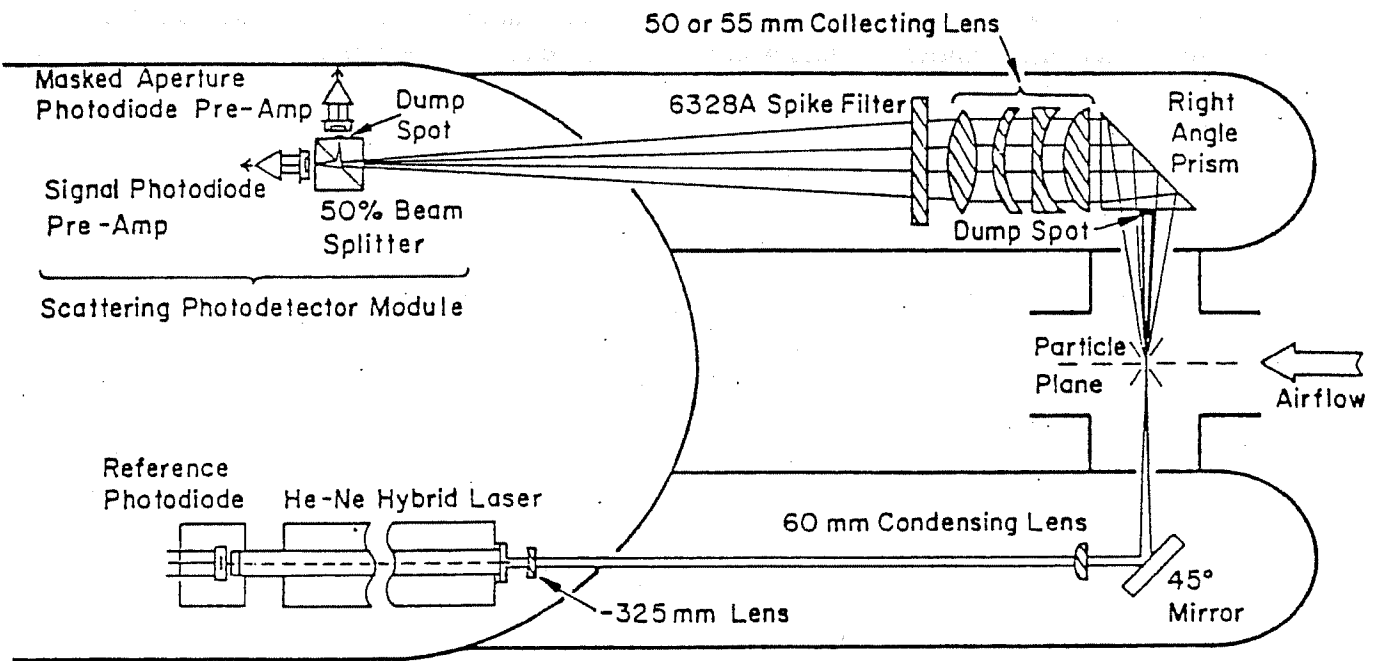
Data Interpretation

The FSSP-100 was developed as a cloud droplet measurement instrument. The size that is determined by the FSSP assumes that the scattered light detected is from a spherical, liquid droplet of refractive index 1.33. The size distributions produced from these measurements must be viewed with great caution when in clouds containing mixtures of water and ice, since ice particles will not be correctly sized due to their different refractive index and non-spherical shapes.

A secondary caution when looking at size distributions is in the presence of precipitation sized drops. These are suspected of colliding with the sample inlet and causing spurious satellite droplets.

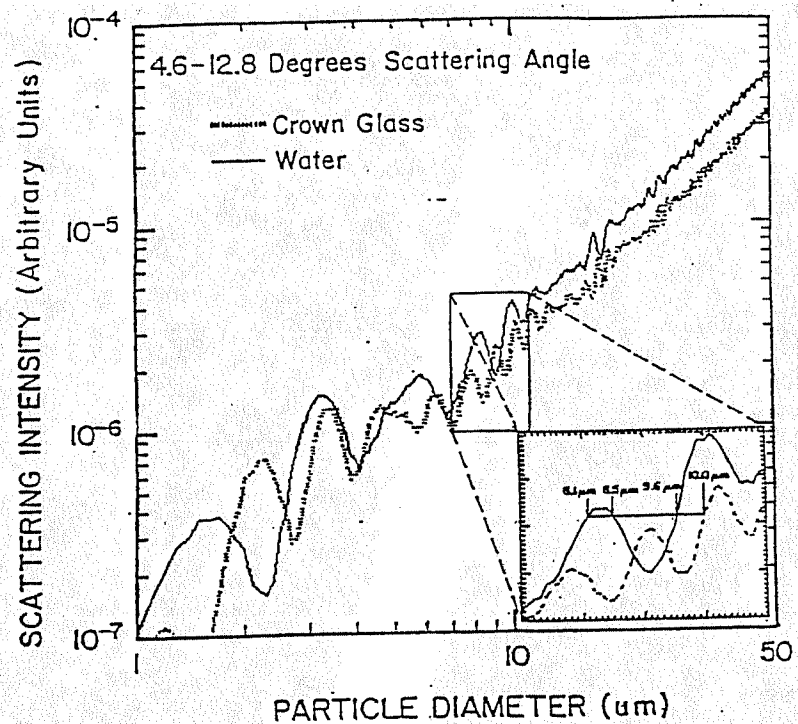
The probability of more than a single particle coinciding in the beam or being missed during the electronic reset time increases with concentration from about 5% losses at 300 cm^{-3} to greater than 30% at 1000 cm^{-3} . Corrections are applied to account for these losses but still lead to concentration uncertainties (Baumgardner, 1983; Baumgarnder, et al, 1985; Baumgardner, 1987; Baumgardner, et al, 1990; Baumgardner and Spowart, 1990; Brenguier, et al, 1994; Dye and Baumgardner, 1984).

The FSSP is a droplet sizing instrument, not a liquid water content probe. Since the liquid water content is derived by integrating the size distribution, uncertainties in the size measurement lead to root sum squared uncertainties in liquid water content a factor of three higher.



Schematic diagram of the Forward Scattering Spectrometer Probe (FSSP-100 Cloud Probe)

Figure 6.10



Variation of scattered light with particle diameter for the FSSP 100

Figure 6.11

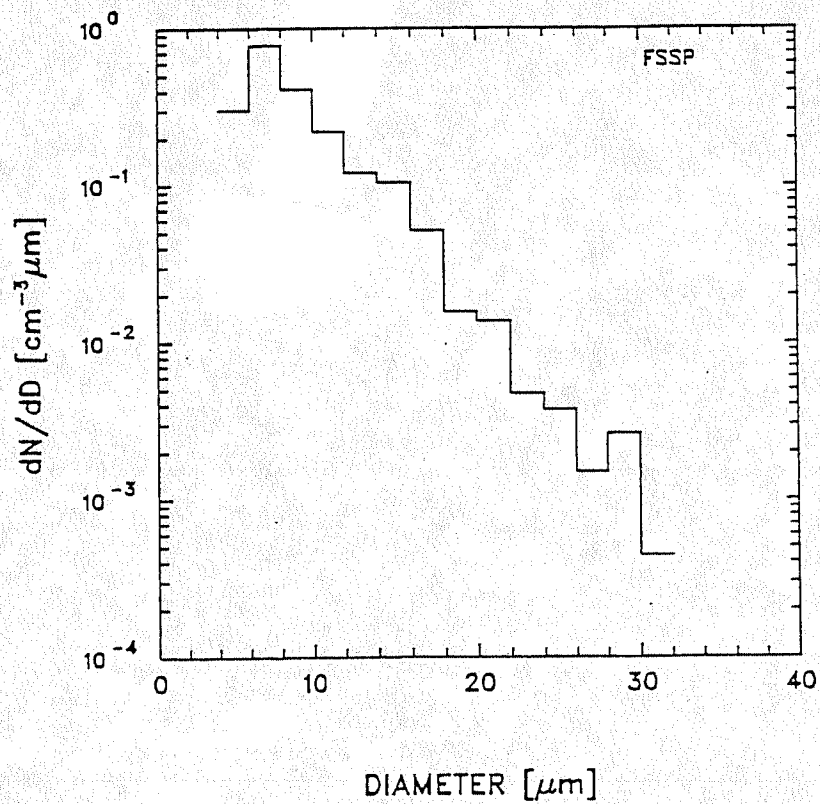
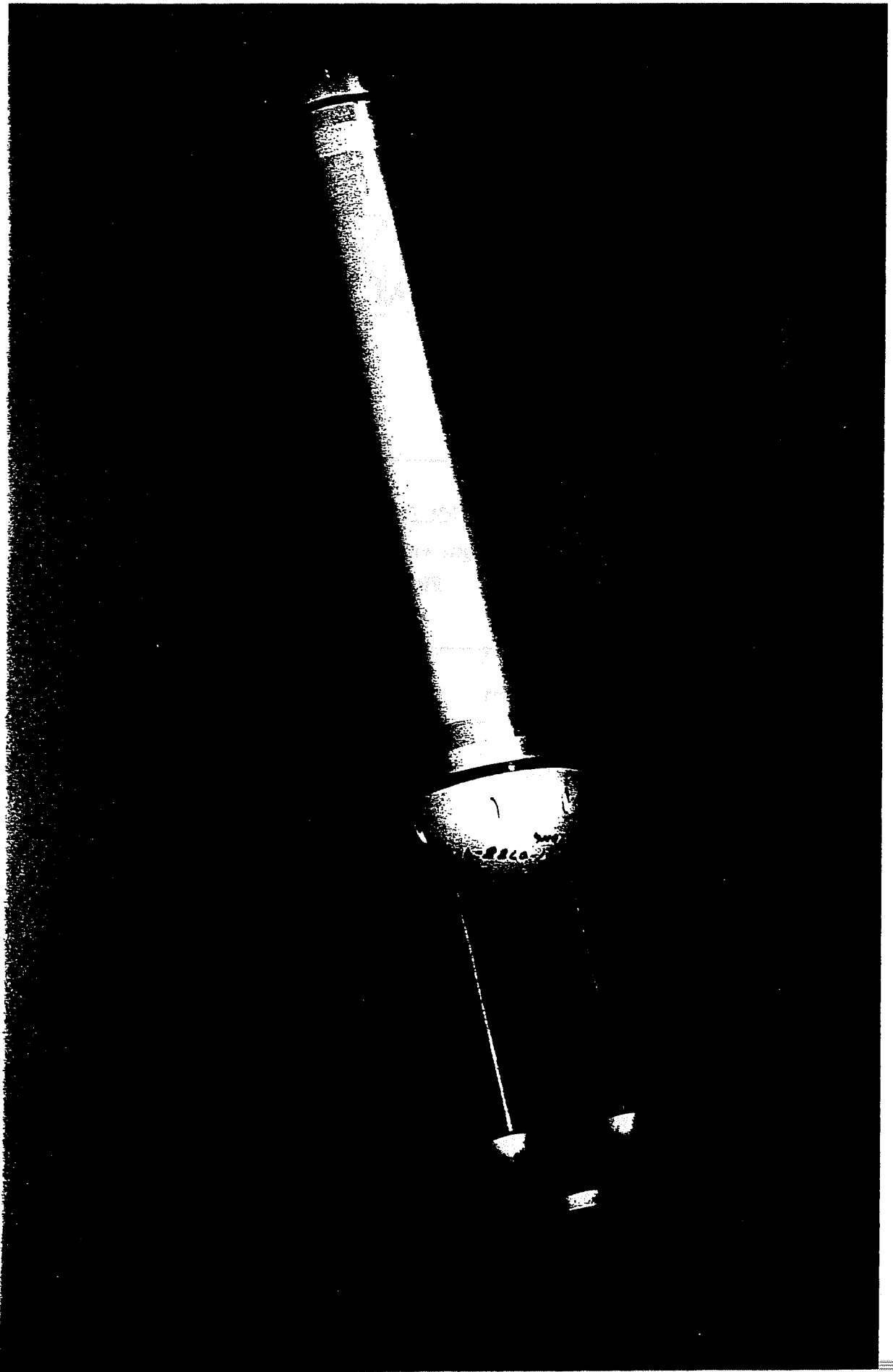


Figure 6.12 – Size distribution from the FSSP 100

Figure 6.13 — Forward Scattering Spectrometer Probe



Rosemount Icing Detector Model 871

Introduction

The Model 871 icing detector is an instrument that was developed by Rosemount Engineering (Eden Prairie, Minnesota) for the detection of supercooled liquid water content and the onset of airframe icing. It has been used by the cloud physics community to detect the presence of supercooled water in mixed phase clouds. It has been particularly useful for detecting supercooled water in cirrus clouds at very cold temperatures when the water levels are below the detection limit of conventional hot wire devices.

Operating Principles

The Model 871 detector, shown schematically in Figure 6.14, measures the amount of ice mass accumulation on a metal cylinder. Using a property known as magnetostriction, the sensing cylinder is driven at a natural frequency of 40 KHz. As the ice accretes on the cylinder, the frequency of the vibration decreases. A phase-locked loop converts this frequency change to a proportional voltage from which the ice mass may be calculated. Once a pre-set amount of mass has been accumulated, the cylinder is heated to melt the ice. Figure 6.15 shows a typical time history of the probe output as the voltage increases with accumulating ice mass then drops to its threshold value as the heater is activated to remove the ice. Figure 6.16 is a photograph of the sensor.

Sensor Output and Specifications

a) general information

Manufacturer:	Rosemount Engineering, Eden Prairie, MN
RAF Resource Person(s):	Darrel Baumgardner
Calibration Method:	Single Drop Freezing
Range:	.001 - 1.0 g m ⁻³ (airspeed, temperature, and liquid water content dependent)
Accuracy:	±20% - 50%

b) primary output

RAF Parameter Name	Plain Language Name	Description
RICE	Detector Volts Out	Raw output voltage

c) derived output

RAF Parameter Name	Plain Language Name	Description
RLWC	Liquid Water Content	Supercooled liquid water content - grams per cubic meter

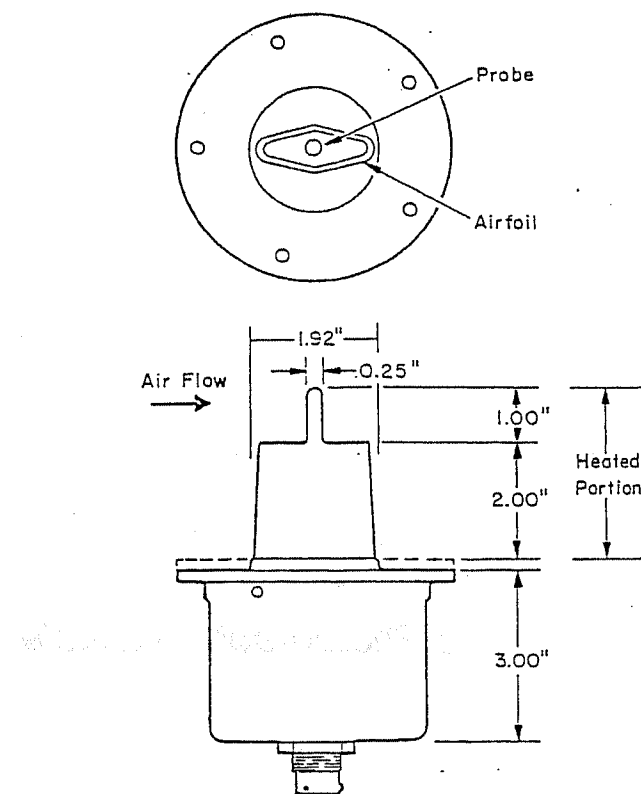
$$LWC = \frac{dM}{dt} \frac{l}{E_c dlv}; \frac{dM}{dt} = G \frac{dV}{dt}$$

where l is the sensor length, d is its width, v is the air velocity, E_c is the collection efficiency, and G is the sensitivity coefficient that relates the rate of mass change to voltage change from the sensor.

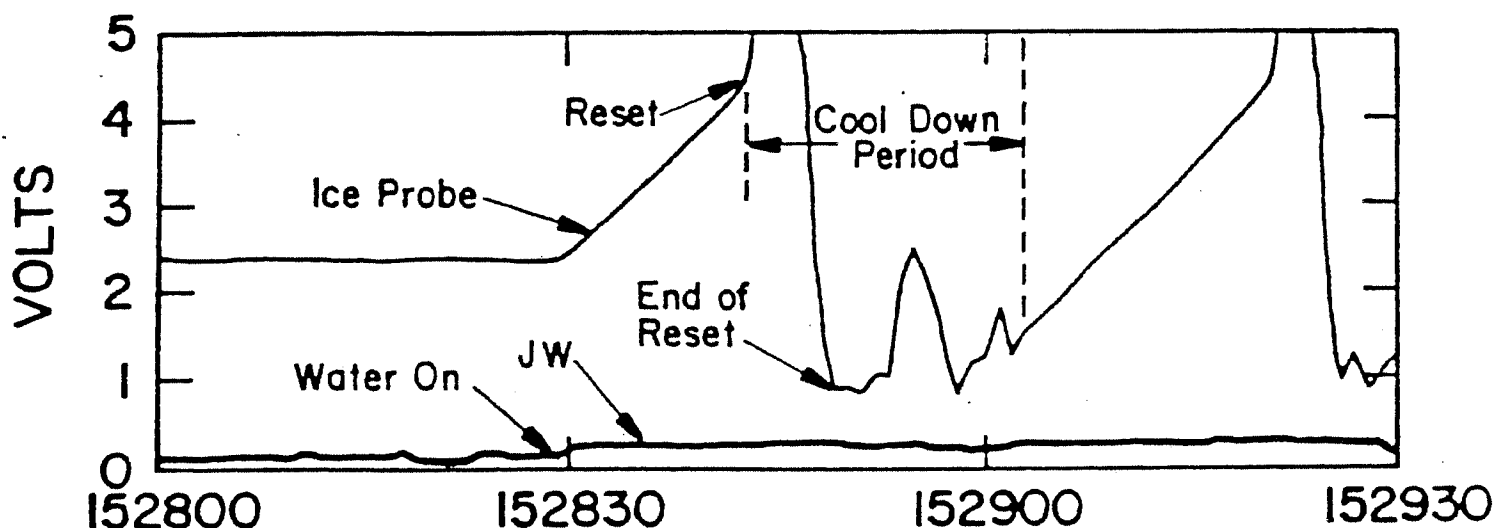
Data Interpretation

The ice detector is limited by collection efficiency considerations on the small droplet end of the spectrum. As ice accumulates and the diameter of the cylinder increases, the collection efficiency decreases. The collection efficiencies are not well characterized but can decrease below 20% for droplets less than 10 μm . An additional uncertainty arises due to the change of diameter with mass accumulation. The mass does not accumulate evenly so there is not a simple expression relating the mass to diameter change. A maximum error of 30% is associated with this source of uncertainty (Baumgardner and Rodi, 1989).

The sensitivity coefficient is a function of where the mass accretes on the sensor. This factor can be determined empirically through comparisons with other instruments and can vary depending upon mounting location.



Schematic diagram of the Rosemount Icing Detector Model 871
Figure 6.14



Output from the Rosemount Icing Detector

Figure 6.15

No Photograph Available

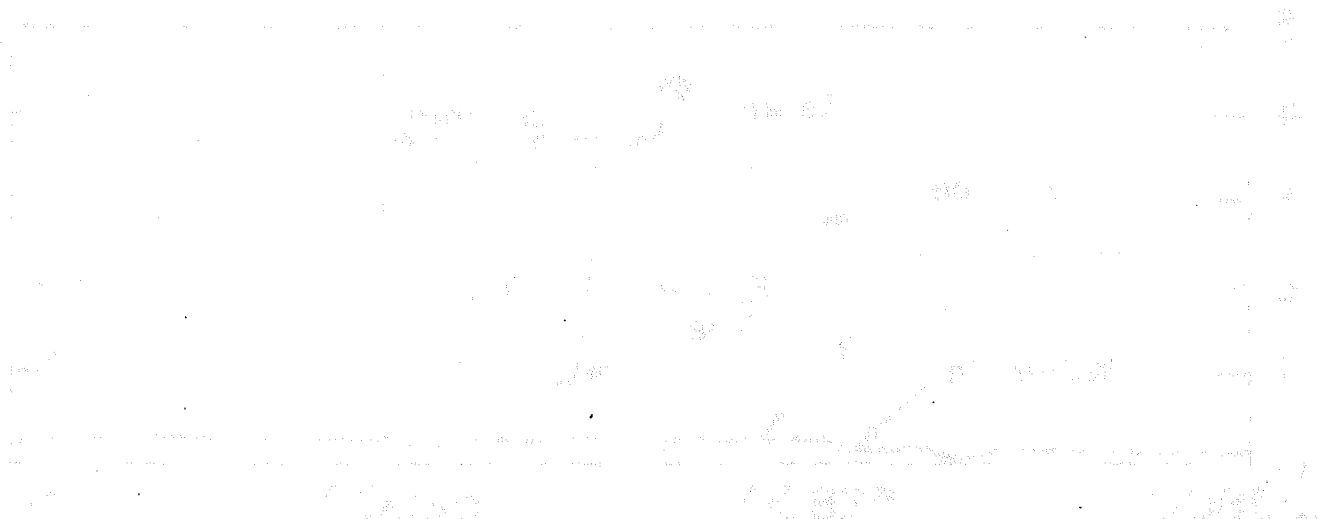


Figure 6.16—Rosemount Icing Detector

PMS/CSIRO Hot Wire Liquid Water Probe

Introduction

The PMS/CSIRO is an instrument developed by King et al (1978) and marketed by Particle Measuring Systems (PMS, Inc., Boulder, Co) for the measurement of cloud liquid water content. This sensor, commonly referred to as the "King" probe, is used primarily for the study of cloud microphysical processes and in icing studies.

Operating Principles

The King probe operates under the principle that liquid water can be calculated from measurements of the amount of heat released when droplets vaporize. As shown in the drawing in Figure 6.17 and photograph in Figure 6.18, a heated cylinder is exposed to the airstream and intercepts oncoming droplets. The electronics maintain this sensor at a constant temperature (approximately 130° C) and monitors the power required to regulate the temperature as droplets vaporize. This power is directly related to the amount of heat taken away by convection plus the heat of vaporization. The convective heat losses are known empirically and vary with airspeed, temperature and pressure.

The liquid water content is calculated from power loss found from the difference between total and convective power losses.

Sensor Output and Specifications

a) general information

Manufacturer:	Particle Measuring Systems, Inc., Boulder, Co.
RAF Resource Person(s):	Darrel Baumgardner
Calibration Method:	None required
Range:	.05 - 3.0 g m ⁻³
Accuracy:	±15%

b) primary output

RAF Parameter Name	Plain Language Name	Description
PLWC	Power	This is the power consumed in watts to maintain the hot wire sensor at a constant temperature.

c) derived output

RAF Parameter Name	Plain Language Name	Description
PLWCC	Liquid Water Content	Cloud Droplet water mass - grams per cubic meter

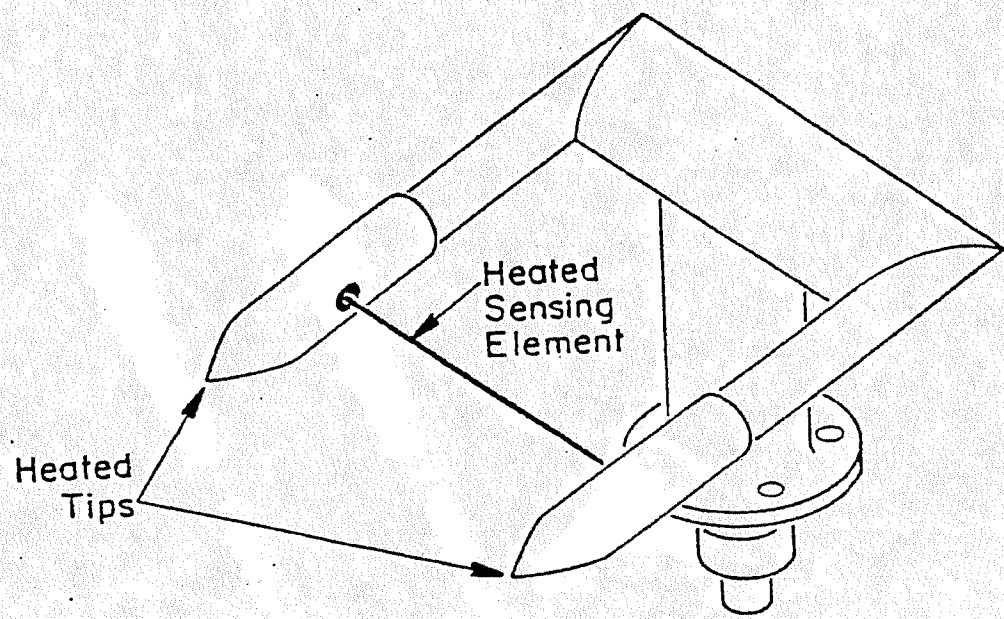
$$PLWCC = \frac{P - P_d}{ldv[L_v + c(T_b - T_a)]} ; P_d = A_0 \pi k (T_s - T_a) Re^x Pr^y$$

where l is the sensor length, d is its width, v is the air velocity, L_v is the latent heat of vaporization, c is the specific heat of water, T_b is the boiling point of water, T_a is the air temperature, T_s is the sensor temperature, k is the thermal conductivity of the air, Re is the Reynold's number, Pr is the Prandtl number and A_0 , x and y are constants for a heated cylinder at high Reynold's number.

Data Interpretation

The King probe sensor is limited by collection efficiency considerations on the small droplet end of the spectrum and by vaporization time on the large end. The sensor has a diameter of approximately 2 mm and small water droplets, less than 10 μm will not impact with 100% efficiency as they follow the airflow around the sensor. These losses are typically about 5% for 10 μm droplets but increase to greater than 20% for diameters less than 5 μm . This is normally not a major problem since the largest fraction of the water mass is typically carried in droplets greater than 10 μm . In developing clouds, however, near cloud base where droplets are still quite small, or in cloud edges where entrainment and evaporation is occurring, the underestimation of liquid water content can be significant.

On the large droplet side, the King probe begins to underestimate the liquid water contained in drops larger than 30-40 μm as a result of incomplete evaporation as these larger droplets impact and are carried away by the airstream before sufficient heat has been transferred to vaporize them.



Schematic diagram of the PMS/CSIRO Hot Wire Liquid Water Probe

Figure 6.17

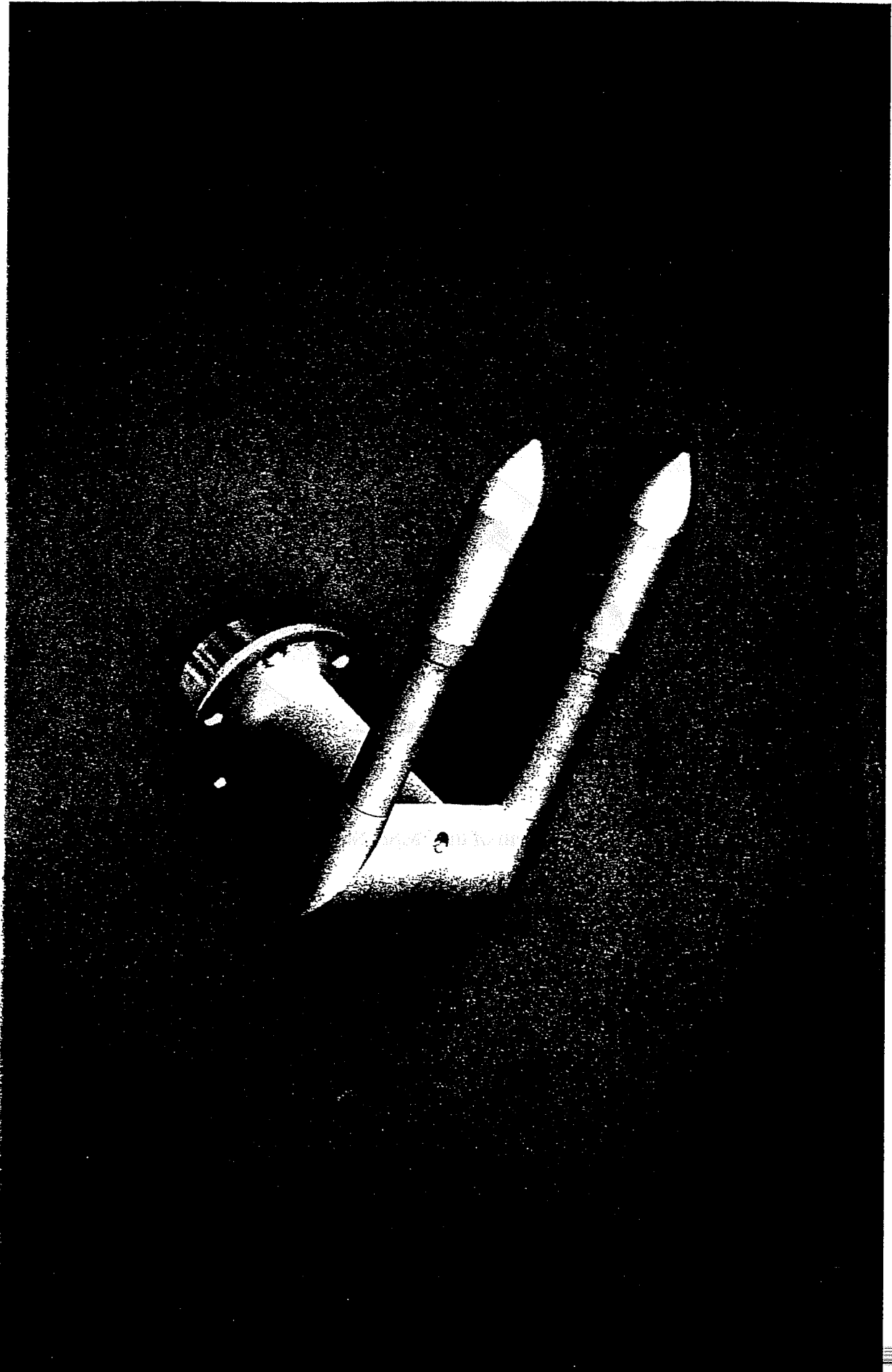


Figure 6.18 — PMS/CSIRO Hot Wire Liquid Water Probe